HISTIDINE PHOSPHORYLATION IN BACTERIAL CHEMOTAXIS

Thesis by

Cindy Maria Quezada

In Partial Fulfillment of the Requirements

for the Degree of

Doctor of Philosophy

California Institute of Technology

Pasadena, California

2003

(Defended June 4, 2003)

Acknowledgements

It has been a great privilege to be a graduate student at Caltech and to have interacted with so many gifted people. Herein, I give thanks to all those who influenced me personally and scientifically during this time.

When I first came to Caltech, I thought I knew who I wanted to work for. But then I met Harry Gray and my mind changed instantly. During our first encounter, he warned me that if I wanted to join his group, I had to like traveling. I still wonder whether he knew exactly who stood before him when he said this to me. After that meeting, I was sold and joined Harry's group. It has been a pleasure to know Harry for all these years. He is a professor who wears many hats. I will describe just three of those. There is Harry the scientist. Six of us joined his group my year- Ivan Dmochowski, Lila Guterman, Elizabeth Krider, Mike Machczynski, and Akif Tezcan. Each of us worked on a completely different project, reflecting Harry's breadth of scientific interests and genius. Secondly, there is Harry the friend. He loves to spend time with students. Harry is just as comfortable in a dive like the Colorado as he is at the Ritz. He is a blast to be around, is extremely generous, always has a story to tell, and has the ability to liven up even the stiffest party. Thirdly, there is Harry the parent, a role that he shares with his wife, Shirley Gray. Both Harry and Shirley enjoy getting to know the person behind the student. I thank them for going to my matriculation at Oxford, for watching me race in the Christ Church regatta, for seeing me off to a formal event when I was dressed in my silk sari, etc. etc. In essence, I thank them for their interest and concern. I am grateful for their friendship.

Through Harry, I met Tom Meade. We worked together on the Redox project. The times with Tom were crazy. He taught me how to properly pack a silica column in the middle of the night, he was conveniently available at odd hours in his office, diet Coke in hand, and he entertained my crazy ideas. Tom had a wonderful group of people working for him. In particular, I would like to thank Arnd Boettcher for helping me with the heinous synthesis of the cobalt acaciden peptide complexes. Angie Louie was not only a great scientific resource, but also became a very good friend. I thank her for her friendship, support, shopping outings, and fun nights out on the town in incredibly uncomfortable, but cute, shoes. Martina Hueber's smile and pleasant demeanor made the BI basement a nice place to work. Mary Flowers made life extremely easy by running the lab so smoothly.

Although I was mainly working in the Beckman Institute, I also had a bench in Noyes. I have many fond memories of the "late night crew" on the third floor of Noyes, namely myself, the young Mr. Chang, and Kevin Hoke. We shared many fun times at work going on late night food runs, watching Jerry Springer, and listening to Puff Daddy with Chris Chang. There are many Gray group members that I've interacted with over the years…there are too many to name, but I thank them all for making life at Caltech more enjoyable.

My scientific interests became more biological over time, and after I returned from an amazing year at Oxford (thank you Harry!), I was introduced to bacterial chemotaxis, which eventually became the subject of my thesis. This work was done in the laboratories of Mel Simon. Mel is a great scientist and I wish I could have learned more from him. He gave me one of the most precious gifts a person can receive because

it is something that you can never get back. That gift would be time. He let me take all the time I needed to be with my family and for that I shall be eternally grateful.

Mel has provided a great environment in which to do science. I know that I will miss it when I leave. The lab is well organized and all I ever had to worry about was doing the experiment. I would like to thank those people who made this possible. In addition to brightening up the hall with the beautiful flowers on her desk, Josephine Macenka ordered my supplies. I especially thank her for fulfilling my numerous last minute rush job requests. Blanca Mariona and Maria made my life easy by providing a constant source of clean and autoclaved glassware. They both also had a sixth sense for when I was hungry and had no food. I thank them for their generosity. Blanca even brought me food from her home during a really busy week so that I could just concentrate on work. I thank her immensely for being so maternal. Santiago and previously, Segundo, saved me a great deal of time by making buffers, media, and pouring plates. I know that I am spoiled. Luz made me laugh, was encouraging, and was extremely generous with food and candy as well. Joyce Kato kept the lab in shape.

I have met many great people in the Simon lab. In particular, I would like to thank Bryan Beel, the only other chemotaxis person in the group, for his encouragement and scientific advice. J.I. was a fun lab mate to have and kept me company during the evenings. I thank him for all those times after 5pm when he was a mini stock room and for being a helpful resource when I was cloning. Emil Bogenmann spent his sabbatical on a bench next to mine. It was a pleasure getting to know him. I enjoyed our talks.

I was extremely fortunate to have met Brian Crane and Alexandrine Bilwes in Mel's lab. Alex is a great scientist, very neat and precise when doing experiments.

Although I will never be able to grease trays as beautifully as she, I hope that some of her experimental technique rubbed off on me. Alex and Brian taught me how to do science. I thank them for their patience and help in crystallography. I was very sorry to see them leave Caltech for their new positions at Cornell. But in the end, I became an honorary member of their lab (thanks Mel for financing all those trips!). I thank them for their hospitality during my numerous visits to Ithaca. Thank you Owen for sharing your bathroom with me and for generously lending me papa's truck when I needed it. Brian became an advisor from a distance and I thank him for his input into my project and this thesis. I would not have been able to accomplish this work without the help and guidance of Brian and Alex. I could never thank them enough.

Members of the Crane group are responsible for all the fond memories I have of Ithaca, even of those bitter winter days. Seong "the player" Kang is a great host and entertainer. The brigade could learn a lot from him. Maddhavan Buddha, lord of the rings, master of intuition, was always a source of amusing conversation. It was fun to collaborate with Sang Park on the chemotaxis project and to hang out in Mexico. He is such a "nice" guy. I owe many thanks to Cristian Gradinaru, mon petit-fils. Not only was he a SHELX genius and a great help in solving the P1 structure, but he was also a wonderful friend. Avec wem could I otherwise write beaucoup de verrueckte multilingual emails. I enjoyed all the mischief we got into…manicures, HOT DOGS, breaking barriers, Christmas at the airport, the beautiful and sunny uptown days at the Marina…. I look forward to more fun in the future. Although Kartikeya Pant initially ratted me out, he eventually made up for this act by introducing me to cycling in the gorges Ithaca environs, by keeping my secrets, by being my talent agent, by graciously

putting up with all his nicknames, by reading my stories, by having such a stately demeanor, by having such gorges hands, by always being of enormous help at CHESS. I thank him for helping me take over the facility and for keeping me company when he could've been sleeping at home.

I also want to thank many of the Caltech staff members. Pat Anderson was a fun person to talk to about clothes, sales, and decorating. Virginia Russell has been incredibly kind to me and I thank her especially for all those years of cheap rent. She never complained about all the sounds that came from my little apartment, even as they got progressively weirder. Tess in the Registrar's office always greeted me with a smile. Natalie Gilmore answered all my questions about graduation. Dian Buchness has also been very helpful, along with Alison Ross. Catherine May was an entertaining person to talk to on the fourth floor of the BI. I would also like to thank my thesis committee: Jack Richards, Sunney Chan, and Pamela Bjorkman for their input.

My thesis was made into a much more interesting story with the help of Professor Rick Dahlquist and his student Damon Hamel at the University of Oregon, Eugene. I thank Rick for letting me do the NMR experiments described in this thesis in his labs and Damon for putting up with me for ten hard working days. Damon was a fun person to collaborate with scientifically and also over some sangritas. I thank him and Carrey for the fun times in Cuernavaca…sorry I made you starve!

There are some people that are not affiliated with Caltech to whom I also owe thanks. Kevin Miller has been a good friend to me for so many years and I was happy that we overlapped for some time in Pasadena. Through him, I met Catherine Cox, who was an excellent and hilarious gal pal. We had many fun nights together. Enrique

Ramirez introduced me to the restaurant world. I thank him for all the good food, martinis, and for showing me a side of LA that I never knew existed. I owe many thanks to Clarita for bringing music and dance into my life. She helped me out enormously while I was finishing up, more than she could ever imagine. Clarita is a great mentor. She is tough, but made the class laugh while we struggled and made us proud when we succeeded. Besides reminding me what hips are meant for, Clarita also taught me to have no fear, to remove the word can't from my vocabulary, and to just go for it. Being around such a positive person was really helpful while I was writing my thesis. I always left her class fired up with plenty of energy to continue working into the night. I am very thankful to her. I hope to make her proud in a tablao one of these days.

Acquaintances come and go. True friendships, those that are maintained no matter what happens, last a lifetime. The following people have been there for me when times got tough and I appreciate their friendship in more ways than I can ever express. I know they will always be my real friends.

Todd Davidson has been a great influence in my life on both an intellectual and personal level. He has introduced me to great thinkers and has been an inspiration to read, read, read. I enjoyed our conversations about politics, philosophy, history, language, and culture. Regardless of what topic I brought up, he always managed to reach over to his bookshelf and pick up at least one book that he had already read on the subject---like I said, a true inspiration. I thank him for exposing me to so many ideas. I have become a better person by knowing him. I also thank him for being so generous and for taking me places and showing me things majarani style.

Although Sven Halstenberg (the most Salvadorean German I know) almost killed me in the Swiss Alps while "teaching" me how to ski, I am extremely thankful for his kindness. He has been very supportive, often making fun of himself in order to make me laugh. I appreciate his sense of humor and friendship. I would also like to thank his parents for including me in their family festivities.

Ari Hershowitz is one of the few people I know who can keep up with my dancing. He is willing to dance anywhere and anytime. Maybe that is why we get along so well. In addition to being a great dancing partner, he has also been a wonderful and caring friend. I appreciate his concern for me. Thanks for being my cheerleader Ari, even when you moved far away.

Kevin Hoke has been an incredible friend to me and I will never be able to repay him for all his kindness. Kevin taught me how to synthesize cobalt acacen compounds, but more importantly, he taught me what it means to be a good friend. Kevin has always been there for me and has offered a helping hand whenever I needed one. I never even had to ask. Thanks for walking me home safely, for keeping me out of trouble (or at least trying to), for keeping me sane during candidacy, for watching updates on carrot arm woman with me, for the fun times on Bourbon Street,..etc. I thank you particularly for sending postcards to my mother when in Europe. That meant a lot to me and to her.

Don Low has been a great friend to talk to. I thank him for his advice and the comfort that he has provided me. Just like a good chemist should be, Don is a great cook. I thank him for all the Sunday night meals that eventually turned me into an X-files addict and for treating a starving grad student to a decent dinner on his visits to Pasadena.

I would likely not be here if it weren't for Kai Martell. I thank him for driving through rain and snow to get me to Caltech, for dodging bullets with me in war zones, for teaching me to sing Hans Albers songs as good as any fisherman from the Hamburg Hafen, and for bringing so much insanity into my life. Most of all, I would like to thank him for all the encouragement he provided me. He never thought an idea was too crazy or that a goal was out of reach. I am grateful that he came into my life, because he significantly changed it.

I read a lot about chemical bonds while writing this thesis, but I failed to run across an important one, perhaps one of the strongest bonds around…the thesis writing bond. This is a bond that I share with Will Wehbi. We happened to write our thesis at the same time. It was incredibly helpful to have someone along for this roller coaster ride. So thank you Will for being a Father, a grandma, a butterfly, an alarm clock, and an ambulating proton to me during this time. I will fondly remember the adventures of the "thesis writing crew"- the regiment, the all-nighters, the "15 more minutes" requests, the tea (plain or otherwise enhanced), the ice-cream, taking a pass on Bass, those "I didn't do a damn thing today" days, the thirty-some countdown ceremonies, and of course the infamous countdown pad. You certainly made the thesis writing experience more enjoyable and words cannot express my gratitude to you. I don't know what I did to deserve a friend like you Will. I suppose some might say that makes me Lady Luck.

And finally, I would like to thank my family. My beautiful boys, Alec and Aaron, never once asked me when I would finally finish. For that, I thank them. I benefited greatly from having two older sisters, Jenny and Nina, who took their bratty little sister everywhere they went, exposing her to many things at a young age.

I was blessed with two wonderful parents. My father has been the source of my academic inspirations. He instilled a love of books in me from a young age. He is a renaissance man and my role model. I would consider myself a success if I were ever to achieve half of his accomplishments. I thank him for proofreading my reports in elementary school, for helping me build the San Juan Capistrano Mission in the 4th grade, for helping me test the effect of various types of light on plant growth for a science fair project, for listening to me practice my arguments for a high school debate on American foreign policy, the list goes on and on. In essence, I thank him for spending so much time with me as a child, even when he had a busy schedule to keep himself. I could not have asked for a better father.

I also could not have asked for a better mother. I thank her for dedicating her life to our family, although that surely got in the way of her own dreams and aspirations. She was a nurturing mother, a great cook, incredibly giving, and a whole lot of fun to be around. I thank her for dancing around the house with me, for making sure I continued to speak Spanish, for the nutritious food, for mending my clothes, for teaching me about manners, kindness, and generosity through her actions, for never letting me give up, for encouraging me to see the world and giving me the funds to so. Whatever resilience I have, I owe to her. She taught me to never give up hope, no matter how grim the outlook might be. She also taught me that if I fall, to get back up and keep going no matter what. I could never thank her appropriately for all that she has done for me, for shaping me into what I have become. I dedicate this thesis to my mother. Mil gracias mami.

Table of Contents

Acknowledgements iii

Table of Contents xii

Abstract xiv

Chapter 1: Introduction 1

Chapter 2: The crystal structure of the CheA histidine phosphotranfer domain from *Thermotoga maritima* 43

Chapter 3: The chemical determinants of histidine reactivity in CheA 81

Chapter 4: Mutations in the conserved hydrogen bonding network of the CheA histidine phosphotransfer domain 134

Appendix 1: ^{1}H and ^{15}N chemical shifts of P1 histidine residues 173

Appendix 2: Biochemical characterization of CheA domains 189

Dedicatoria

A mi madre, por ser quien fue, por haberme hecho quien soy

Abstract

Bacterial chemotaxis, the directed movement of bacteria in a chemical environment, represents one of the best biochemically and structurally characterized signal transduction pathways. The histidine kinase CheA is a central player in this two-component regulatory system. Its active site is spread across two domains: the histidine phosphotransfer domain (P1) and the kinase domain (P4). Our efforts focus on elucidating the mechanistic contribution of P1 residues to the autophosphorylation reaction.

An atomic resolution structure (0.98Å) of the *Thermotoga maritima* CheA histidine phosphotransfer domain was obtained, affording a unique opportunity to view the environment surrounding His45, the phosphoaccepting histidine, in detail. His45, participates in a hydrogen bonding network including three other residues: Glu67, Lys48, and His64, which are conserved in CheA. Employing a combination of site-directed mutagenesis studies, protein crystallography, and 2-D heteronuclear NMR techniques, we explored the functional roles of these residues involved in the largely conserved hydrogen bonding network.

Our experiments revealed that the P1 domain provides the nucleophile for phosphate transfer (His45) and the activating glutamate (Glu67) completing a catalytic center observed in the GHL family of ATPases. Glu67 tunes the reactivity of His45 through a hydrogen bond. This interaction activates His45 to the normally unfavored $N^{\delta 1}H$ tautomeric state. As a result, His45 possesses an altered pKa. Upon mutation of Glu67 to a Gln, the chemical properties of His45 change. When existing in the

predominantly $N^{\varepsilon 2}H$ tautomeric state, its pKa is similar to that of a solvent exposed histidine and its phosphorylation is dramatically reduced *in vitro* and *in vivo*.

Hence, the phosphoaccepting histidine must exist in the normally unfavored $N^{\delta 1}H$ tautomeric state in order for CheA autophosphorylation to occur. The other two residues, Lys48 and His64, do not affect the reactivity of His45. Instead they contribute towards the structural integrity of the P1 active site. The results obtained in this thesis provide a solid structural and biochemical basis for further understanding the CheA phosphotransfer mechanism and may provide critical insight for the development of novel antibiotic agents.

Chapter 1

Introduction

This chapter was adapted from Bilwes A. M., Park, S. Y., Quezada, C. M., Simon, M. I., and Crane, B.R. "Structure and Function of CheA, the Histidine Kinase Central to Bacterial Chemotaxis." in *Histidine Kinases in Signal Transduction* (eds. Inouye, M. & Dutta, R.) 47-72 (Academic Press, New York, 2003).

Bacteria are continuously exposed to environmental changes. Signal transducing circuits, referred to as "two-component" regulatory systems or "His-Asp phosphorelays," process the extracellular information into a usable intracellular response [1-3]. These pathways have also been found in lower eukaryotes, like yeast, slime mold, and plants [4-7] and are utilized to control diverse cell responses such as bacterial chemotaxis, sporulation, osmoregulation, pathogenesis, plant response to hormones, cell growth and differentiation [1, 8]. These adaptable and sensitive circuits can function over a broad time range extending from milliseconds to hours.

In the simplest case, the mechanism of a two-component regulatory system is described by a phosphotransfer event from an autophosphorylating protein histidine kinase (PHK) to a response regulator (RR) (Figure 1). In *E. coli*, 29 PHK genes and 32 RR genes have been found and constitute, at the very least, 29 independent His-Asp phosphorelay systems, each responding to a specific subset of stimuli [9]. Current estimates of the number of two-component proteins from other bacterial genomes are 70 for *B. subtilis* [10]; 9 for *Haemophilus influenzae* [11]; 11 for *Helicobacter pylori* [11]; and 19 for *Thermotoga maritima* [12].

Protein histidine kinases, which act as sensors for individual external signals, catalyze the transfer of the ATP γ-phosphoryl group to one of its histidine residues. Upon autophosphorylation, the dimeric PHK then transfers the reactive phosphoryl group from its histidine to a conserved aspartate residue of another component in the response regulator (RR). The phosphorylated RR modifies an effector which leads to the appropriate change in cellular behavior.

Five conserved regions of sequence are used to identify histidine kinases [2, 13, 14]. These consist of the H box, which contains the phospho-accepting histidine, and the N, G1, F, and G2 boxes, which delineate the ATP binding domain. PHKs can be further classified by the relative position of the H box to the ATP binding domain (Figure 2). In Class I PHKs, the H box is located in the dimerization domain which is located directly adjacent to the ATP binding region. Alternatively, in Class II PHKs, the H-box lies in an N-terminal monomeric domain distal to the ATP binding region and the dimerization domain does not contain a histidine residue. A further difference between these two classes is that Class I members are typically membrane bound, possessing a periplasmic sensor domain. Conversely, the Class II histidine kinase CheA is regulated by interaction with an independent receptor.

The second player in two-component regulatory systems is the response regulator and it is typically the terminal component of the signaling pathway. It consists of two domains: a regulatory domain and an effector domain (Figure 3). In some cases, as observed with the response regulator CheY, the effector domain is missing altogether [15-18]. Aspartyl phosphorylation of the conserved regulatory domain by a protein histidine kinase or small molecule phosphodonors activates the effector domains to elicit specific cellular responses such as transcription regulation or enzymatic catalysis [19].

The core structures of two-component systems, their activities, and phosphorelay sequences are maintained across the prokaryotic, archaeal, and eukaryotic kingdoms. However, much diversity is observed in the organization of elements in a particular pathway. The EnvZ/OmpR osmoregulatory system exemplifies a simple two-component regulatory pathway in *E. coli* (Figure 4a). The orthodox PHK EnvZ transfers its

phosphoryl group to an aspartyl residue of the RR OmpR. Although the signal transducing circuit of bacterial chemotaxis also uses a single phosphoryl transfer event, the unorthodox PHK CheA exhibits an alternative arrangement of domains (Figure 4b).

Some "His-Asp phosphorelay" systems are even more complex, displaying variations in the number and modular organization of PHK and RR components. These hybrid histidine kinases possess other functional domains that are directly linked to one another. For example, the anaerobic hybrid sensor ArcB has a RR domain and a histidine phosphotransfer (HPt) domain that are connected to the C- terminus of its ATP binding domain. The terminal RR ArcA can receive a phosphoryl group directly from the catalytic core of the PHK or from the HPt domain [20] (Figure 4c). The yeast osmoregulatory control system presents another variation on multi-step phosphorelays [5, 21]. It is similar to that of ArcB, except for its HPt domain is an independent protein (Figure 4d). Another four step His-Asp-His-Asp phosphorelay system is the *B. subtilis* sporulation control system. Its signaling domains consist entirely of independent proteins (Figure 4e).

Significant progress has been made in understanding the biology and chemistry of these ubiquitous two-component signaling pathways. They are prevalent in prokaryotes, but seldom found in eukaryotes, making proteins involved in these His-Asp phosphotransfer systems attractive targets for antibiotics, herbicides, and fungicides. Given that histidine kinases initiate most bacterial signaling pathways, it is of great interest to obtain a detailed understanding of their chemical and biological nature. We have begun a detailed study of one of the best characterized histidine kinases, CheA,

involved in one of the most extensively studied two-component signaling pathways, bacterial chemotaxis.

Bacterial Chemotaxis: A Paradigm for the Study of Two-Component Signal Transduction

Bacterial chemotaxis describes the directed movement of bacteria in a chemical gradient [22]. A direct correlation between flagellar rotation and bacterial movement exists [23]. When flagella turn counterclockwise, a coherent bundle is formed and bacteria swim "smoothly" in a straight line. In contrast, clockwise rotation results in dispersion of the flagellar bundle, causing an abrupt change in the swimming course and is termed "tumbling." (Figure 5)

A combination of smooth swimming, interrupted by brief tumbling episodes that reorient the cell, is normally observed when a bacterium swims in a homogeneous environment [24]. Alternatively, in a spatial chemical gradient, a bacterium measures changes in chemical concentration over time, adapting its swimming behavior to the local environment [25]. Smooth swimming is observed for lengthier periods of time when a bacterium is moving towards a chemoattractant or away from a chemorepellent. Conversely, the tumbling frequency is augmented if a bacterium encounters sharply increasing repellent or decreasing attractant concentrations. This behavior enhances the chance of a bacterium to translocate to more favorable surroundings [24-26]. Therefore bacterial chemotaxis is said to be achieved by a "biased random walk."

The signaling components involved in bacterial chemotaxis

Bacterial chemotaxis has been described at the molecular level (Figure 6). Its excitation pathway, which occurs within milliseconds, involves an intricate phosphorylation cascade. A repellent bound receptor triggers the autophosphorylation of the PHK CheA [27]. The rate of autophosphorylation is enhanced by the binding of the adaptor protein CheW to CheA and receptor [28]. CheA autophosphorylation initiates a phosphorylation cascade transferring its histidine bound phosphoryl group to the aspartate residue of the response regulator CheY [29, 30]. Phosphorylated CheY then interacts with the flagellar motor component FLiM. The bacterium then tumbles and can swim in another direction [31].

As the fast excitation response proceeds, a slower adaptation response, which occurs within minutes, is concurrently set in motion. CheA activity is regulated by receptor methylation [27, 32]. These methyl groups are added by CheR. Low levels of receptor methylation are associated with low CheA kinase activity and high levels of receptor methylation are associated with higher CheA kinase activity. In addition to CheY, CheA can also phosphorylate a methyl esterase CheB [33]. In its activated form, CheB removes methyl groups from glutamate residues found on the C terminal tail of the receptor thereby inhibiting CheA activity and eventually reducing the occurrence of tumbling. These competing pathways provide bacteria with an elegant way to reset its memory, allowing for the sensitive continuous detection and response to changes in the environment continuously.

The modular structure of CheA

Our understanding of the bacterial chemotaxis process has been further enhanced by the structural elucidation of all the proteins known to be involved in the pathway. For the remainder of this chapter, we focus on the protein histidine kinase CheA. The modular character of CheA was inferred from functional assays [34-36] with isolated fragments and later demonstrated by protein crystallography and NMR. CheA is a homodimer that is composed of five domains in *T. maritima* (Figure 7).

The P1, or histidine phosphotransfer (HPt) domain, consists of a four-helix bundle that possesses a solvent accessible histidine which becomes phosphorylated [37, 38]. A fifth helix connects P1 to the P2 domain, which binds the response regulators CheY and CheB. This domain facilitates the transfer of the P1 phosphoryl group to a response regulator. P2 is formed by a small alpha/beta sandwich fold [39-42]. The structures of the last three domains of *T. maritima*, termed CheA Δ289, were solved as an entity [43]. P3 is the dimerization domain. It consists of two antiparallel helices that pack against the analogous two helices of the second subunit to form the central four helix bundle that modulates CheA transphosphorylation. The kinase domain, P4, contains the ATP binding pocket and is formed by a two layered α-β sandwich composed of five β- strands and seven α- helices [44]. The regulatory domain, P5, consists of two intertwined five stranded beta barrels. It regulates kinase activity by binding to the adaptor protein CheW, coupling it to the receptor [34, 45, 46].

Each CheA domain has a distinct and critical function that optimizes bacterial response to the extracellular environment. Although P1 and P4 must interact with one another within a dimeric CheA for physiological activity, some ATP-dependent histidine

phosphorylation can be achieved *in vitro* by the two separated domains [44]. Hence, all the elements necessary for the chemistry of histidine phosphorylation are contained in the domains P1 and P4. The features of the kinase domain, P4, are first examined, followed by those of the histidine phosphotransfer domain, P1.

The P4 histidine kinase domain belongs to a superfamily of ATPases

The CheA histidine kinase domain (P4) is structurally similar to the ATP-binding domain of a class of ATPases named the GHL family [47] after the three structurally defined members: the type II DNA topoisomerase GyraseB [48], the chaperone Hsp90 [49] and the DNA-repair enzyme MutL [50]. These functionally divergent ATPases are multi-domain proteins whose other domains are unrelated to histidine kinases. The core structural elements in common between CheA, GyrB, Hsp90, and MutL consist primarily of the 4 β-strands and 3 α-helices that form a deep cavity for binding ATP (Figure 8a-b). Histidine kinases are therefore unrelated to mammalian Ser/Thr or Tyr kinases and instead probably derive from an ancestor common to GyrB, Hsp90 and MutL.

Nucleotide binding by CheA P4 and the GHL ATPases

The ATP-binding sites of PHKs and GHL ATPases are highly conserved. ATP analogs bind CheA in a deep cavity, whose back wall is formed by the P4 β-sheet (Figure 8). The cavity edges include four regions of sequence similarity that characterize the histidine kinase family. These are (1) the N box (helix α4); (2) the G1 box (the segment running in front of the sheet and forming a right angle turn after strand β2); (3) the F box (the end of helix α2); and (4) the G2 box (beginning of the helix α3 with the end of the

loop preceding it). The residues pointing into the cavity from the β strands form a mainly hydrophobic lawn on which the adenine ring hydrogen bonds with the invariant Asp (449 in *T. maritima* CheA). Four buried water molecules that bridge interactions between the nucleotide base and the cavity are also found in the nucleotide complexes of Hsp90 [51, 52] and MutL [47]. A conserved Asn (409 *T. maritima* CheA) coordinates nucleotide - bound Mg^{2+} in CheA [44], MutL [47], GyrB [48] and Hsp90 [52].

Despite striking similarities in nucleotide binding by PHKs and GHL ATPases, there are some compelling differences. For example, an essential glutamate of the GHL ATPases presumed to be the general base involved in water activation for ATP hydrolysis[53] (Glu 29 for MutL) is replaced by His 405 in CheA (Figure 9). His 405 stabilizes the G2 box when Mg^{2+} is bound. In contrast, the general base for histidine activation likely resides on the P1 domain (see below).

Moreover, CheA and the GHL ATPases appear to recognize the ATP phosphates in different ways. For example, the functional analog of a CheA residue that hydrogen bonds to the ATP β- phosphate (His 413) comes from a different loop in the ATPases. Furthermore, interactions between nucleotide phosphates and main-chain nitrogens of the P-loop (a glycine-rich segment found in many ATP-binding proteins that coordinates the α- and γ- phosphates of bound ATP) are not nearly as extensive in CheA as they are in GyrB and MutL. Perhaps P1 binding drives a more extensive interaction between nucleotide and the CheA P-loop that resembles structures observed for the ATPases. In fact, the G2 box (P-loop) mutation Gly 502 to Lys (*E. coli* residue 470) does not affect nucleotide affinity but is inactive [54].

The conformation of P4 is linked to ATP hydrolysis

PHKs and GHL ATPases contain a region that varies in conformation upon nucleotide-binding: the ATP-lid (Figure 9). In CheA, the ATP-lid (composed of the flexible loop between α2 and α3) changes conformation significantly among ATP-analog, ADP, and nucleotide-free structures. Only in the structure of separately expressed P4 with Mg^{2+}-ADPCP is the ATP-lid completely discerned [44]. The high mobility of the lid region is indicated by its poor order in all other P4 structures, the nucleotide-free structure of CheA Δ289 [43], and the NMR structure of the type I EnvZ PHK. In the P4:ADPCP-Mg^{2+}structure, the ATP-lid forms a helix that borders the nucleotide-binding cavity (Figure 9a). The resulting concave groove on the face of P4 surrounds the exposed γ-phosphate and has dimensions appropriate for binding P1 (Figure 10).

The shape of this groove, particularly its width nearest the bound nucleotide, depends on the presence of ATP analogs and Mg^{2+}. In P4 structures where the ATP pocket size is contracted due to molecular packing within the crystal lattice, Mg^{2+} does not bind and the γ-phosphate of non-hydrolyzable ATP analogs cannot be resolved due to disorder. This contracted conformation is also observed when ADP is bound by P4 (Figure 9d). Change in cavity size and loss of Mg^{2+} on ATP hydrolysis can be linked by the movement of His 405, which in the absence of Mg^{2+}, swivels up from the position where it coordinates the metal ion and instead hydrogen bonds to the ADP β-phosphate.

In the ADP complex, the G2 box residues change conformation because His 405 no longer stabilizes the G2 box; this destabilizes the entire ATP-lid structure (Figure 10d). If direct coordination to Mn^{2+} instead of Mg^{2+} forces His 405 to swivel, the

conformation of the ATP-lid is similarly affected and interactions of the P-loop with the γ-phosphate are weakened (Figure 9b). As confirmed by biochemical studies, conformational changes in regions that likely compose the P1-binding site on P4 (the ATP-lid) are coupled to ATP hydrolysis and Mg^{2+} release by movement of His 405 [55].

Biochemical investigations of other mutations at the N, G1, G2, and F boxes were made [55]. Results suggested these conserved residues contribute to the CheA kinase activity and ATP binding. Mutations that affect ATP binding were also found to stabilize the transition-state complex during CheA autophosphorylation in an unknown fashion. Alterations at a glycine residue in the G1 box are not tolerated, consistent with prior structural analysis that mutations at this location would disrupt the structure of the ATP binding cavity [44]. In correlating biochemical to structural studies, some of the functional roles of conserved residues residing in the P4 domain have begun to be assigned providing insight into the CheA mechanism.

The site of phosphorylation is located in the P1 domain

P1 contains the substrate histidine that transfers phosphate from kinase bound ATP to the response regulators CheY and CheB [33, 56]. It is composed of a small 3_{10} helix followed by an antiparallel four-helix bundle (helices A-D) and helix (E) that connects to P2 via a 25-35 residue linker [37, 38]. Helix E does not contribute to helix cluster stability nor to the phosphorylation reaction[37].

The P1 helices are amphipathic with most hydrophobic residues buried in the core and most polar residues exposed to the surface. Inter-helix salt bridges and hydrogen bonds are found only between helices A and D and helices B and C[38]. The five helices

each display very different dynamic features. Residues from helices A, C, and D show strong protection from hydrogen exchange, indicative of local stability around the amide hydrogen[37]. However, helix B, which contains the phospho-accepting histidine, may be more variable in conformation as its amide protons are not strongly protected from solvent exchange.

Sequence similarity among CheA P1 homologs is concentrated in helices B and C, where the active site residues are located. Despite the high sequence similarity between *E. coli* and *T. maritima* CheA P1 in this region[37], *T. maritima* CheA Δ289 cannot phosphorylate an *E. coli* P1-P2 fragment (unpublished data). The interface between P1 and the kinase domain is therefore likely to include residues on P1 not immediately surrounding His45.

NMR studies of protein backbone dynamics indicate that *E. coli* P1 forms a rigid and compact helix bundle in both the unphosphorylated and phosphorylated states. Both these forms of P1 have very similar backbone conformation[37]. Phosphorylation of P1 does not deprotonate His48 $N^{\delta 1}H$ and results in only small chemical shift changes for residues on helices B and C surrounding His48. Alternations in the local electronic environment caused by phosphorylation are likely responsible for these changes[57]. No interaction between P2 and phosphorylated P1 was detected by NMR[58].

The reactivity of the phospho-accepting His48, located in the middle of helix B, is tuned by its local environment. A hydrogen bond between the His48 $N^{\delta 1}H$ and the Glu70 carboxylate may be responsible for the high pKa (7.8) of the His48 imidazole ring, which is the site of phosphorylation. NMR studies indicate that its $N^{\varepsilon 2}$ atom does not hydrogen bond with other P1 residues, but that His48 $N^{\delta 1}H$ is a hydrogen bond donor that remains

protonated at high pHs and after phosphorylation [57]. Three out of the four molecules in the crystal structure of *Salmonella* P1 reveal that His48 $N^{\delta 1}H$ hydrogen bonds to Glu70 on Helix C. Furthermore, Lys51Ala and Glu70Ala mutations in *Salmonella* reduce the ATP phosphotransfer rate[38]. However, these experiments could not distinguish if the decreased transfer rate was due to loss of binding between the P1 and the kinases or a catalytic defect.

Investigating the mechanism of CheA phosphotransfer

In contrast to GyrB, MutL, and Hsp90, which hydrolyse ATP, PHKs must transfer phosphate to a histidine residue. Therefore, the nucleophilic mechanism for attack on the ATP γ-phosphate must differ between the two enzymes. In GyrB, mutagenesis studies [53] implicate the conserved Glu 42 (Glu 29 in MutL, Glu 47 in human Hsp90) as an essential general base for water activation. Despite high conservation of active site residues between GyrB and histidine kinases, the latter do not contain a Glu at this position (His 405 for CheA proteins, Asn for other histidine kinases) (Figure 11). Thus, the CheA P1 domain may provide not only the nucleophile for phosphate transfer (His45) but also the activating glutamate (Glu70), thereby completing the catalytic center observed in GyrB.

Despite the fact that CheA is one of the best-characterized histidine kinases, little is known about its biochemical mechanism. The CheA active site is distributed across two domains, P1 and P4. The investigations described in this thesis focus on the least studied domain encompassing the CheA active site. In order to gain insight into the

biochemical mechanism of CheA, structure-function studies of the histidine phosphotransfer domain are performed.

The remainder of this thesis focuses on two questions: (1) Do the GHL family of ATPases and CheA share a conserved mechanism? and (2) What are the chemical and structural determinants for histidine phosphorylation in bacterial chemotaxis? These questions will be addressed in the following chapters. Chapter 2 describes the atomic resolution structure of helices A-D of the CheA HPt domain from *T. maritima*. A conserved hydrogen bonding network involving residues His45, Lys48, His65, and Glu67 is identified. Their contributions to the CheA phosphorylation reaction are further explored. In Chapter 3, the functional role of Glu67 is explored using an interdisciplinary approach involving site directed mutagenesis, macromolecular protein crystallography, and two dimensional NMR techniques. The same approach is used in Chapter 4 to assess the putative functional roles of Lys48 and His64, the remaining participants in the hydrogen bonding network.

Figure 1: Organization of a prototypical two-component regulatory system

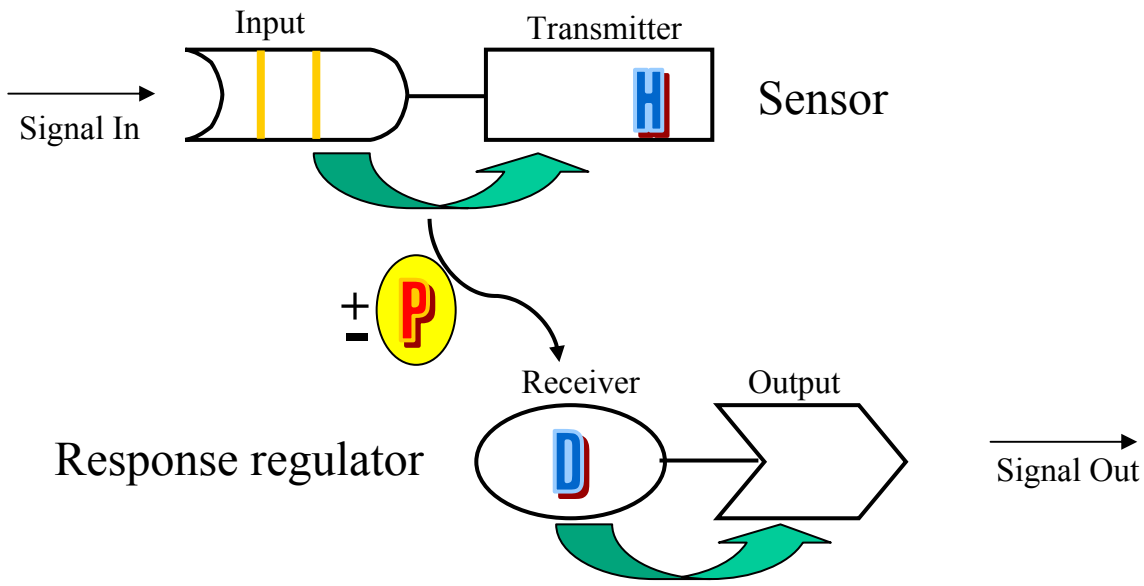
Input
Transmitter
Signal In
Sensor
H
+
-
P
Receiver
Output
Response regulator
D
Signal Out

Figure 2: Protein histidine kinases can be divided into two classes. A schematic depiction of the classification of PHKs based on the position of the H-box relative to the ATP binding domain.

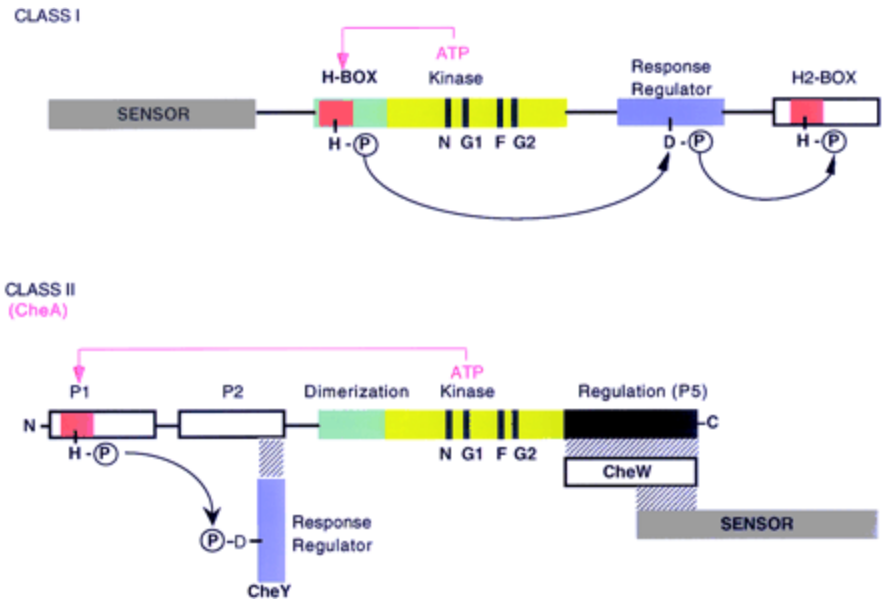
CLASS I
ATP
H-BOX
Kinase
Response
Regulator
H2-BOX
SENSOR
H - P
N G1 F G2
D - P
H - P
CLASS II
(CheA)
ATP
P1
P2
Dimerization
Kinase
Regulation (P5)
N
C
H - P
N G1 F G2
CheW
SENSOR
P - D
Response
Regulator
CheY

Figure 3: Typical architecture of a response regulator

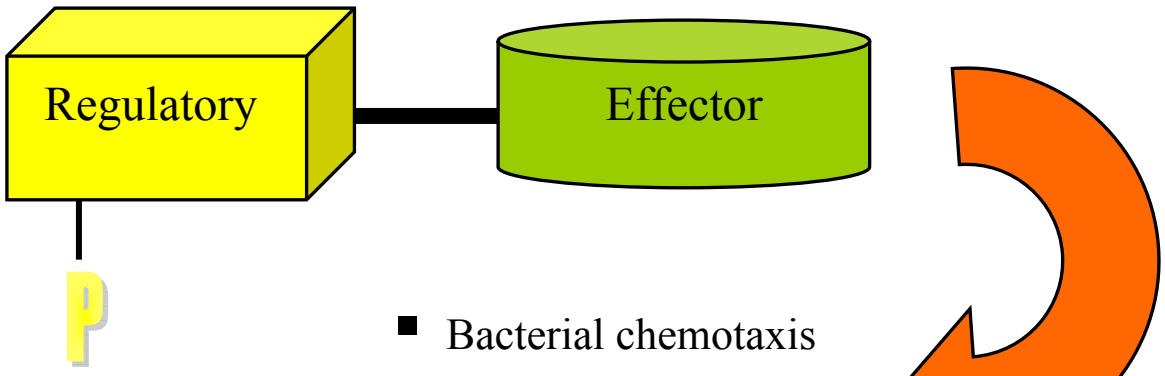

- Bacterial chemotaxis
- Osmoregulation
- Sporulation
- Pathogenesis
- Plant response to hormones

Figure 4: Diversity of domain organization in His-Asp phosphorelays. (a) The osmoregulatory system of *E. coli* employs the PHK EnvZ and the RR OmpR. (b) Bacterial chemotaxis involves the Class II PHK CheA and the RR CheY. (c) Anoxic redox control in *E. coli* is regulated by the PHK ArcB and the RR ArcA. (d) *S. cerevisiae* employs the PHK Sln1, the HPt domain Ypd1, and the RR Ssk1 in the osmosensing system. (e) The *B. subtilis* sporulation pathway involves a multicomponent His-Asp phosphorelay in which all signaling components are individual proteins.

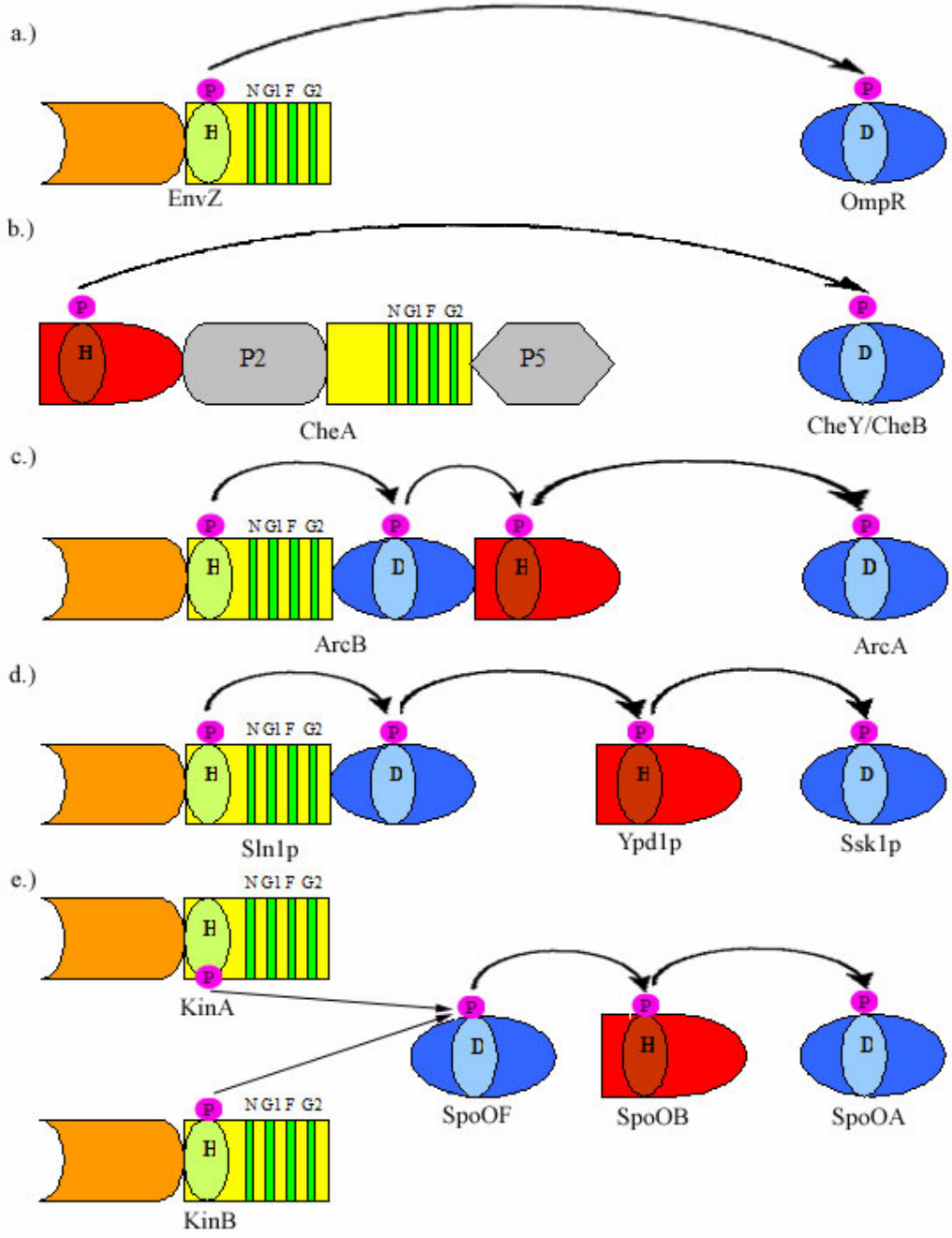
a.)
P
N G1 F G2
H
EnvZ
P
D
OmpR
b.)
P
H
P2
N G1 F G2
P5
CheA
P
D
CheY/CheB
c.)
P
N G1 F G2
H
P
D
P
H
ArcB
P
D
ArcA
d.)
P
N G1 F G2
H
P
D
Sln1p
P
H
Ypd1p
P
D
Ssk1p
e.)
N G1 F G2
H
P
KinA
P
D
SpoOF
P
H
SpoOB
P
D
SpoOA
P
N G1 F G2
H
KinB

Figure 5: Bacterial movement is controlled by flagellar rotation. Counterclockwise rotation of flagella results in “smooth” swimming and clockwise rotation results in “tumbling.”

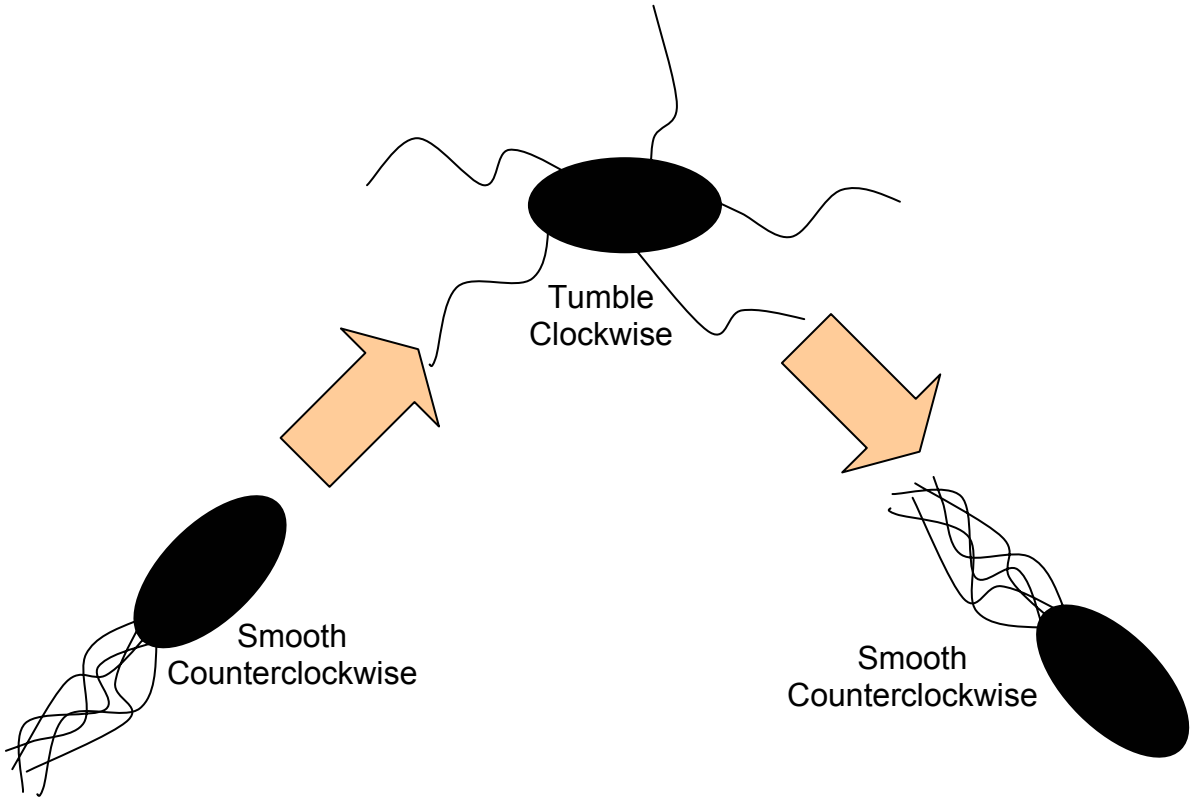
Tumble
Clockwise
Smooth
Counterclockwise
Smooth
Counterclockwise

Figure 6: The molecular components involved in the bacterial chemotaxis signal transduction pathway

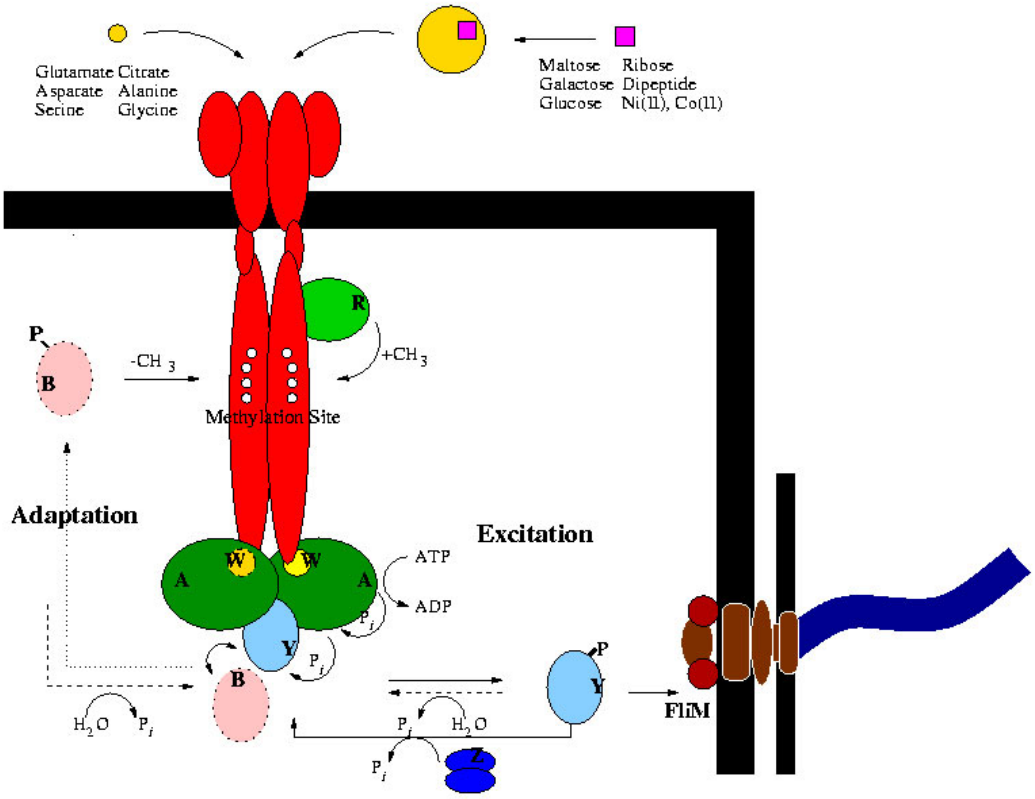
Glutamate Citrate
Asparate Alanine
Serine Glycine
Maltose Ribose
Galactose Dipeptide
Glucose Ni(II), Co(II)
R
P
B
-CH 3
+CH 3
Methylation Site
Adaptation
Excitation
W
W
A
A
ATP
ADP
Y
B
H2O
Pi
P
Y
FliM
Z

Figure 7: CheA is a homodimer consisting of five domains (P1-P5). P1 is the phosphotransfer domain, P2 is the response regulator binding domain, P3 is the dimerization domain, P4 is the kinase domain, and P5 is the regulatory domain. Dotted lines represent missing residues and putative linker regions between domains. One monomer is colored in red, orange and yellow hues, while the other is represented in purple and grey tones.

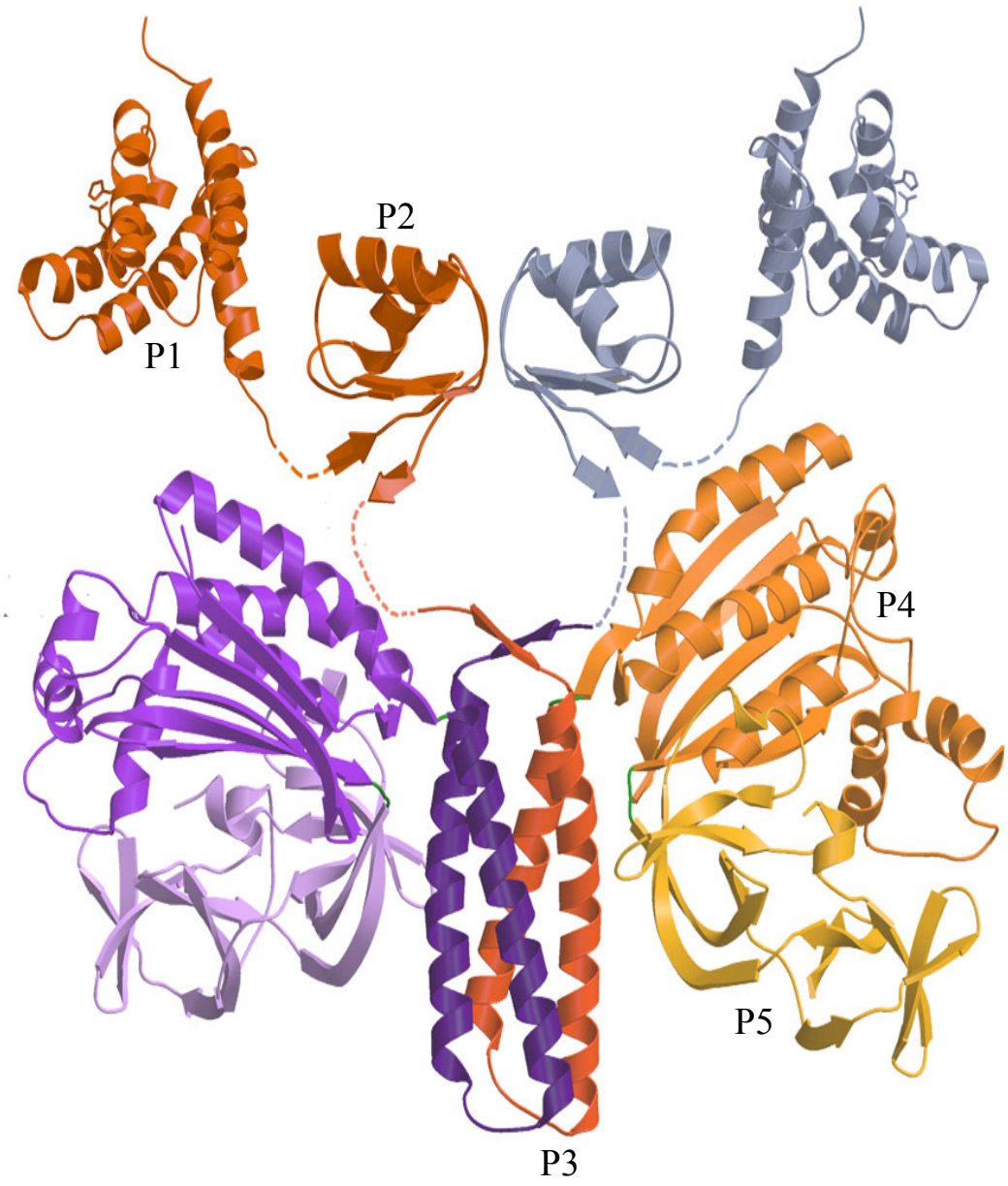
P1
P2
P3
P4
P5

Figure 8: The CheA kinase domain (a) is topologically similar to the ATP binding domain of GyrB (b).

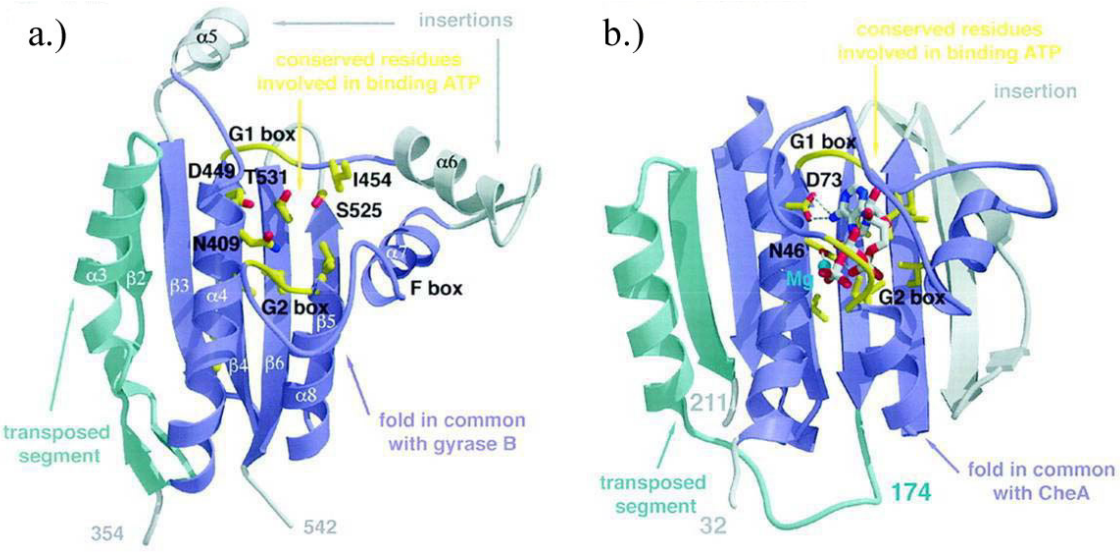
a.)
insertions
α5
conserved residues
involved in binding ATP
G1 box
D449
T531
I454
S525
α6
N409
α7
α3
β2
β3
α4
G2 box
F box
β5
β4
β6
α8
transposed
segment
fold in common
with gyrase B
354
542
b.)
conserved residues
involved in binding ATP
insertion
G1 box
D73
N46
Mg
G2 box
211
transposed
segment
32
174
fold in common
with CheA

Figure 9: Nucleotide binding alters the conformation of the CheA kinase domain

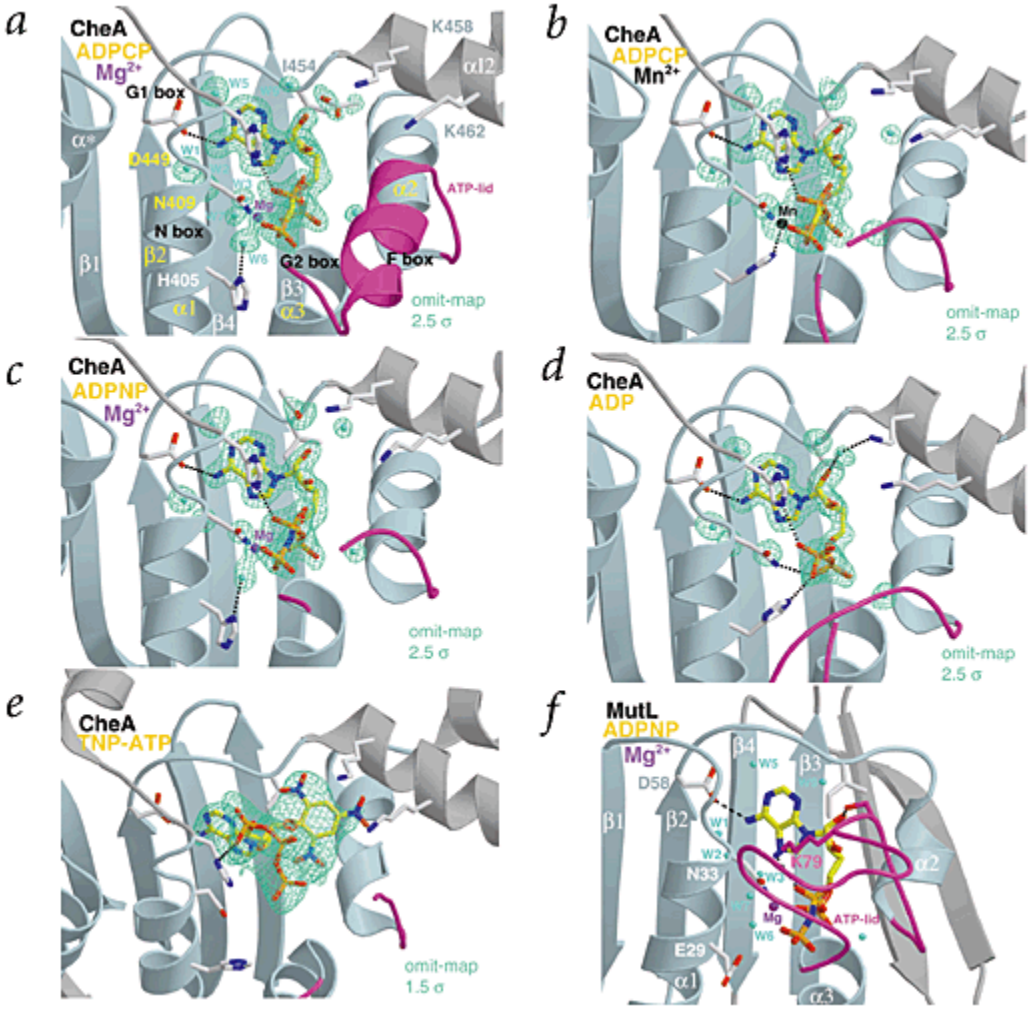
a
CheA
ADPCP
Mg2+
G1 box
K458
I454
α12
K462
D449
N409
N box
β2
H405
α1
β4
G2 box
F box
ATP-lid
α2
β3
α3
omit-map
2.5 σ
b
CheA
ADPCP
Mn2+
Mn
omit-map
2.5 σ
c
CheA
ADPNP
Mg2+
omit-map
2.5 σ
d
CheA
ADP
omit-map
2.5 σ
e
CheA
TNP-ATP
omit-map
1.5 σ
f
MutL
ADPNP
Mg2+
D58
β1
β2
β3
β4
N33
K79
α2
α3
E29
α1
ATP-lid

Figure 10: The CheA kinase domain forms a concave groove for binding to P1

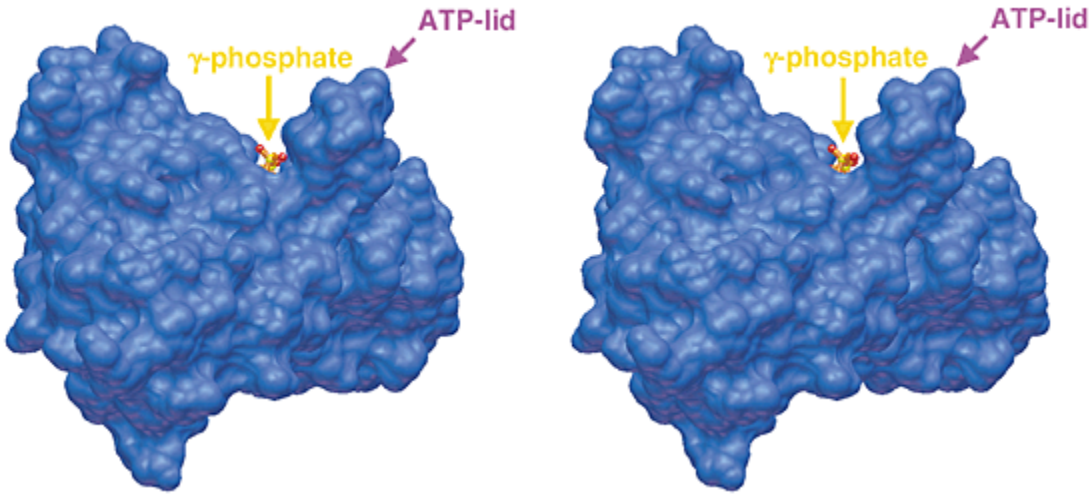
ATP-lid
γ-phosphate
ATP-lid
γ-phosphate

Figure 11: Sequence similarity between PHKs and the GHL family of ATPases

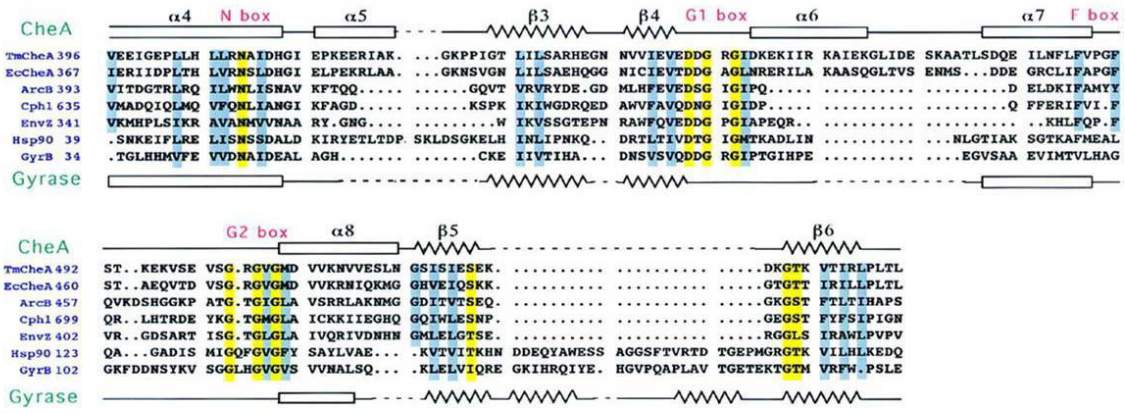
CheA
α4 N box α5 β3 β4 G1 box α6 α7 F box
TmCheA 396 VEEIGEPLLH LLRNAIDHGI EPKEERIAK. ...GKPPIGT LILSARHEGN NVVIEVEDDG RGIDKEKIIR KAIEKGLIDE SKAATLSDQE ILNFLFVPGF
EcCheA 367 IERIIDPLTH LVRNSLDHGI ELPEKRLAA. ...GKNSVGN LILSAEHQGG NICIEVTDDG AGLNRERILA KAASQGLTVS ENMS...DDE GRCLIFAPGF
ArcB 393 VITDGTRLRQ ILWNLISNAV KFTQQ..... ......GQVT VRVRYDE.GD MLHFEVEDSG IGIPQ..... .....D ELDKIFAMYY
Cph1 635 VMADQIQLMQ VFQNLIANGI KFAGD..... ......KSPK IKIWGDRQED AWVFAVQDNG IGIDP..... .....Q FFERIFVI.F
EnvZ 341 VKMHPLSIKR AVANMVVNAA RY.GNG.... .....W IKVSSGTEPN RAWFQVEDDG PGIAPEQR.. ....KHLFQP.F
Hsp90 39 .SNKEIFLRE LISNSSDALD KIRYETLTDP SKLDSGKELH INLIPNKQ.. DRTLTIVDTG IGMTKADLIN ....NLGTIAK SGTKAFMEAL
GyrB 34 .TGLHHMVFE VVDNAIDEAL AGH..... .....CKE IIVTIHA... DNSVSVQDDG RGIPTGIHPE ....EGVSAA EVIMTVLHAG
Gyrase
G2 box α8 β5 β6
CheA
TmCheA 492 ST..KEKVSE VSG.RGVGMD VVKNVVESLN GSISIESEK. ....DKGTK VTIRLPLTL
EcCheA 460 ST..AEQVTD VSG.RGVGMD VVKRNIQKMG GHVEIQSKK. ....GTGTT IRILLPLTL
ArcB 457 QVKDSHGGKP ATG.TGIGLA VSRRLAKNMG GDITVTSEQ. ....GKGST FTLTIHAPS
Cph1 699 QR..LHTRDE YKG.TGMGLA ICKKIIEGHQ GQIWLESNP. ....GEGST FYFSIPIGN
EnvZ 402 VR..GDSART ISG.TGLGLA IVQRIVDNHN GMLELGTSE. ....RGGLS IRAWLPVPV
Hsp90 123 QA...GADIS MIGQFGVGFY SAYLVAE... .KVTVITKHN DDEQYAWESS AGGSFTVRTD TGEPMGRGTK VILHLKEDQ
GyrB 102 GKFDDNSYKV SGGLHGVGVS VVNALSQ... .KLELVIQRE GKIHRQIYE. HGVPQAPLAV TGETEKTGTM VRFW.PSLE
Gyrase

REFERENCES

1. Stock, A.M., V.L. Robinson, and P.N. Goudreau, *Two-component signal transduction.* Annu. Rev. Biochem., 2000. **69**: p. 183-215.

2. Parkinson, J.S., and Kofoid, E.C., *Communication modules in bacterial signaling proteins.* Annu. Rev. Genet., 1992. **26**: p. 71-112.

3. Inouye, M. and R. Dutta, eds. *Histidine Kinases in Signal Transduction*. 2003, Academic Press. 520.

4. Chang, C., Kwok, S.F., Bleecker, A.B., and Meyerowitz, E.M., *Arabidopsis ethylene-response gene ETR1: similarity of product to two-component regulators.* Science, 1993. **262**: p. 539-544.

5. Ota, I.M. and A. Varshavsky, *A Yeast Protein Similar to Bacterial Two-Component Regulators.* Science, 1993. **262**(5133): p. 566-569.

6. Alex, L.A., K.A. Borkovich, and M.I. Simon, *Hyphal development in Neurospora crassa: Involvement of a two- component histidine kinase.* Proceedings of the National Academy of Sciences of the United States of America, 1996. **93**(8): p. 3416-3421.

7. Maeda, T., S.M. Wurglermurphy, and H. Saito, *A 2-Component System That Regulates an Osmosensing Map Kinase Cascade in Yeast.* Nature, 1994. **369**(6477): p. 242-245.

8. Parkinson, J.S. and E.C. Kofoid, *Communication modules in bacterial signaling proteins.* Annu. Rev. Genet., 1992. **26**: p. 71-112.

9. Mizuno, T., *Compilation of All Genes Encoding Two-component Phosphotransfer Signal Transducers in the Genome of Escherichia coli.* DNA Research, 1997. **4**: p. 161-168.

10. Fabret, C., V.A. Feher, and J.A. Hoch, *Two-component signal transduction in Bacillus subtilis: How one organism sees its world.* Journal of Bacteriology, 1999. **181**(7): p. 1975-1983.

11. Mizuno, T., *His-Asp phosphotransfer signal transduction.* Journal of Biochemistry, 1998. **123**(4): p. 555-563.

12. Nelson, K.E., et al., *Evidence for lateral gene transfer between Archaea and Bacteria from genome sequence of Thermotoga maritima.* Nature, 1999. **399**(6734): p. 323-329.

13. Alex, L.A., and Simon, M.I., *Protein histidine kinases and signal transduction in prokaryotes and eukaryotes.* Trends Genet . 1994. **10**: p. 133-138.

14. Swanson, R.V., Alex, L.A., and Simon, M.I., *Histidine and aspartate phosphorylation: two-component systems and the limits of homology.* Trends Biochem. Sci., 1994. **19**: p. 485-490.

15. Usher, K.C., et al., *Crystal structures of CheY from Thermotoga maritima do not support conventional explanations for the structural basis of enhanced thermostability.* Protein Science, 1998. **7**(2): p. 403-412.

16. Lukat, G.S., et al., *Phosphorylation of Bacterial Response Regulator Proteins by Low-Molecular-Weight Phospho-Donors.* Proceedings of the National Academy of Sciences of the United States of America, 1992. **89**(2): p. 718-722.

17. Volz, K. and P. Matsumura, *Crystal Structure of Escherichia coli CheY Refined at 1.7A Resolution.* Journal of Biological Chemistry, 1991. **266**(23): p. 15511-15519.

18. Stock, A.M., et al., *Three Dimensional Structure of CheY, the Response Regulator of Bacterial Chemotaxis.* Nature, 1989. **337**(6209): p. 745-749.

19. Lukat, G.S., et al., *Phosphorylation of Bacterial Response Regulator Proteins by Low-Molecular-Weight Phospho-Donors.* Proc. Natl. Acad. Sci. U.S.A., 1992. **89**(2): p. 718-722.

20. Ishige, K., et al., *A Novel Device of Bacterial Signal Transducers.* Embo Journal, 1994. **13**(21): p. 5195-5202.

21. Posas, F., et al., *Yeast HOG1 MAP kinase cascade is regulated by a multistep phosphorelay mechanism in the SLN1-YPD1-SSK1 "two-component" osmosensor.* Cell, 1996. **86**(6): p. 865-875.

22. Berg, H.C., *Bacterial Behavior.* Nature, 1975. **254**(5499): p. 389-392.

23. Larsen, S.H., et al., *Change in Direction of Flagellar Rotation Is Basis of Chemotactic Response in Escherichia coli.* Nature, 1974. **249**(5452): p. 74-77.

24. Berg, H.C. and D.A. Brown, *Chemotaxis in Escherichia coli Analyzed by Three Dimensional Tracking.* Nature, 1972. **239**(5374): p. 500-&.

25. Macnab, R.M. and D.E. Koshland, *Gradient-Sensing Mechanism in Bacterial Chemotaxis.* Proceedings of the National Academy of Sciences of the United States of America, 1972. **69**(9): p. 2509-&.

26. Tsang, N., R. Macnab, and D.E. Koshland, *Common Mechanism for Repellents and Attractants in Bacterial Chemotaxis.* Science, 1973. **181**(4094): p. 60-63.

27. Li, G.Y. and R.M. Weis, *Covalent modification regulates ligand binding to receptor complexes in the chemosensory system of Escherichia coli.* Cell, 2000. **100**(3): p. 357-365.

28. Maddock, J.R. and L. Shapiro, *Polar Location of the Chemoreceptor Complex in the Escherichia coli Cell.* Science, 1993. **259**(5102): p. 1717-1723.

29. Borkovich, K.A. and M.I. Simon, *The Dynamics of Protein-Phosphorylation in Bacterial Chemotaxis.* Cell, 1990. **63**(6): p. 1339-1348.

30. Hess, J.F., Bourret, R.B., & Simon, M.I., *Histidine phosphorylation and phosphoryl group transfer in bacterial chemotaxis.* Nature, 1988. **336**: p. 139-143.

31. Welch, M., et al., *Phosphorylation-Dependent Binding of a Signal Molecule to the Flagellar Switch of Bacteria.* Proceedings of the National Academy of Sciences of the United States of America, 1993. **90**(19): p. 8787-8791.

32. Borkovich, K.A., and Simon, M.I., *Coupling of receptor function to phosphate-transfer reactions in bacterial chemotaxis.* Methods Enzymol., 1991. **200**: p. 205-214.

33. Li, J.Y., et al., *The Response Regulators CheB and CheY Exhibit Competitive Binding to the Kinase CheA.* Biochemistry, 1995. **34**(45): p. 14626-14636.

34. Bourret, R.B., Davagnino, J., and Simon, M.I., *The carboxy-terminal portion of the CheA kinase mediates regulation of autophosphorylation by transducer and CheW.* J. Bacteriol., 1993. **175**: p. 2097-2101.

35. Morrison, T.N., and Parkinson, J.S., *A fragment liberated from the E. coli kinase that blocks stimulatory, but not inhibitory, chemoreceptor signaling.* J. Bacteriol., 1997. **179**: p. 5543-5550.

36. Swanson, R.V., Schuster, S.C., and Simon, M.I., *Expression of CheA fragments which define domains encoding kinase, phosphotransfer and CheY binding activities.* Biochemistry, 1993. **32**: p. 7623-7629.

37. Zhou, H., Lowry, D.F., Swanson, R.V., Simon, M.I., Dahlquist, F.W., *NMR studies of the phosphotransfer domain of the histidine kinase CheA from Escherichia coli: assignments, secondary structure, general fold, and backbone dynamics.* Biochemistry, 1995. **34**: p. 13858-13870.

38. Mourey, L., Da Re, S., Pedelacq, J.D., Tolstykh, T., Faurie, C., Guillet, V., Stock, J.B., and Samama, J.P., *Crystal structure of the CheA histidine phosphotransfer domain that mediates response regulator phosphorylation in bacterial chemotaxis.* J. Biol. Chem., 2001.

39. McEvoy, M.M., et al., *Nuclear Magnetic Resonance Assignments and Global Fold of a CheY Binding Domain in CheA, the Chemotaxis Specific Kinase of Escherichia coli.* Biochemistry, 1995. **34**(42): p. 13871-13880.

40. Welch, M., Chinardet, N., Mourey, L., Birck, C., and Samama, J. P., *Structure of the CheY-binding domain of histidine kinase CheA in complex with CheY.* Nat Struct Biol., 1998. **5**: p. 25-29.

41. McEvoy, M.M., et al., *Structure and dynamics of a CheY-binding domain of the chemotaxis kinase CheA determined by nuclear magnetic resonance spectroscopy.* Biochemistry, 1996. **35**(18): p. 5633-5640.

42. McEvoy, M.M., Hausrath, A. C., Randolph, G. B., Remington, S. J., and Dahlquist, F. W., *Two binding modes reveal flexibility in kinase/response*

regulator interactions in the bacterial chemotaxis pathway. Proc. Natl. Acad. Sci. U.S.A., 1998. **95**: p. 7333-7338.

43. Bilwes, A.M., Alex, L.A., Crane, B.R., and Simon, M.I., *Structure of CheA, a signal-transducing histidine kinase.* Cell, 1999. **96**: p. 131-141.

44. Bilwes, A.M., Quezada, C.M., Croal, L.R., Crane, B.R., and Simon, M.I., *Nucleotide binding by the histidine kinase CheA.* Nature Struct. Biol., 2001. **8**: p. 353-360.

45. Boukhvalova, M., R. VanBruggen, and R.C. Stewart, *CheA kinase and chemoreceptor interaction surfaces on CheW.* Journal of Biological Chemistry, 2002. **277**(26): p. 23596-23603.

46. Boukhvalova, M.S., F.W. Dahlquist, and R.C. Stewart, *CheW binding interactions with CheA and Tar - Importance for chemotaxis signaling in Escherichia coli.* Journal of Biological Chemistry, 2002. **277**(25): p. 22251-22259.

47. Ban, C., Junop, M., and Yang, W., *Transformation of MutL by ATP binding and hydrolysis: a switch in DNA mismatch repair.* Cell, 1999. **97**: p. 85-97.

48. Wigley, D.B., Davies, G.J., Dodson E.J., Maxwell, A. and Dodson, G., *Crystal structure of an N-terminal fragment of the DNA gyrase B protein.* Nature, 1991. **351**: p. 624-629.

49. Stebbins, C.E., Russo, A.A., Schneider, C., Rosen, N., Hartl, F.U., and Pavletich, N.P., *Crystal structure of an Hsp90-geldamycin complex: targeting of a protein chaperone by an antitumor agent.* Cell, 1997. **89**: p. 239-250.

50. Ban, C., and Yang, W., *Crystal structure and ATPase activity of MutL: implications for DNA repair and mutagenesis.* Cell, 1998. **95**: p. 541-552.

51. Prodromou, C., Roe, S.M., O'Brien, R., Ladbury, J.E., Piper, P.W. and Pearl, L.H., *A molecular clamp in the crystal structure of the N-terminal domain of the yeast Hsp90 chaperone.* Cell, 1997. **90**: p. 65-75.

52. Obermann, W.M.J., Sondermann, H., Russo, A.A., Pavletich, N.P., and Hartl, F.U., *In vivo function of Hsp90 is dependent on ATP binding and ATP hydrolysis.* J. Cell Biol., 1998. **143**: p. 901-910.

53. Jackson, A.P., and Maxwell, A., *Identifying the catalytic residue of the ATPase reaction of DNA gyrase.* Proc. Natl. Acad. Sci. USA, 1993. **90**: p. 11232-11236.

54. Stewart, R.C., VanBruggen, R., Ellefson, D.D., and Wolfe, A.J., *TNP-ATP and TNP-ADP as probes of the nucleotide binding site of CheA, the histidine protein kinase in the chemotaxis signal transduction pathway of Escherichia Coli.* Biochemistry, 1998. **37**: p. 12269-12279.

55. Hirschman, A., et al., *Active Site Mutations in CheA, the Signal-Transducing Protein Kinase of the Chemotaxis System in Escherichia coli.* Biochemistry, 2001. **40**: p. 13876-13887.

56. Hess, J.F., Oosawa, K., Kaplan, N., and Simon, M.I., *Phosphorylation of three proteins in the signaling pathway of bacterial chemotaxis.* Cell, 1988. **53**: p. 79-87.

57. Zhou, H.D., F. W., *Phosphotransfer site of the chemotaxis-specific protein kinase CheA as revealed by NMR.* Biochemitry, 1997. **36**: p. 699-710.

58. Zhou, H.J., et al., *Phosphotransfer and CheY-binding domains of the histidine autokinase CheA are joined by a flexible linker.* Biochemistry, 1996. **35**(2): p. 433-443.

Chapter 2

The crystal structure of the CheA histidine phosphotransfer domain from **Thermotoga maritima**

CheA plays a central role in the bacterial chemotaxis signal transduction pathway that controls bacterial motor behavior in response to environmental stimuli. The focus of these studies is on the CheA histidine phosphotransfer domain, P1. It mediates the transfer of the γ-phosphoryl group from ATP to the response regulators CheY and CheB. The global fold of the P1 domain has been determined by NMR [1] and by crystallography to a resolution of 2.1Å [2]. It consists of five alpha helices, including an antiparallel four helix bundle, flanked by a helix at its C-terminus [1, 2].

Crystallographic and NMR studies suggested the P1 phospho-accepting histidine forms a hydrogen bond to a neighboring glutamate residue [2, 3]. Furthermore, the phospho-accepting histidine, His48 in *E. coli*, possesses an altered pKa of 7.8 at 30°C; approximately one pH unit higher than a normal solvent accessible histidine [3]. Learning more about the detailed hydrogen bonding interactions with the phospho-accepting histidine and their effects on histidine reactivity prompted an attempt to improve the resolution of the CheA histidine phosphotransfer domain crystal structure.

The 0.98 Å resolution structure of helices A-D of the CheA histidine phosphotransfer domain from *T. maritima* is reported in this chapter. Structural issues concerning the phosphotransfer mechanism of the histidine kinase CheA, which are better assessed due to the improvement in accuracy of the atomic coordinates, are discussed. The phospho-accepting histidine, His45, participates in an elaborate hydrogen bond network including three other residues. Insight into the dynamic properties of the CheA histidine phosphotransfer domain is also obtained.

MATERIALS AND METHODS

Protein Cloning, Expression, and Purification

T. maritima Δ289 (residues 290-671), domain P1 (residues 4-133), and a fragment of domain P1 termed $P1_{short}$ (residues 4-105) were subcloned in the vector pET28(a) (Novagen). The plasmid was transformed into *E. coli* strain BL21(DE3) (Novagen) and protein expressed in 2L TB cultures. Protein purification was achieved by affinity chromatography on Nickel-NTA beads (Qiagen), followed by an overnight digestion of the His_6 tag at 4°C by thrombin. The protein was further purified by gel filtration on a superdex 75 or 200 column (Pharmacia) using a buffer composed of 50 mM Tris(pH 7.5), 150 mM NaCl and 2 mM DTT. Centrifugation with an Amicon centriprep concentrator yielded the concentrated protein. A cysteine mutant, T81C, for derivatization with heavy atoms was generated using Quickchange mutagenesis (Stratagene). The selenomethionine protein was expressed using the *E. coli* methionine auxotroph strain B834(DE3) (Novagen). It was purified in the manner described above.

Crystallization

The hanging drop method of crystallization produced crystals that grew overnight at room temperature. Crystals were obtained by mixing 2 μL of the reservoir solution (28% PEG 8K, 0.1M NaAc pH 4.5, 0.2M AmAc) with 2 μL of 7-15 mg/ml $P1_{short}$. Crystals were briefly soaked in a cryogenic solution (38% PEG 8K, 0.1M NaAc pH 4.5, 0.2M AmAc) and then flash cooled in liquid nitrogen. The crystal belongs to the orthorhombic space group $P222_1$ and has unit cell dimensions of a=27.38Å, b=37.42Å,

and c=87.54Å. The asymmetric unit contains one molecule. Orthorhombic crystals of the native and mutant protein, T81C, were soaked in saturated EMP (ethylmercuric phosphate) for a week and in a 1/100 saturated solution of phenylmercury acetate for two days.

Data Collection

High resolution data to 1.1 Å were initially collected on beamline 9-2 at the Stanford Synchrotron Radiation Laboratory (SSRL) using an ADSC Quantum-4 CCD detector and a wavelength of 1.0332 Å. A low resolution dataset of an isomorphous crystal was collected at a home x-ray source on an R-AXIS 2 phosphoimaging plate detector mounted on a rotating-anode generator with a wavelength of 1.54 Å. The F1 beamline at CHESS, possessing a Dual ADSC Quantum-4 CCD and a wavelength of 0.9Å was used to collect the high resolution dataset described in this paper. The crystal diffracted to 0.98 Å. Derivative datasets were collected at the home source with the R-AXIS 4 mounted on a rotating anode x-ray generator using a wavelength of 1.54 Å. The F2 line at CHESS was used to perform a multiwavelength anomalous dispersion experiment on a single crystal of the selenomethionine protein using an ADSC Quantum-210 CCD detector and the following wavelengths 0.9795 (inflection), 0.9791 (peak), and 0.96112 (high remote). The A1 line at CHESS was tuned to the Hg inflection point to accentuate the anomalous signal from one of the mercury soaked crystals. Data were processed, scaled, and reduced using the DENZO/SCALEPACK suite of programs [4]. A total of 5% of the total reflections were randomly selected to provide a test set for the calculation of R_{free} [5].

MIR and MAD Phasing

The phases for the native P1 crystal were determined by a combination of MIR and MAD. The primary mercury site was at the only cysteine in P1. This position was determined by Patterson map analysis [6]. A second mercury derivative came from a site-directed mutant (T81C) designed to place a cysteine on the protein surface. Secondary sites were determined from difference Fouriers using phases derived from the primary site. MIR data from two mercury derivatives were calculated with the program PHASES[7]. The isomorphous phasing figure of merit was 0.58 to 2.5Å.

The X-ray flourescence spectrum of the selenomethionine derivative was measured directly from the crystal on the F2 beam line at CHESS. Selection of the wavelengths of the peak and the inflection point for the multiple anomalous dispersion (MAD) data collection was made on the basis of the f' and f'' anomalous scattering factors, as determined by the program CHOOCH. The peak and inflection point were determined to be at 0.9791Å and 0.9795Å, respectively. The high energy remote peak was chosen at 0.9611Å. Datasets at each wavelength were collected to a resolution of at least 2.8Å and then reduced with denzo and scaled with scalepack [4]. Selenium sites were positioned by difference Fouriers using the mercury MIR phases. MAD data was phased in MADPHSREF [8] and a figure of merit of 0.48 to 2.8Å was obtained. MIR and MAD were combined probabilistically with MADPHSREF to give an overall figure of merit of 0.63 to 2.5Å. Phases were improved by solvent flattening, histogram matching, and the application of Sayre's equation as implemented in DM [9].

Structure Determination and Model Refinement

Once an interpretable electron density map was obtained, the model was built manually using XFIT [6]. Methionine positions were identified from Bivjoet difference Fourier maps of seleno-methionine modified crystals phased with the isomorphous mercury phases. Initial refinement was performed using the Crystallography and NMR System (CNS) [10]. The starting model was first optimized using rigid body refinement followed by least squares minimization and unrestrained B-factor refinement. The molecular graphics program Xfit was used to adjust the model during the rebuilding cycles using both 2Fo-Fc σ_a-weighted and Fo-Fc σ_a-weighted maps [6]. The initial solvent water model was built using automated water picking in CNS [10].

The final CNS model was isotropically refined in SHELX97 employing conjugate gradient least-squares minimization [11]. Inspection of omit maps revealed the presence of alternate conformations in discrete residues (Thr14, Glu16, Gln19, Leu21, Met51, Met55, Ser58, Asp72, Glu78) and in contiguous regions of helices A and D (residues 22-32 and 82-105). Individual occupancies were refined for each of the residues located in the extended regions of disorder and found to be approximately the same. These sections exhibiting conformational heterogeneity were therefore assigned a common occupancy factor. The refinement of individual anisotropic displacement parameters (ADPs) for all atoms resulted in an 8% drop in R_{free}. The final R_{work} and R_{free} were determined to be 0.1702% and 0.2049%. Inclusion of all data yielded an R-factor of 0.1714%. The final SHELXL model is comprised of 105/105 residues and 207 water molecules.

Although the final model is consistent with the electron density and expected stereochemistry, the R factors are higher than expected for a 0.98Å structure. A possible

explanation is that current methods of refinement are not able to accurately model the extent of disorder observed in this protein crystal. The extended region of conformational heterogeneity observed in helices A and D is a result of the displacement of the entire main chain. Although techniques such as translation-libration-screw (TLS) and multiconformer refinement have previously been used to model ambiguous electron disorder, they are not as effective at modeling areas that exhibit spatially well-resolved disorder [12]. P1 and its solvent may well be sampling a larger number of conformational substates than we have been able to model, thus yielding a higher than expected R_{work} and R_{free}.

K_m determination

Initial velocities of P1 and $P1_{short}$ phosphorylation by Δ289 (2 μM) were measured in 50 mM Tris pH 8.5, 50 mM KCl, and 2 mM DTT at 50°C over a range of concentrations. Reactions were initiated upon addition of [γ-^{32}P] ATP. At specific time intervals, aliquots were quenched with 2X sodium dodecyl sulfate (SDS) electrophoresis buffer containing 25 mM ethylenediaminetetra acetic acid (EDTA). Samples were then electrophoresed on 18% Criterion Tris-HCl gels (Biorad) using a Criterion Dodeca cell. Gels were dried under vacuum and phosphorylation quantified using a Storm phosphoimager (Molecular Dynamics). The apparent K_m value was obtained by plotting the inverse of P1 or $P1_{short}$ concentration versus the inverse of the initial velocities.

Thermal Denaturation

CD spectra were recorded with an AVIV (Lakewood, NJ) 62A DS spectrometer equipped with a Peltier-type temperature control system and using a 0.1cm quartz cuvette (Wilmad). Protein concentrations were determined by UV spectrophotometry [13]. Samples were at a concentration of 30 to 40 μM in 20 mM sodium phosphate buffer at pH 8.0. Thermal denaturation was monitored at 222 nm. Data were collected every 1°C with an equilibration time of 6 minutes, an averaging time of 10 s and a bandwidth of 1.5 nm. The melting temperature, Tm, was extracted from a Boltzmann fit to the data using the program Kaleidagraph (Synergy Software).

RESULTS

X-ray structure of the CheA histidine phosphotransfer domain at 0.98 Å resolution

We report the crystal structure of the CheA phosphotransfer domain at 0.98Å (Figure1a). The model consists of helices A-D, a four-helix bundle that is characteristic of histidine phosphotransfer (HPt) domains [2, 14-16]. Hereafter, this protein fragment will be referred to as $P1_{short}$. The protein crystallized in the orthorhombic space group $P222_1$, with unit-cell parameters a=27.38Å, b=37.42Å, and c=87.54Å. The structure of the native crystal was solved by the MIR method with Hg derivatives and the MAD method with a seleno-methionine derivative. The final model consisted of residues 4-105, including three N-terminal residues corresponding to the residual histidine tag. Crystallographic refinement converged to a final R_{work} of 17% and an R_{free} of 20%.

Details of the structural determination and crystallographic refinement can be found in Table 1 .

Figure 1b demonstrates the typical electron density observed in the protein's ordered regions. The $2F_{obs} - F_{calc}$ σ_A- weighted electron density map is continuous between covalently bonded atoms at lower contour levels, and discrete at higher contour levels showing density for individual atoms. Calculation of the Ramachandran plot [17] by the program PROCHECK [18] revealed that 97.6% of the residues in the final model are found in the most favored regions and the remaining 2.4% in additionally allowed regions (Table 1).

P1 helices A-D form an anti-parallel four helix bundle

The present atomic resolution structure shows the same overall fold as observed in the low resolution *E. coli* NMR structure and the *Salmonella* 2.1Å crystal structure [1, 2]. The α-helical structure consists of four α-helices ranging in length from 18 to 28 residues, as calculated by the program PROMOTIF [19]. The autophosphorylation site, His45, was also observed to be solvent exposed and located on Helix B [1, 2]. Nonetheless, an atomic resolution structure is more accurate, providing a wealth of detailed information on hydrogen bonding networks and a molecule's inherent flexibility.

Dynamic features of P1$_{short}$

In addition to improving the accuracy of the atomic coordinates in the histidine phosphotransfer domain active site, extensive conformational heterogeneity was observed throughout the molecule. Approximately 45% of P1 residues exist in an alternate

conformation, a substantially higher percentage than the 6-24% observed in other proteins of comparable resolution [12, 20]. A number of side chains (Thr14, Glu16, Gln19, Leu21, Met51, Met55, Ser58, Asp72, and Glu78) throughout the model reveal the presence of alternate conformations.

Interestingly, two distinct main chain conformations are observed for the terminal portion of helix A (residues 22-32) and the entire helix D (residues 82-105) (Figure 2a). Only residues 31, 32, and 82 are located in connecting loops. The quality of the electron density map of the extended disordered regions is in general poorer than the rest of the molecule, providing evidence of appreciable disorder for every residue in this region. Side chain density is not as well defined as that for the main chain.

Electron density from omit maps provides clear evidence that the mainchain exists in an alternate conformation (Figure 2b-2c). This displacement is correlated. The ranges of conformer separation between equivalent backbone atoms in helix A range between 1.27Å and 1.85Å. The occupancies of these atoms are 0.52 and 0.48. Helix D displays an incremental increase in mainchain separation in going from its N- to C-terminus. The ranges of distances between equivalent atoms are 0.84Å to 1.07Å for residues 82-87; 1.11Å to 1.28Å for residues 88-91; 1.21Å to 1.43Å for residues 92-98; and 1.25Å to 1.73Å for residues 99-103. The occupancies of helix D are 0.53 and 0.48, respectively. Although two discrete conformations for these helices are resolved, additional conformers that we are not able to accurately model with current refinement techniques may exist.

The intrahelical hydrogen bonds of each conformer are maintained as well as side chain interactions. The disordered region of helix A (residues 22-32) shares a

hydrophobic interface with residues 81-93 of helix D. Although the side chains of these residues exist in two conformations, the interhelical packing is not disturbed. The same is observed with the hydrophobic residues of helix D that face helix C.

$P1_{short}$ exhibits wild-type activity and stability

Highly diffracting crystals of the CheA histidine phosphotransfer domain were obtained by truncating the C-terminal helix of P1, helix E. Prior studies indicated that helix E was not critical to the phosphorylation reaction and had little interaction with the other helices of the phosphotransfer domain [1, 21, 22]. In order to ascertain that removal of the terminal helix did not affect phosphorylation activity, we compared the Km value of P1 (helices A-E) and $P1_{short}$(helices A-D) for Δ289, a CheA fragment consisting of the dimerization, kinase and regulatory domains was monitored as a function of temperature. Although it was not possible to measure the initial velocities of either protein at saturating conditions, their respective K_m values were estimated to be 270μM and 230μM (Table 4). Therefore, phosphorylation activity was not altered by the removal of helix E.

Circular dichroism was used to monitor the thermal denaturation of P1 and $P1_{short}$. The melting temperature, T_m, was 98ºC and 99ºC, respectively (Table 3). The parameters of the two protein fragments show good correlation to one another. Hence, we conclude that truncation of the terminal helix is not affecting the protein's structure or activity.

The active site architecture

The high resolution structure of the CheA histidine phosphotransfer domain has afforded the unique opportunity to accurately determine the geometric arrangement of residues surrounding the active site histidine. An important issue that can be addressed at a resolution of 0.98Å is the clear distinction between carbon, nitrogen, and oxygen.

Based on the volume density observed at higher contour levels, the position of the His45 side chain nitrogen atoms could be indisputably assigned (Figure 3). It was first predicted [23] and later suggested that the hydrogen bonding partner of the phospho-accepting histidine was Glu67 [2]. The distance between the nitrogen atom ($N^{\delta 1}$) of His45 and the oxygen atom ($O^{\delta 2}$) of Glu67 is 2.70Å (Figure 4). The site of phosphorylation, the $N^{\varepsilon 2}$ atom of His 45, is exposed to solvent and not within the hydrogen bonding distance of any atoms. We have thus unambiguously identified the hydrogen bonding partner of His45.

Further information about the active site environment was extracted by removing the stereochemical restraints on Glu67 during refinement. In general, neutral carboxyls have bond lengths around 1.21Å and 1.32Å for the C=O and C-OH bonds, respectively. On the other hand, ionized carboxyls have identical C-O bond lengths due to electron resonance. The differences in the carboxyl bond lengths were also calculated to deduce the protonation state [24]. Using unrestrained positional refinement, the C-O bond lengths of Glu67 were calculated to be 1.23Å and 1.24Å. In addition, the electron density of the carboxyl moiety at higher contour levels is equally distributed exhibiting properties of delocalized charge (Figure 3). Together, these data reveal that Glu67 exists in an ionized state, allowing it to act as a hydrogen bond acceptor. The bond lengths of histidines 45 and 64 were also calculated. The distances between the carbon nitrogen

bonds ($C^{\varepsilon 1}$ and $N^{\varepsilon 2}$) and ($C^{\varepsilon 1}$ and $N^{\delta 1}$) are nearly equivalent, as expected for an imidazole side chain that is undergoing rapid tautomerization [25].

The P1 active site exhibits a hydrogen bond network between four largely conserved residues: His45, Glu67, Lys48, and His64 (Figure 4). Glu67 acts as the hydrogen bond acceptor of the phospho-accepting His45, and neighboring atoms Lys48 and His64. Interestingly, these four residues only interact with one another, forming hydrogen bonds with no other residues (Table 4).

His45 exhibits an altered pKa

Experiments measuring the pH dependence of P1 phosphorylation by Δ289 revealed the optimal phosphorylation activity to be at approximately pH 8.5, as observed in *E.coli* CheA [26]. The experimentally determined pH profile of the *T. maritima* P1 domain was overlaid with the calculated fraction of histidine molecules that would be found in the deprotonated state when using a pKa value of 6.9, the pKa value determined for the *T. maritima* phospho-accepting histidine at 50°C; and using a pKa value of 5.9, the estimated average pKa value of a solvent exposed histidine at 50°C (this value was determined in Chapter 3). The histidine pKa value is expected to be lower at 50°C than the previously measured value at 30°C[3] due to the dependence of temperature on pKa.

Figures 4a-b reveal that the pH activity profile of the phosphotransfer domain is consistent with the phospho-accepting histidine having a higher pKa than that found for an average solvent exposed histidine. Using a pKa of 5.9, close to 80% of the histidine molecules are calculated to exist in the deprotonated state at pH 6.5. Yet, only ~20% of maximal phosphorylation activity is observed *in vitro*. Conversely, approximately 30%

of the histidine molecules are expected to exist in the deprotonated state at pH6.5 using a pKa of 6.9, correlating closely to the experimentally determined value.

DISCUSSION

The CheA phosphotransfer domain, P1, of *T. maritima* consists of a four-helix bundle structure, which is common to the histidine phosphotransfer domains belonging to other two component systems, such as ArcB and Ypd1 [14-16, 27]. Protein backbone dynamic studies show that with the exception of the N- and C- terminal residues and some of the loop regions, the *E.coli* P1 domain forms a tight and compact structure with little flexibility both in helices and turns [1].

Despite the previously reported overall rigidity of P1 and other histidine phosphotransfer domains, multiple occupancies from various residues have been identified in the *T. maritima* P1 structure. In fact, two regions possessing extended disorder are observed in helices A and D. The unprecedented number of residues that exist in heterogeneous conformations suggests that there are likely more substates than we can model, including perhaps smaller scale fluctuations throughout the entire molecule. The dynamic properties that $P1_{short}$ exhibits may be important contributors to the domain's biological function. The molecule's flexibility could possibly facilitate conformational adjustments that may be required to bind the kinase domain.

Alternatively, the observed dynamic features could result from the removal of the terminal E helix. Crystallographic and NMR studies suggested that Helix E had minimal contact with the four N-terminal helices [1, 2]. Data presented in this paper revealed that

it does not contribute towards helix cluster stability or to the phosphorylation reaction (Table 3). Hydrogen exchange studies demonstrated that the five helices show different degrees of protection [1]. Helix D showed the strongest protection against solvent, suggesting it has extensive contacts with the other helices. If the truncation of helix E results in the destabilization of helix D, the extensive disorder found in helix D could be propagated to helix A. This is likely the case considering that the occupancies of the alternate conformations in these two helices are virtually identical.

The high resolution structure of P1 may reveal important principles of the structure and dynamics of histidine phosphotransfer domains. The same general protein fold appears to be utilized by prokaryotes and lower eukaryotes to undergo phosphotransfer reactions. The four-helix bundle motif that is characteristic of HPt domains is always flanked by other helices in the structures solved to date. It is tempting to speculate that the four-helix bundle core of the various HPt domains is stabilized by surrounding helices.

While the general fold of the P1 domain is conserved between the organisms, *E.coli, Salmonella* and *T. maritima*, the detailed interaction of residues surrounding the phospho-accepting histidine differs. In addition to the hydrogen bonding network that is observed between His45, Glu67, and Lys48 in the *Salmonella* structure [2], the *T. maritima* P1 structure revealed that His64 participates in the hydrogen bonding network as well.

At the higher resolution of 0.98Å, there is a dramatic increase in the quality and detail of the electron density map in comparison to that of a 2.1Å structure. The ambiguity in the geometry and architecture of the hydrogen bonding network caused by

crystal packing interactions in the *Salmonella* structure is clarified in this paper (Table 4). Residues involved in this hydrogen bonding network are important to CheA function. Site directed mutagenesis of Glu67 and Lys48 (Glu70 and Lys50 in *Salmonella*), diminish CheA auto-phosphorylation [2].

The phospho-accepting histidine was reported to exist in the unusual $N^{\delta 1}H$ tautomeric state [3]. We have been able to unambiguously confirm the existence of a hydrogen bond between the conserved glutamate, Glu67 in *T. maritima*, and the $N^{\delta 1}H$ position of the histidine. Glu67 exists in an ionized state, as observed by the delocalized electron density and C-O bond lengths. The results of the P1 pH profile (Figure 4) further support the existence of a perturbed pKa for the phospho-accepting histidine.

These findings have mechanistic implications. The crystal structure of the CheA kinase domain revealed that it does not resemble Ser/Thr or Tyr kinases [23, 28]. Instead, it is structurally similar to the GHL family of ATPases. Despite the striking topological and sequence similarities, some compelling differences exist between these two protein families. An essential glutamate of the GHL ATPases, presumed to be the general base involved in water activation for ATP hydrolysis, is missing from the CheA kinase domain P4 [29]. We propose that the conserved Glu67 completes the catalytic center observed in GyrB. The CheA P1 domain may therefore provide not just the nucleophile for phosphate transfer (His45), but also the activating glutamate (Glu67).

Bacterial chemotaxis represents one of the best biochemically and structurally characterized signal transduction pathways. The structures, or fragments, of all the identified players have been solved. A wealth of structural and biochemical data exists for CheA. With high resolution structures of the phosphotransfer domain (P1) and the

kinase domain (P4), there is a unique opportunity to identify the key determinants of activity in this protein family. These results will provide a solid structural basis for further understanding the phosphotransfer mechanism involved in bacterial chemotaxis and may provide critical insight for the development of novel antibiotic agents. In addition, the observed conformational heterogeneity provides evidence for protein dynamic motions, known to occur in solution, but rarely observed in crystal structures.

Table 1: Data collection and refinement statistics

	P1$_{short}$	*EMP*	*PMA*	*Hg-anom*	*Se6*
Data Collection Statistics					
Resolution (Å)	0.98	1.798	2.1	1.6	2.0
Wavelength (Å)	0.9	1.54	1.54	1.006	0.93
Total reflections	362996	63326	61390	76550	72990
Unique reflections	52070	8753	5742	12897	6586
Completeness (%)	98	97.2	99.6	93.3	99.1
	(88.2)	(90.5)	(98.1)	(96.5)	(98.8)
I/σ(I)	19.2		14.5	25.8	41.0
	(2)		(6.7)	(6.6)	(17.1)
Rsym(%)	0.063	0.039	0.067	0.064	0.032
	(0.33)	(0.10)	(0.19)	(0.21)	(0.047)
Mosaicity	0.356	0.601	0.578	0.406	0.345
Wilson B (Å^2)	11.354	23.856	27.129		
Refinement Statistics					
Resolution limits	15 – 0.98				
R_{work}[c]	0.17				
R_{free}[d]	0.20				
RMS deviations from ideal values					
Bond lengths (Å)	0.015				
Bond angles (°)	2.70				
Dihedral angles (°)	21.13				
Improper torsion angles (°)	2.17				
Ramachandran plot[e] residues in					
Most favored regions (%)	97.6				
Additional allowed regions(%)	2.4				
Generously allowed regions(%)	0.0				
Disallowed regions (%)	0.0				

[a] Numbers in parentheses correspond to values in the highest resolution shell

[b] $R_{sym} = (\Sigma_{hkl}\Sigma_i | I_i(hkl) - < I(hkl) > |)/(\Sigma_{hkl}\Sigma_i I(hkl))$

[c] $R_{work} = \Sigma(|F_{obs}| - |F_{calc}|)/\Sigma|F_{obs}|$

[d] R_{free} is the R-factor calculated for a 5% test set of reflections excluded from the refinement calculation

[e] As determined by PROCHECK [18]

Table 2: MIR and MAD phasing statistics

	Number of sites	Resolution	Phasing Power	Anomalous Ratio[a]	Dispersive Ratio[b]	Figure of merit
EMP	2	2.5	1.65			0.58
PMA	2	2.5	1.37			
Hg-anom	2	2.5	0.56			
Se6	6	2.5	1.05			
Inflection		2.8		0.021		
Peak		2.8		0.026	0.037	0.48
High remote		2.8		0.022	0.048	
Combined		2.5				0.63

[a]Anomalous ratio = rms$\big|\,|F^{+}|-|F^{-}|\,\big|$/rms F
[b]Dispersive ratio = rms$\big|\,|F_{\lambda 1}|-|F_{\lambda 2}|\,\big|$/rms F

Table 4: Comparison of kinetic and stability parameters between P1 and P1short

	Km(μM)	*Tm (°C)*
P1	270	99
$P1_{short}$	230	98

Table 5: Stereochemical parameters of conserved residues involved in the P1 hydrogen bonding network

Donor (D-H)	Acceptor	(D-A) distance	*DHA angle*
His45 $N^{\delta 1}$-H	Glu67 $O^{\varepsilon 1}$	2.70	*150.1*
Lys48 NZ-H	Glu67 $O^{\varepsilon 2}$	2.62	*135.07*
His64 $N^{\delta 1}$-H	Glu67 $O^{\varepsilon 2}$	2.78	146.9

Figure 1: Structure of the HPt domain of *T. maritima* CheA. (a) A ribbon representation of the P1 domain demonstrates the overall fold to be a four helix bundle. (b) The $2F_o$-F_c σ_A- weighted electron density map of 1.1Å data contoured at 2σ (green) and 4σ (purple).

1a.)

b.)

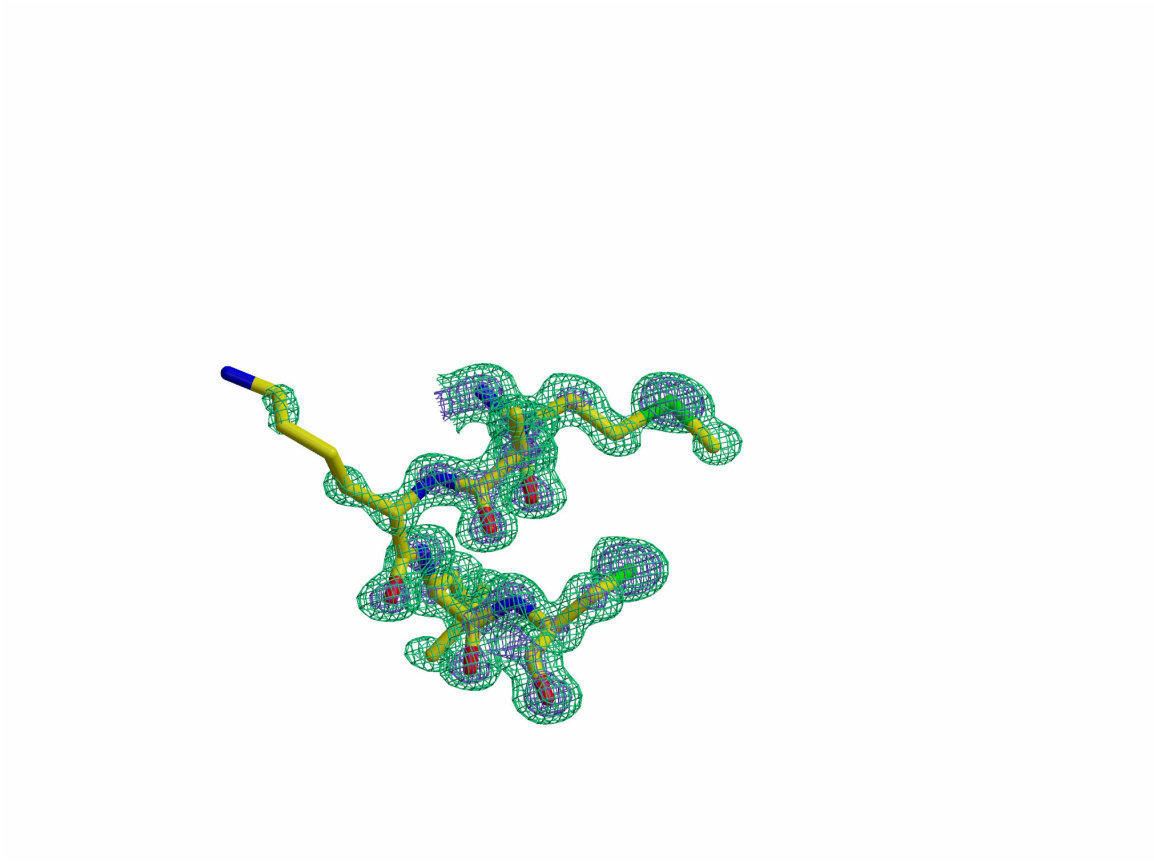

Figure 2: (a) The P1 mainchain exists in two conformations (b) Fo-Fc σ_A- weighted omit maps contoured at 2σ of a region exhibiting an alternate conformation

a.)

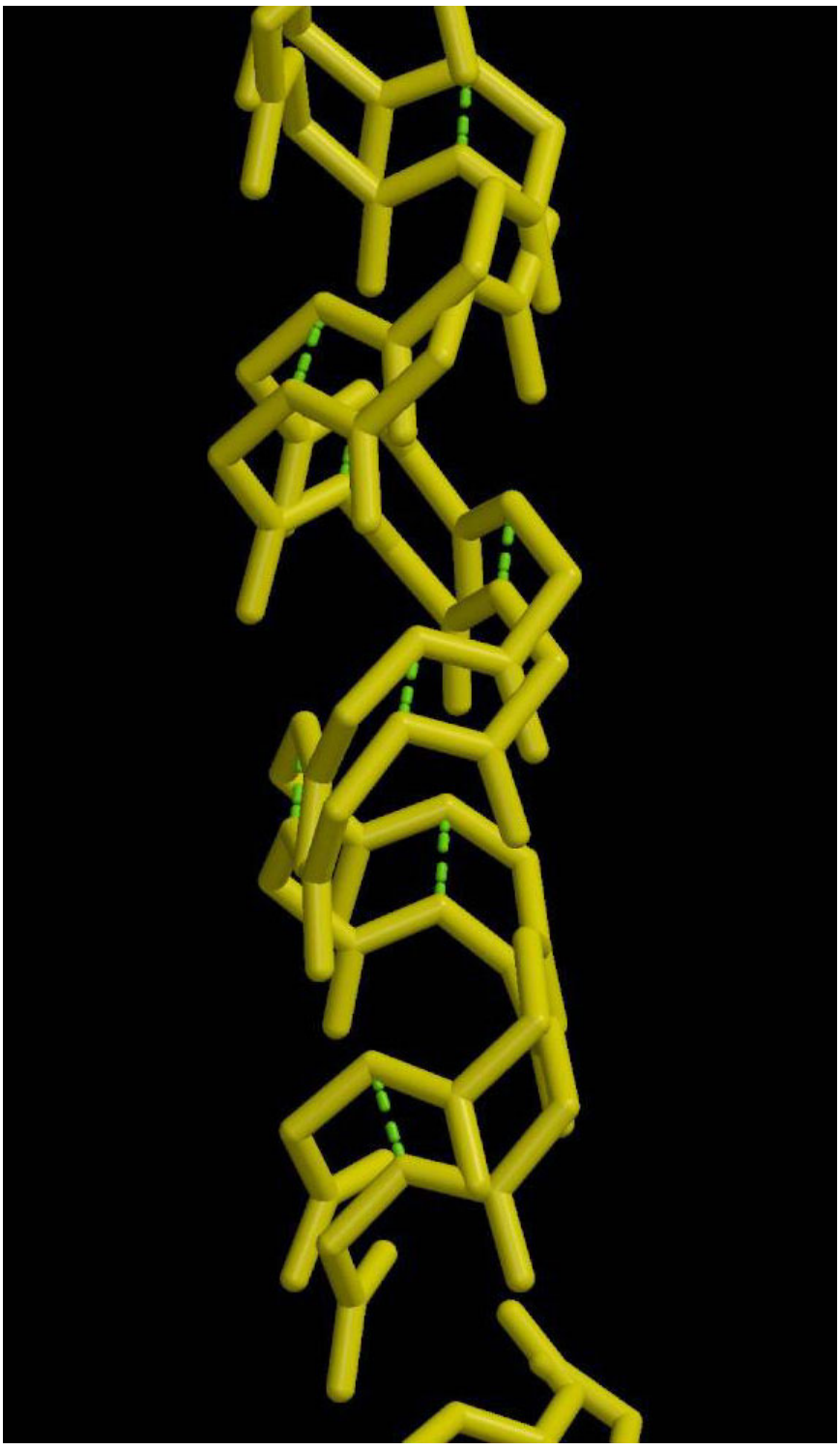

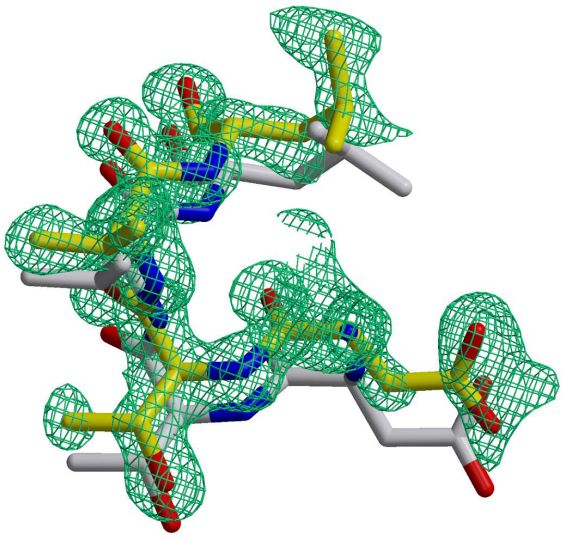

b.)

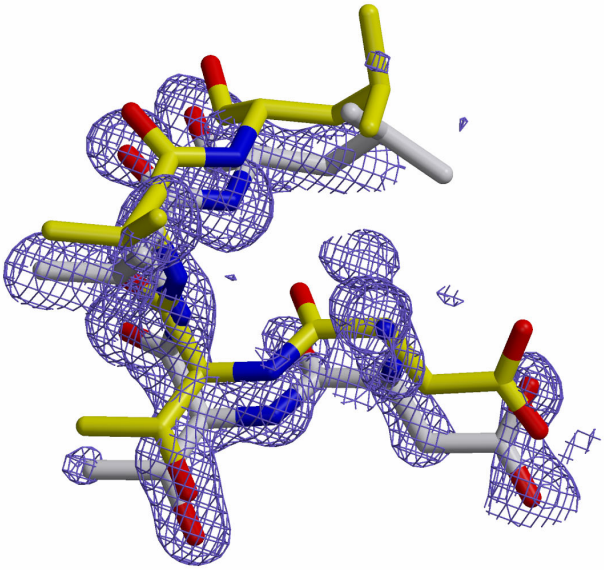

Figure 3: The $2F_o$-F_c σ_A- weighted electron density map of the P1 active site contoured at 2.2σ (green) and 3.2σ (purple).

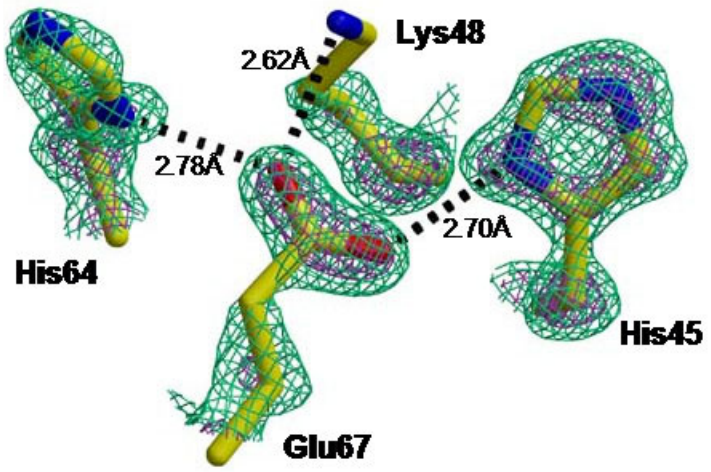
Lys48
2.62Å
2.78Å
2.70Å
His64
His45
Glu67

Figure 4: The pH profile of the *T. maritima* P1 domain overlaid with the calculated percentage of histidine molecules existing in the deprotonated state at pHs (a) 5.9 and (b) 6.9

a.)


% deprotonated histidines
% maximal phosphorylation activity
100
80
60
40
20
0
105
85
65
45
25
5
-15
pH 6.5
pH 7.13
pH 7.66
pH 8.26
pH 8.59
pH 9.24
pH 9.63

b.)

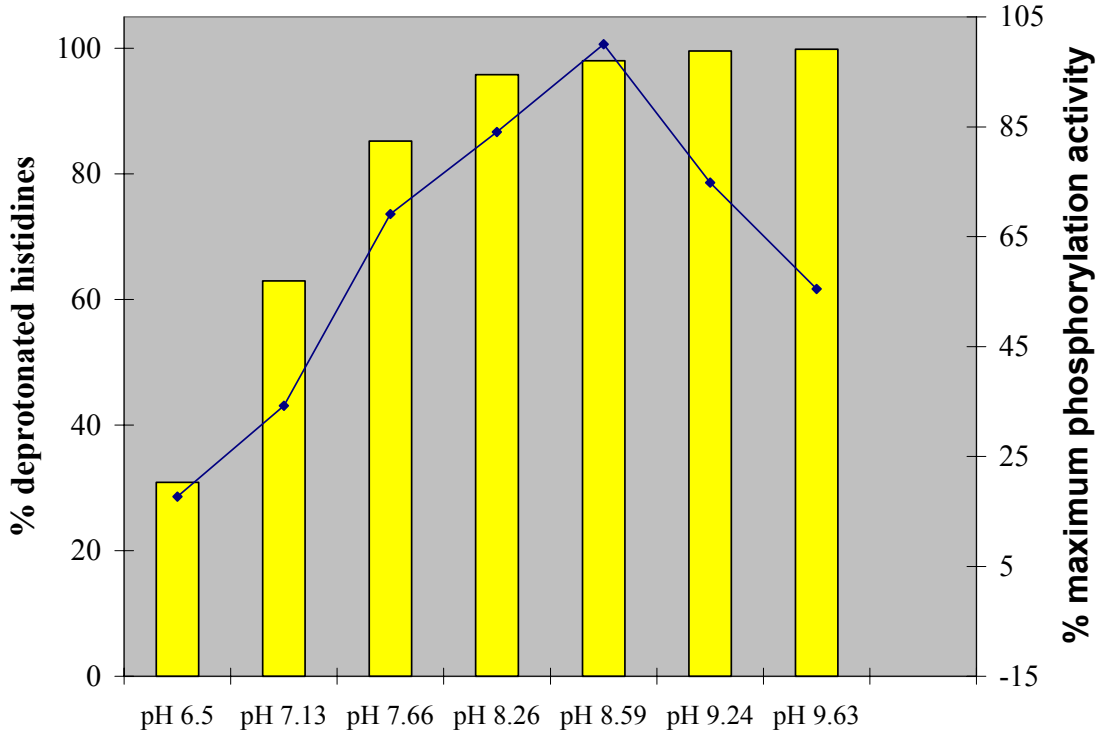
% deprotonated histidines
% maximum phosphorylation activity
100
80
60
40
20
0
105
85
65
45
25
5
-15
pH 6.5
pH 7.13
pH 7.66
pH 8.26
pH 8.59
pH 9.24
pH 9.63

REFERENCES

1. Zhou, H., et al., *NMR Studies of the Phosphotransfer Domain of the Histidine Kinase CheA from Escherichia coli: Assignments, Secondary Structure, General Fold, and Backbone Dynamics.* Biochemistry, 1995. **34**: p. 13858-13870.

2. Mourey, L., et al., *Crystal Structure of the CheA Histidine Phosphotransfer Domain that Mediates Response Regulator Phosphorylation in Bacterial Chemotaxis.* The Journal of Biological Chemistry, 2001. **276**(33): p. 31074-31082.

3. Zhou, H. and F.W.Dahlquist, *Phosphotransfer site of the Chemotaxis-Specific Protein Kinase CheA as Revealed by NMR.* Biochemistry, 1997. **36**: p. 699-710.

4. Otwinowski, A. and W. Minor, *Processing of X-ray diffraction data in oscillation mode.* Methods in Enzymolozy, 1997. **276**: p. 307-325.

5. Brunger, A.T., *Free R-Value - a Novel Statistical Quantity for Assessing the Accuracy of Crystal-Structures.* Nature, 1992. **355**(6359): p. 472-475.

6. McRee, D.E., *XtalView: a visual protein crystallographic software system for X11/Xview.* J. Mol. Graph., 1992. **10**: p. 44-47.

7. Furey, W. and S. Swaminathan, *PHASES: A Program Package for the Processing and Analysis of Diffraction Data from Macromolecules*, in *ACA meeting Abstracts*. 1990, American Crystallographic Association.

8. Crane, B.R. and E.D. Getzoff, *Determining phases and anomalous scattering models from the multiwavelength anomalous diffraction of native protein metal clusters. Improved MAD phase error estimates and anomalous- scatterer positions.* Acta Crystallographica Section D-Biological Crystallography, 1997. **53**: p. 23-40.

9. Collaborative Computational Project, N., *The CCP4 suite: programs for protein crystallography.* Acta Crystallographica, 1994. **D50**: p. 760-763.

10. Brunger, A.T., et al., *Crystallography & NMR system: a new software suite for macromolecular structure determination.* Acta Crystallographica Section D, 1998. **54**: p. 905-921.

11. Sheldrick, G.M. and T.R. Schneider, *SHELXL:high resolution refinement.* Methods in Enzymology, 1997. **277**: p. 319-343.

12. Wilson, M.A. and A.T. Brunger, *The 1.0A Crystal Structure of Ca2+-bound Calmodulin: an Analysis of Disorder and Implications for Functionally Relevant Plasticity.* Journal of Molecular Biology, 2000. **301**: p. 1237-1256.

13. Gill, S.C. and P.H. Vonhippel, *Calculation of Protein Extinction Coefficients from Amino-Acid Sequence Data.* Analytical Biochemistry, 1989. **182**(2): p. 319-326.

14. Kato, M., et al., *Insights into Multistep Phosphorelay from the Crystal Structure of the C-Terminal HPt Domain of ArcB.* Cell, 1997. **88**: p. 717-723.

15. Kato, M., et al., *Refined structure of the histidine-containing phosphotransfer (HPt) domain of the anaerobic sensor kinase ArcB from Escherichia coli at 1.57A resolution.* Acta Crystallographica, 1999. **D55**: p. 1842-1849.

16. Xu, Q. and A.H. West, *Conservation of Structure and Function Among Histidine-containing Phosphotransfer (HPt) Domains as Revealed by the Crystal Structure of YPD1.* Journal of Molecular Biology, 1999. **292**: p. 1039-1050.

17. Ramakrishnan, C. and G. Ramachandran, *Stereochemical Criteria for Polypeptide and Protein Chain Conformations .2. Allowed Conformations for a Pair of Peptide Units.* Biophysical Journal, 1965. **5**(6): p. 909-933.

18. Laskowski, R.A., et al., *PROCHECK: a program to check the stereochemical quality of protein structures.* J. Appl. Crystallogr., 1993. **26**: p. 283-291.

19. Hutchinson, E. and J. Thornton, *PROMOTIF: a program to identify and analyze structural motifs in proteins.* Protein Science, 1996. **5**: p. 212-220.

20. Smith, J.L., et al., *Structural Heterogeneity in Protein Crystals.* Biochemistry, 1986. **25**: p. 5018-5027.

21. Morrison, T.B. and J.S. Parkinson, *Liberation of an interaction domain from the phosphotransfer region of CheA, a signaling kinase of Excherichia coli.* Proc. Natl. Acad. Sci. U.S.A., 1994. **91**: p. 5485-5489.

22. Zhou, H., et al., *Phosphotransfer and CheY-Binding Domains of the Histidine Autokinase CheA Are Joined by a Flexible Linker.* Biochemistry, 1996. **35**: p. 433-443.

23. Bilwes, A., et al., *Structure of CheA, a Signal-Transducing Histidine Kinase.* Cell, 1999. **96**: p. 131-141.

24. Deacon, A., et al., *The structure of concanavalin A and its bound solvent determined with small-molecule accuracy at 0.94 angstrom resolution.* Journal of the Chemical Society-Faraday Transactions, 1997. **93**(24): p. 4305-4312.

25. Schuster, II and J.D. Roberts, *N-15 Nuclear Magnetic-Resonance Spectroscopy - Effects of Hydrogen-Bonding and Protonation on Nitrogen Chemical-Shifts in Imidazoles.* Journal of Organic Chemistry, 1979. **44**(22): p. 3864-3867.

26. Conley, M.P., et al., *pH Dependence of CheA Autophosphorylation in Escherichia coli.* Journal of Bacteriology, 1994. **176**(13): p. 3870-3877.

27. Song, H.K., et al., *Insights into eukaryotic multistep phosphorelay signal transduction revealed by the crystal structure of Ypd1p from Saccharomyces cerevisiae.* Journal of Molecular Biology, 1999. **293**(4): p. 753-761.

28. Bilwes, A.M., et al., *Nucleotide binding by the histidine kinase CheA.* Nature Structural Biology, 2001. **8**(4): p. 353-360.

29. Jackson, A.P. and A. Maxwell, *Identifying the catalytic residue of the ATPase reaction of DNA gyrase.* Proceedings of the National Academy of Sciences, 1993. **90**: p. 11232-11236.

Chapter 3

The chemical determinants of histidine reactivity in CheA

Protein phosphorylation is a key mechanism for intracellular signal transduction in both eukaryotic and prokaryotic cells. Histidine phosphorylation is central to bacterial signaling [1-3]. Histidine kinases initiate signal processing, transmitting information from the extracellular environment and triggering an appropriate response. Since histidine phosphorylation is prevalent in prokaryotes, and rarely found in higher eukaryotes, it is of extreme interest to elucidate the determinants of histidine reactivity. Distinguishing features could lead toward the development of novel antibiotics.

One of the best characterized histidine kinases is CheA, an autophosphorylating dimeric protein that initiates the phosphorylation cascade which results in chemotaxis, the directed movement of bacteria in a chemical environment. The structure of CheA's catalytic core revealed that it is not similar to the Ser/Thr or Tyr kinases. Instead, CheA surprisingly resembles the functionally divergent GHL (for GyrB, Hsp90, MutL) ATPase family [4]. Histidine kinases use ATP as a phosphodonor, transferring its γ-phosphoryl group to a histidine residue. In contrast, ATPases cleave the ATP γ-phosphoryl group and release it into water.

CheA and the GHL family of ATPases share a common structural element, a deep cavity for ATP binding to the active site. In addition to possessing similar topologies, the sequences of the ATP-binding sites of protein histidine kinases (PHKs) and GHL ATPases are highly conserved. The edges of the ATP-binding cavities of these proteins include four regions of sequence similarity: the N, G1, F, and G2 boxes [4, 5].

Despite the striking topological and sequence similarities, some critical differences exist between these two protein families. An essential glutamate of the GHL ATPases presumed to be the general base involved in water activation for ATP

hydrolysis [6] is replaced by His 405 in CheA. This glutamate is missing from the kinase domain. However, there is a conserved glutamate in the CheA histidine phosphotransfer domain, P1, which is in the vicinity of the active site histidine.

CheA phosphorylation activity is sensitive to pH in the range between 6.5 and 10 [7] (Chapter 2 Fig. 4). The phosphoaccepting histidine (His48 in *E.coli*) was previously determined by NMR to have a higher than normal pKa of 7.8 and to exist in the normally unfavored tautomeric form, $N^{\delta 1}H$. [8]. The phosphorylatable histidine remains strongly hydrogen bonded, even at pHs above its pKa value, via the $N^{\delta 1}$ atom, which serves as a hydrogen bond donor. However, due to the low resolution of the P1 NMR structure, it was initially not possible to identify the histidine hydrogen bonding partner [9]. A crystal structure of the *Salmonella* P1 domain identified a glutamate residue as a potential hydrogen bonding partner [10].

In an effort to determine whether the conserved P1 glutamate (Glu67 in *Thermotoga maritima*) plays a similar role as the activating glutamate of the GHL ATPases, in depth structural and biochemical studies were carried out at the 67th position of the *T. maritima* histidine phosphotransfer domain. Herein, we explore the putative catalytic role of Glu67 to the CheA autophosphorylation reaction by site-directed mutagenesis, protein crystallography, and 2-D NMR techniques.

MATERIALS AND METHODS

Protein cloning, expression, and purification

T. maritima CheA, Δ289 (residues 290-671), domain P1 (residues 4-133), and P1E67Q_{short} (residues 4-104) were subcloned in the vector pET28(a) (Novagen). The plasmid was transformed into *E. coli* strain BL21(DE3) (Novagen) and protein expressed in 2L TB cultures. Protein purification was achieved by affinity chromatography on Nickel-NTA beads (Qiagen), followed by an overnight digestion of the His_6 tag at 4°C. The protein was further purified by gel filtration on a superdex 75 or 200 column (Pharmacia) using a buffer composed of 50 mM Tris pH7.5, 150 mM NaCl and 2 mM DTT. Centrifugation with an Amicon centriprep concentrator yielded the concentrated protein. Mutations were made using the QuickChange Site-Directed Mutagenesis Kit (Stratagene).

Phosphorylation Assays

Initial velocities of full length CheA and its mutants (2-10 μM) or P1(30 μM) incubated with Δ289(2 μM) were measured in 50 mM Tris pH 8.5, 50 mM KCl, and 2 mM DTT at 50°C. Reactions were initiated upon addition of [γ-^{32}P] ATP. At specific time intervals, aliquots were quenched with 2X sodium dodecyl sulfate (SDS) electrophoresis buffer containing 25 mM ethylenediaminetetra acetic acid (EDTA). Samples were then electrophoresed on 12-18% Criterion Tris-HCl gels (Biorad) using a Criterion Dodeca Cell (Biorad). Gels were dried under vacuum and phosphorylation quantified using a Storm phosphoimager (Molecular Dynamics). pH dependence studies were performed in the same manner over a pH range of 6 to 9.5. The same protocol was

used when P1(30 μM) was incubated with Δ289(2 μM) in the presence of a tenfold excess of P1 mutant (300 μM) or the control BSA(300 μM).

Swarm assays

Tryptone swarm plates consist of 0.25% Difco Bacto Agar in tryptone broth (1% tryptone, 0.5% NaCl) 100 μg/ml ampicillin, and 5 μM IPTG. Strain RP9538, a derivative of *E.coli* K-12 carrying a deletion for the CheA gene, was transformed with pAR1:cheA derivatives containing the wild-typeor mutant alleles. Tryptone swarm plates were stabbed in the center with fresh transformants and immediately incubated at 37°C. Ring diameters were measured after twelve hours. RP9538 and pAR1:cheA were kindly provided by Prof. Rick Stewart (University of Maryland, College Park).

CD experiments

CD spectra were recorded with an AVIV (Lakewood, NJ) 62A DS spectrometer equipped with a Peltier-type temperature control system and using a 0.1 cm quartz cuvette (Wilmad). Samples were prepared in 20 mM NaPi buffer at pH 8. Data were collected in the far UV (from 250 to 190 nm) with an averaging time of 5 s and a bandwidth of 1.5 nm.

Crystallization, data collection, structure determination, and refinement

Orthorhombic crystals belonging to the $P222_1$ space group were obtained by mixing 2 μL of 7-15 mg/ml $P1E67Q_{short}$ with 2 μL of the reservoir solution (14% PEG 2K, 0.1M NaAc pH 4.5, 0.2M AmAc). Crystals were briefly soaked in a cryoprotectant solution (36% PEG 8K, 0.1M NaAc pH4.5, and 0.2M AmAc) and then flash frozen.

Diffraction data were colleted to 1.1Å resolution at the Cornell University synchrotron source, CHESS, on beamline F1. Data were processed, scaled, and merged using the DENZO/SCALEPACK suite of programs [11] (Table1).

The "warpNtrace" feature of ARP/wARP was used to automatically build the initial protein model [12]. The asymmetric unit consists of one molecule. Iterative cycles of refinement using the program SHELXL [13] and manual rebuilding of the model in XtalView [14] yielded an R_{work} and R_{free} of 0.146 and 0.194, respectively. Inclusion of all data yielded a crystallographic R factor of 0.148 (Table 1). As previously observed in the wild-type structure of P1 (Chapter 2 Fig. 2), several discrete residues (14, 16, 39, 51, 54, and 55) exist in alternate conformations. Extended regions displaying alternate conformations in helices A and D (residues 21-32 and 82-105) are also observed in the P1E67Q_{short} crystal structure.

NMR spectroscopy

NMR experiments were performed on a 600 MHz Inova spectrometer equipped with ^{1}H [$^{13}C/^{15}N$] pulsed-field gradient probes. NMR samples contained 50mM sodium phosphate, 0.05% sodium azide and 10% D_20. All experiments were recorded at 50˚C. Assignments for all non-proline backbone amides of wild-type P1 were obtained from the Dahlquist Lab (Hamel et al. unpublished results). For this work, 3-D ^{15}N-NOESY-HSQC, 2-D HSQC-aliphatic and 2-D HSQC-aromatic correlation experiments were acquired on uniformly ^{15}N-labeled proteins [15]. For aliphatic (aromatic) HSQC spectra, the ^{15}N carrier frequency was set to approximately 121(190) ppm, using a delay of 4.8(50) ms to refocus chemical shift evolution arising from the coupling between the

backbone amide proton and nitrogen (carbon-bound proton and imidazole nitrogen). In all correlation experiments 100(128) complex t_1 increments were recorded. Spectral widths were 1600(4800) Hz in F_1 and 8000 Hz in F_2. The number of scans in individual 2D experiments ranged from 4 to 128 depending on the signal-to-noise ratio. Quadrature detection in the ^{15}N dimension used the States-TPPI method [16]. 3D ^{15}N-NOESY-HSQC spectra were recorded for each mutant and used to verify backbone amide resonance assignments. These spectra had the same parameters listed above with 64 complex t_2 increments, spectral width of 8000 Hz in F_3 and 150 ms mixing time. In the pH titration experiments, a series of spectra were recorded for each protein, ranging from approximately pH 4 to pH 10. The pH was adjusted with small amounts of HCl or NaOH. The aliphatic HSQC experiments were used to measure chemical shift changes with pH of the amides. The aromatic HSQC experiments were used to measure pH-dependent chemical shift changes of the histidine rings. All data was processed using the FELIX software package from MSI.

Analysis of NMR data

The protonation state of a nitrogen nucleus results in a unique chemical shift [17-21]. The charged (type α+) and neutral (type α) protonated imidazole ^{15}N nucleus have chemical shifts of 176.5 and 167.5 ppm, respectively. The deprotonated ^{15}N (type β) possesses a chemical shift of 249.5 ppm. These values are according to that of Pelton et al., which differ from those of Bachovchin [22, 23] (Table 2).

At low pH, the observed chemical shifts reflect that of the pure protonated state, whereas at high pH, the chemical shifts consist of the weighted averaged of the neutral

tautomer shifts [23]. Fast equilibration of the two tautomers, $N^{\delta 1}H$ and $N^{\varepsilon 2}H$, is observed in solution [24]. Important information about the predominant histidine tautomeric state and potential hydrogen bonding interactions can be obtained by comparing the observed chemical shift values to those obtained from model compounds. Hydrogen bonding results in changes to the ^{15}N chemical shifts that are similar to those produced by nitrogen protonation and deprotonation [24]. However, the magnitude is much smaller, up to 10ppm. Another indication of hydrogen bond formation is the predominance of the normally unfavored tautomer $N^{\delta 1}H$ [8, 23, 25].

The pKa values of the imidazole rings were determined by a least squares fit of the chemical shifts over a range of pH values using the Henderson-Hasselbach equation:

$$\delta_{obs} = \delta_1 10^{-pH}/(10^{-pH} + 10^{-pKa}) + \delta_2 10^{-pKa}/(10^{-pH} + 10^{-pKa}) \qquad \text{(Eqn 1)}$$

The chemical shifts at the low and high pH limits are δ_1 and δ_2 respectively. The observed chemical shift, δ_{obs}, at any given pH is assumed to result from the weighted average of fast exchange between the limiting values δ_1 and δ_2, respectively. The fraction of each tautomer present was calculated as previously described [8].

RESULTS

A conserved residue, Glu67, is critical to CheA auto-phosphorylation

As a first step in probing whether GHL ATPases and PHKs share a common mechanism of ATP cleavage, we investigated the role Glu67 plays in CheA

autophosphorylation. A series of mutations at this position were designed to examine whether hydrogen bonding ability or charge were critical to the phosphorylation reaction. Using site directed mutagenesis, the conserved residue Glu67 was altered to Gln, Asp, and Ala.

The first mutation, E67Q, replaces the oxygen moiety of the carboxyl side chain with an amide. This conservative mutation maintains hydrogen bonding ability, but removes charge from this location. In addition, other histidine phosphotransfer (HPt) domains, such as $ArcB_c$ and Ypd1, have a glutamine at this position. It was of interest to probe whether a glutamine residue is interchangeable for a glutamate at this site. The Asp mutation keeps the charge, but being one carbon shorter than a Glu, could weaken or abolish a hydrogen bond. The Ala mutation removes both charge and the ability to hydrogen bond. The effects of a Glu to Ala mutation have already been described for *Salmonella* [10]. However, the conservative and semi-conservative mutations reported in this study investigate the role of Glu67 in further detail by assessing the effect of varying hydrogen bonding degrees and charge on the phosphorylation reaction of *T. maritima* CheA.

To initially characterize each Glu67 mutant, the phosphorylation level of wild-type protein was compared to that of mutant protein following a thirty-minute incubation with $^{\gamma 32}$P ATP *in vitro*. Mutations were made both in the isolated phosphotransfer domain, P1, as well as the intact CheA protein. CheA containing the mutations E67Q, E67D, and E67A showed dramatically reduced autophosphorylation activity (5.7%, 8.4%, and 2.4%, respectively; Figure 1a). An even more dramatic reduction in

phosphotransfer activity to P1 was observed, averaging about 1% of wild-type activity for all mutants (Figure 1b).

The effect of each mutation was further investigated *in vivo* by measuring the ability of *E. coli* mutant strains to migrate in semisolid agar medium [26]. Plasmids expressing each E67 mutation in intact CheA were transformed into a host strain, ΔcheA, lacking the CheA allele. All E67 CheA mutants exhibit significantly reduced chemotactic swarming ability, approximately 20% of that observed with wild-type (Figure 2). Therefore, a point mutation of a critical residue in CheA can disrupt the normal chemotaxis signal transduction pathway in intact cells.

To probe whether an increase in pH rescues the activity of the E67 mutants by making His45 more nucleophilic through deprotonation and therefore more amenable to phosphorylation, the activity of E67 mutants was monitored as a function of pH at 50ºC. The phosphotransfer reaction of the mutants is not markedly affected by a change in pH (Figure 3). Phosphotransfer to the mutant proteins is therefore independent of pH or the deprotonation of the active site histidine.

Far-UV CD spectra of wild-type P1 and the E67 mutants are virtually identical, indicating that the mutation does not alter the secondary structure of the phosphotransfer domain (Figure 4a). In order to probe whether the P1E67Q mutant binds the kinase domain as P1, it was incubated in a tenfold excess to its wild-type counterpart in the presence of the kinase fragment Δ289. The time course of this reaction was monitored and revealed that P1E67Q inhibits the normal progression of phosphotransfer. A tenfold excess of P1E67Q results in 26% of normal phosphotransfer activity (Figure 4b). To further investigate whether P1E67Q is specifically inhibiting the phosphorylation

reaction, a ten fold excess of a non-specific protein, BSA, was added to a solution containing P1 and Δ289. 90% of normal activity is retained. Taken together, these data suggest P1E67Q is a catalytic mutation of the wild-type reaction. Both charge and the ability to hydrogen bond are important at this position.

The high resolution structure of P1E67Q reveals a disrupted hydrogen bond network

In order to further elucidate the role that Glu67 plays in the phosphotransfer reaction, the crystal structure of $P1E67Q_{short}$ (helices A-D) was solved to a resolution of 1.1Å (Table 1). The protein crystal belongs to the orthorhombic $P222_1$ space group with cell dimensions a= 27.36Å, b= 37.49Å, and c= 87.47Å. Refinement converged to an R_{work} of 14.6% and an R_{free} of 19.4%.

At a resolution of 1.1 Å, individual atoms such as N and O can be unambiguously assigned based on the electron density volume. Additionally, the shape of the electron density at single and double bonds can be distinguished. As observed in Figure 5, the glutamine carbonyl exhibits continuous electron density, as expected for a double bond, between the carbon and oxygen atoms. On the other hand, the nitrogen moiety of the Gln residue shows discrete density, as expected for a single bond. The high resolution structure of P1E67Q therefore affords a unique opportunity to see the structural effects of a single point mutation in atomic detail.

The E67Q structure is almost indistinguishable from that of the native P1 structure, with the exception of a few but critical details. An overlay of the active site region of wild-typeP1 and P1E67Q reveals the disruption of the hydrogen bond network involving His45, Glu67, Lys48, and His64 (Figure 6a). At pH 4.5, the $N^{\delta 1}$ position of

the phosphoaccepting histidine is within hydrogen bonding distance, 2.82Å, of the Gln67 carbonyl oxygen atom. The slight change in side chain orientation results in the disturbance of the hydrogen bond interactions to Lys48 and His64 observed in the wild-type at this position (Figure 6b).

Glu67 tunes the reactivity of the phosphoaccepting His45

In solution, histidine side chains readily exist in three protonation states: a charged state and two neutral tautomers $N^{\delta 1}$and $N^{\varepsilon 2}$, which undergo fast exchange in solution [23, 24]. Based on the chemical shift value, it is possible to identify hydrogen bonding interactions, protonation and tautomeric states. (Table 2). In order to evaluate how a conservative mutation at the 67th position affects the reactivity of the phosphoaccepting histidine, we expressed ^{15}N labeled P1E67Q. P1E67Q contains three histidines, the site of phosphorylation, His45, a participant in the hydrogen bond network, His64, and a residual N-terminal histidine from the histidine tag used for protein purification. Histidine deprotonation was monitored as a function of pH using two dimensional NMR techniques.

The pH titration of the P1E67Q His45 imidazole is depicted in Figure 7a. Using equation 1, its pKa was determined to be 5.8. At pH 3.97, the chemical shift values of $N^{\delta 1}$ and $N^{\varepsilon 2}$ are 178.4 and 174.3ppm, respectively. These values closely correspond to the expected 176.5 ppm for a charged imidazole nitrogen. At the high pH limit, the chemical shift values of $N^{\delta 1}$ and $N^{\varepsilon 2}$ are 226.7 and 184.5 ppm, respectively (Table 3). The larger shift of the $N^{\delta 1}$ atom indicates that the phosphoaccepting histidine primarily

exists in the $N^{\varepsilon 2}H$ tautomeric state. In fact, the $N^{\delta 1}H$:$N^{\varepsilon 2}H$ tautomeric ratio was calculated to be 1:3.3 (Table 4).

The protonation states of the remaining two histidines were also examined (Figures 7b-c). His64 is involved in the conserved hydrogen bonding network of P1 (Figure 4b). The $N^{\delta 1}$ atom has a much larger chemical shift, 237.1 ppm, than the 176.1ppm of $N^{\varepsilon 2}$ indicating that the $N^{\varepsilon 2}H$ tautomer is dominant. The pKa value of His64 is 5.9 and the $N^{\delta 1}H$:$N^{\varepsilon 2}H$ tautomeric ratio was calculated to be 1:4.3 (Table 4). The final histidine, located at the N-terminus, is a residual amino acid from the histidine tag. It plays the role of an internal control, serving as a model solvent-exposed histidine residue (Table4). Its pKa was measured to be 5.9 and its $N^{\delta 1}H$/ $N^{\varepsilon 2}H$ tautomeric ratio is 1:4.2. The pH titration of the imidazole ^{1}H chemical shifts for all histidines can be found in Appendix 1.

DISCUSSION

The activation of a phosphoaccepting histidine residue

Using site-directed mutagenesis, crystallography, and 2-D heteronuclear NMR, Glu67 was identified as an indispensable residue to the CheA autophosphorylation reaction. A systematic mutational study investigating whether hydrogen bonding or charge were important contributing factors to the phosphorylation reaction *in vitro* and *in vivo* revealed that both properties are important (Figures 1-2). A Gln side chain that maintains hydrogen bonding ability and an Asp side chain that preserves charge at this location both result in the dramatic inhibition of phosphorylation activity. Interestingly, a

Gln residue, although found in the same position in other HPt domains [27, 28], is not interchangeable for a Glu residue in CheA (Figure 1). These results indicate that a negatively charged residue that simultaneously acts as a hydrogen bond acceptor of the phosphoaccepting histidine is required for efficient CheA autophosphorylation to take place.

Although the E67A mutation in *Salmonella* was shown to reduce the ATP phosphotransfer rate, these experiments could not distinguish whether the decrease in activity was due to the disruption of secondary structure, the loss of binding between the P1 and the kinase domain, or a catalytic defect [10]. Point mutations at Glu67 do not perturb the secondary structure content of P1 as evidenced by far-UV circular dichroism studies (Figure 4a). The crystal structure of P1E67Q further confirms that the overall structure remains intact. Additionally, phosphorylation of wild-typeP1 by the catalytic core fragment, Δ289, was inhibited in the presence of an excess of P1E67Q. On the other hand, an excess of a random protein, bovine serum albumin (BSA), that is not expected to bind P4, did not affect P1 phosphorylation (Figure 4b). We infer that P1E67Q is recognizing the kinase domain P4 and acting specifically.

The pH profile of *E. coli* and *T. maritima* CheA demonstrated optimal activity at pH 8.5, consistent with the existence of a higher than normal histidine pKa (Chapter2 Figure 4) [7]. The phosphorylation activity of E67 mutants are independent of pH. In fact, the phosphorylation level at pH 6.5, where roughly 70% of histidines exist in the protonated state, is similar to that at pH 8.5 and higher, where greater than 99% of the histidines are expected to exist in the deprotonated state. Histidine reactivity in E67

mutants is unaffected by the histidine protonation state. Hence, the mere deprotonation of His45 does not lead to histidine phosphorylation (Figure 3).

The atomic resolution structure of P1E67Q provided further insight into the functional role of Glu67. In changing one atom of a side chain from an oxygen to an amide, the side chain orientation at the 67th position is altered. This slight change disrupts the hydrogen bonding network observed in the native structure (Figure 6). The crystal structure of wild-type P1 demonstrated that Glu67 acts as a hydrogen bond acceptor to both Lys48 and His64. In P1E67Q, the neutral Gln no longer forms a salt bridge with a positively charged Lys48. Furthermore, the Gln amide cannot act as a hydrogen bond acceptor to His64.

Despite the disruption to the intricate hydrogen bonding network the position of His45 is curiously not altered by this mutation. Glu67 is thus not involved in the positioning or alignment of the phosphoaccepting histidine. Although structural perturbations cannot be ruled out as a cause for the decreased efficiency of histidine phosphorylation, a change in the chemical and electronic properties of the phosphorylatable histidine is likely most responsible for the drastic change in activity. The P1E67Q phosphoaccepting histidine exists in the $N^{\varepsilon 2}H$ tautomeric state (Figure 7a). Since its phosphorylation activity is dramatically reduced, this indicates that the phosphoaccepting histidine must exist in the correct tautomer, $N^{\delta 1}H$, in order for it to be phosphorylated. Curiously, the same strategy is employed by the conserved Asp and His catalytic residues of the serine proteases.

Ypd1, $ArcB_c$, and P1E67Q share structural and chemical properties. Their Gln residues have similar side chain orientations and are able to hydrogen bond to the $N^{\delta 1}H$

atom of the phosphoaccepting histidine. Interestingly, $ArcB_c$ and P1E67Q both predominantly exist in the $N^{\varepsilon 2}H$ tautomeric state and have pKas that correspond to that of a normal solvent exposed histidine [27]. The requirements for histidine phosphorylation therefore differ between these two proteins (see discussion below). A mere hydrogen bond with the $N^{\delta 1}$ atom of the phosphoaccepting histidine is not sufficient to phosphorylate the CheA P1 domain. The histidine must predominantly exist in the $N^{\delta 1}H$ tautomeric state in order for phosphorylation to occur.

The native crystal structure revealed that the electrons of the carboxyl moiety of Glu67 are resonating (Chapter 2 Figure3). Therefore His45 is acting as a hydrogen bond donor to a negatively charged oxygen in the case of the wild-type and to a neutral oxygen in P1E67Q. The disparity in electronegativity between Glu and Gln is likely responsible for the effect on histidine reactivity. A negatively charged oxygen atom from a glutamate acts as a stronger base than a neutral glutamine. Glu67 can therefore stabilize the existence of an otherwise unfavorable $N^{\delta 1}H$ histidine tautomer over a large pH range.

Experiments described in this paper have enabled us to clarify the functional role that Glu67 plays in the phosphorylation reaction. Glu67 does not fix the orientation of the histidine. Instead, it tunes the reactivity of the phosphorylatable histidine, making it more nucleophilic. Taken together, the data suggest the P1 domain not only possesses the nucleophile for phosphate transfer, His45, but also the activating glutamate, Glu70.

Towards understanding the biochemical mechanism of CheA

Despite the fact that CheA is one of the best characterized histidine kinases, a detailed biochemical mechanism for CheA autophosphorylation has not been elucidated.

Based on the results reported in this paper and on the extensive structural [4, 5, 9, 10, 29], biochemical [30-32], and mutagenesis investigations of CheA [33-37], we are now beginning to unravel the details of its biochemical mechanism.

The CheA active site spans two domains. All necessary elements for histidine phosphorylation are contained in the phosphotransfer (P1) and kinase (P4) domains [5] (Figure 8). Conserved residues from P4 provide stabilizing contacts necessary for ATP binding and form a pocket that optimally positions the gamma phosphoryl for transfer to the histidine residue [5, 34]. Amino acids present in the kinase domain have also been shown to be catalytically important [34]. P1 possesses a residue that tunes the reactivity of the phosphoaccepting histidine. His45 is made nucleophilic as a result of a hydrogen bond to the strong base Glu67. Thus, we conclude that the P1 domain provides the nucleophile for phosphate transfer (His45) and the activating glutamate (Glu67) completing the GyrB catalytic center.

It therefore appears that in addition to sharing a common fold and ATP binding site, CheA and GyrB also share a common mechanism. The main difference between CheA and the GHL family of ATPases is in the molecule that the conserved glutamate residue activates. In the case of the ATPases, the glutamate is postulated to activate a water molecule that attacks the γ-phosphoryl group [6]. Alternatively, in CheA, the glutamate activates the phosphoaccepting histidine by perturbing its pKa and stabilizing the normally unfavored $N^{\delta 1}H$ tautomeric state.

Since some crucial residues for CheA autophosphorylation have been identified, there is a solid foundation from which to undertake detailed mechanistic studies. It is clear that the kinase domain binds and positions ATP for phosphotransfer, however the

question of exactly how the conserved residues contribute to catalysis has yet to be answered. The challenge remains in not only deciphering the exact functional role of conserved residues, but also in determining the role protein dynamics play in the phosphorylation reaction. Future studies will lead to a deeper understanding of the CheA mechanism and facilitate the development of novel antibiotic agents.

Mechanisms of phosphotransfer between components in bacterial signaling differ

The phosphorelay schemes of two component systems are highly adaptable allowing for variation that has likely evolved to optimize specific signaling systems (Chapter 1 Figure 4). Despite significant diversity in domain organization, the core structures and activities of these domains are conserved. The phosphorylation of histidine residues is central to the transmission of environmental information for prokaryotes [2]. Therefore, it is of key interest to understand the chemical determinants of histidine reactivity.

Despite the low sequence similarities observed in histidine phosphotransfer domains of two-component systems, a four-helix bundle is used as a generic scaffold for the transfer of phosphoryl groups to and from solvent exposed histidines [9, 10, 28, 38, 39]. Furthermore, monomeric HPt domains are reported to be rigid [9, 27] and even upon phosphorylation, minor structural changes occur that are limited to the region surrounding the phosphoaccepting histidine [8, 40-45]. Does a common rigid helical bundle topology imply that HPt domains also share a common biochemical mechanism of phosphotransfer? More specifically, are the chemical determinants of phosphate flow to

a histidine conserved among monomeric HPt domains such as the CheA P1 domain, $ArcB_c$, and Ypd1? We think not.

We propose that two flavors of phosphotransfer exist for monomeric HPt domains that can be divided into two categories: kinase acceptors and phosphotransfer acceptors. Kinase acceptors, exemplified by the CheA P1 domain, accept a γ-phosphoryl group from ATP. These histidines are chemically distinguishable from those of phosphotransfer acceptors. The histidine residue of a kinase acceptor must be activated in a specific way. A hydrogen bond via the $N^{\delta 1}$ atom to a strong base, a glutamate, results in an altered histidine pKa and in the existence of the normally unfavored $N^{\delta 1}H$ tautomeric state of the histidine. This results in a highly nucleophilic histidine that is phosphorylated at the Nε2 atom.

Bacterial chemotaxis demands a very fast response time, in the order of milliseconds. Hence, an activated histidine, one that is so to speak "ready to go," may be essential for CheA. Its phosphotransfer domain lies distal to the kinase domain. The binding interaction between the two domains is weak (Chapter 2, Table 3)[32], so when making contact there is no time to waste.

On the other hand, histidines of phosphotransfer acceptors, like $ArcB_c$ and Ypd1, do not require such reactive histidines. The pKa of the $ArcB_c$ phosphoaccepting histidine was measured and found to be around 6.5, that of a solvent exposed histidine at room temperature. Moreover, it possesses an almost equal population of each tautomer. Enough of the unprotonated $N^{\varepsilon 2}$ form therefore exists to allow for phosphorylation at this location [27]. Interestingly, mutations of the conserved Gln residue in $ArcB_c$ [46] and Ypd1[47] affected neither phosphotransfer to or from these proteins. Accepting a

phosphoryl group from a phosphorylated aspartyl, a reactive species, does not require the tuning of the active site histidine. Conversely, CheA necessitates an activated histidine in order for phosphorylation to occur at the $N^{\varepsilon 2}$ site. Glu67 is needed in order for the $N^{\delta 1}H$ tautomer to dominate.

In summary, the phosphotransfer mechanism is by no means common to all histidine phosphotransfer domains. The details of this mechanism lie in the environment surrounding the phosphoaccepting histidine. Slight differences in the atomic details of various phosphorylation sites may result in differences in phosphorylation mechanism that may be exploited to develop selective drugs. Distinguishing features could lead toward the development of novel antibiotics specific to a particular regulation point in a bacterial signal transduction pathway. In addition to further elucidating how bacteria interpret environmental stimuli, this work could be applied towards the design of chemically tuned peptide-based catalysts used for the phosphorylation of small molecule compounds [48, 49].

Table 1: Summary of data collection and refinement statistics

	P1E67Q$_{short}$
Data Collection Statistics	
Maximum resolution (Å)	1.1
Wavelength (Å)	0.900
Total reflections	295,210
Unique reflections	37261
Completeness (%)[a]	98.5 (90.0)
I/σ (I)	10.4 (2.0)
Rsym (%)[b]	0.133 (0.393)
Mosaicity	0.519
Wilson B (Å^2)	19.2
Refinement Statistics	
Resolution limits	30-1.1
R_{work}[c]	14.6
R_{free}[d]	19.4
RMS deviations from ideal values	
Bond lengths (Å)	0.0268
Bond angles (°)	3.86
Dihedral angles (°)	21.32
Improper torsion angles (°)	2.06
Ramachandran plot[e] residues in	
Most favored regions (%)	95.9
Additional allowed regions (%)	4.1
Generously allowed regions (%)	0.0
Disallowed regions (%)	0.0

[a] Numbers in parentheses correspond to values in the highest resolution shell

[b] $R_{sym} = (\Sigma_{hkl}\Sigma_i | I_i(hkl) - < I(hkl) > |)/(\Sigma_{hkl}\Sigma_i I(hkl))$

[c] $R_{work} = \Sigma(| F_{obs} | - | F_{calc} |)/\Sigma | F_{obs} |$

[d] R_{free} is the R-factor calculated for a 5% test set of reflections excluded from the refinement calculation

[e] As determined by PROCHECK [50]

Table 2: Nitrogen types and characteristic ^{15}N chemical shifts (ppm)

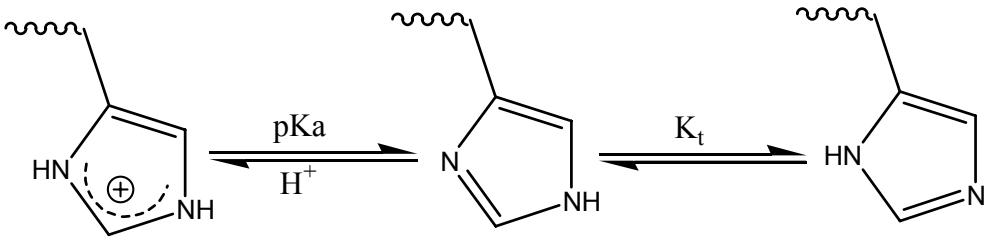

Structure	Nitrogen type	^{15}N Shift (ppm)	H-bond type	^{15}N Shift (ppm)	Δδ (ppm)
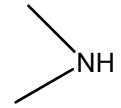	α	167.5	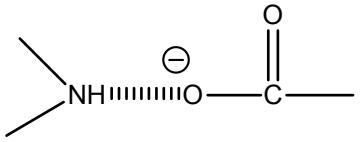	178	~+10
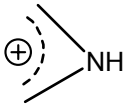	α+	176.5	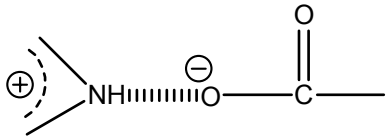	186	~-10
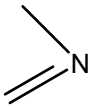	β	249.5	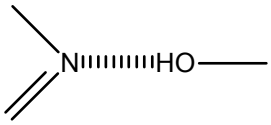	239	~+10

Table 3: Expected and observed ^{15}N chemical shifts for P1E67Q histidine residues

Residue	Nitrogen	Protonation State	δ_{obs} (ppm)	δ_{th} (ppm)	δ_{obs}- δ_{th}	$\Delta\delta$[Nδ1-Nε2]
His45						
low pH	Nδ1	protonated	178.4	176.5	11.6	4.1
	Nε2	protonated	174.3	176.5	0.7	
high pH	Nδ1	deprotonated	227.5*	249.5	-22.0	42.5
	Nε2	protonated	185.0	249.5	64.5	
His64						
low pH	Nδ1		199.4*	176.5	22.9	25.3
	Nε2	protonated	174.2*	176.5	-2.4	
high pH	Nδ1	deprotonated	237.1	249.5	-12.4	61.0
	Nε2	protonated	176.1	249.5	73.4	
HisTag						
low pH	Nδ1	protonated	177.0	176.5	0.5	8.1
	Nε2	protonated	173.6	176.5	0.3	
high pH	Nδ1	deprotonated	236.2	249.5	-13.3	60.3
	Nε2	protonated	175.9	249.5	-73.6	

*theoretical values obtained from the limits as calculated by the Henderson-Hasselbach equation

Table 5: Apparent pKa values and tautomeric states of P1E67Q histidine residues

	Ave pKa	Predominant Tautomeric state	Tautomeric ratio (Nε2:Nδ1)
His45	5.8	Nε2	3.3:1
His64	5.9	Nε2	4.3:1
HisTag	5.9	Nε2	4.2:1

Figure 1: (a) Relative phosphorylation of CheA and CheA E67 mutants (b) Relative phosphorylation of the isolated P1 domain and its mutants

(a)

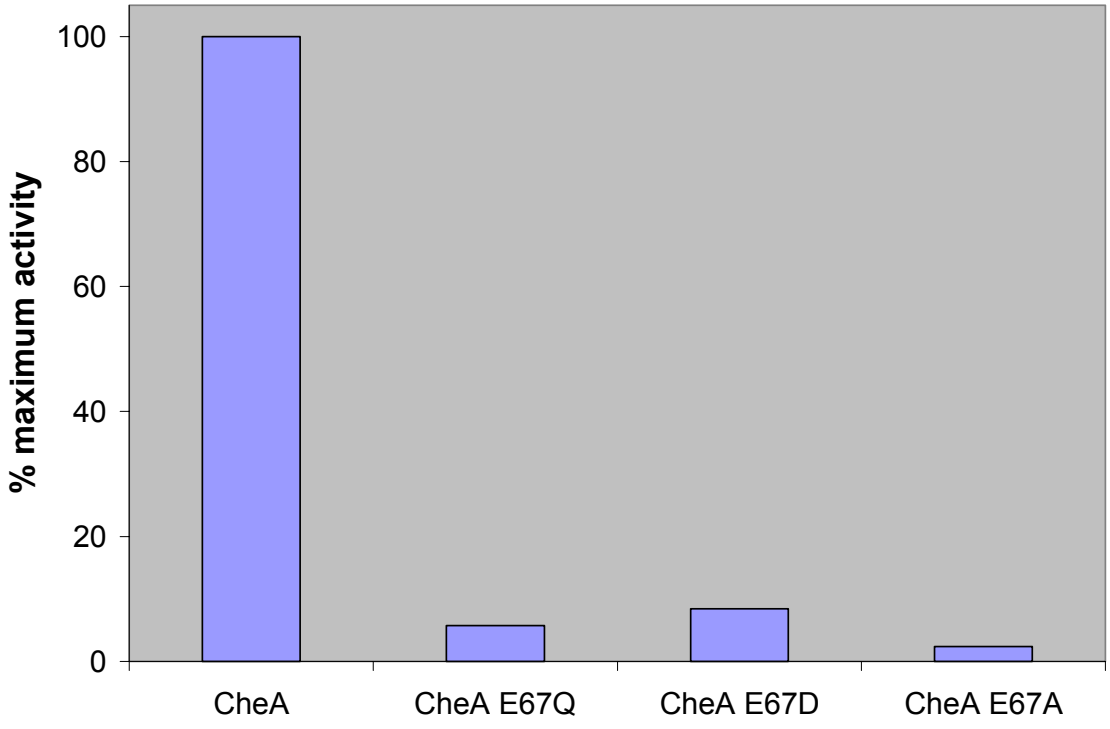
% maximum activity
100
80
60
40
20
0
CheA
CheA E67Q
CheA E67D
CheA E67A

(b)

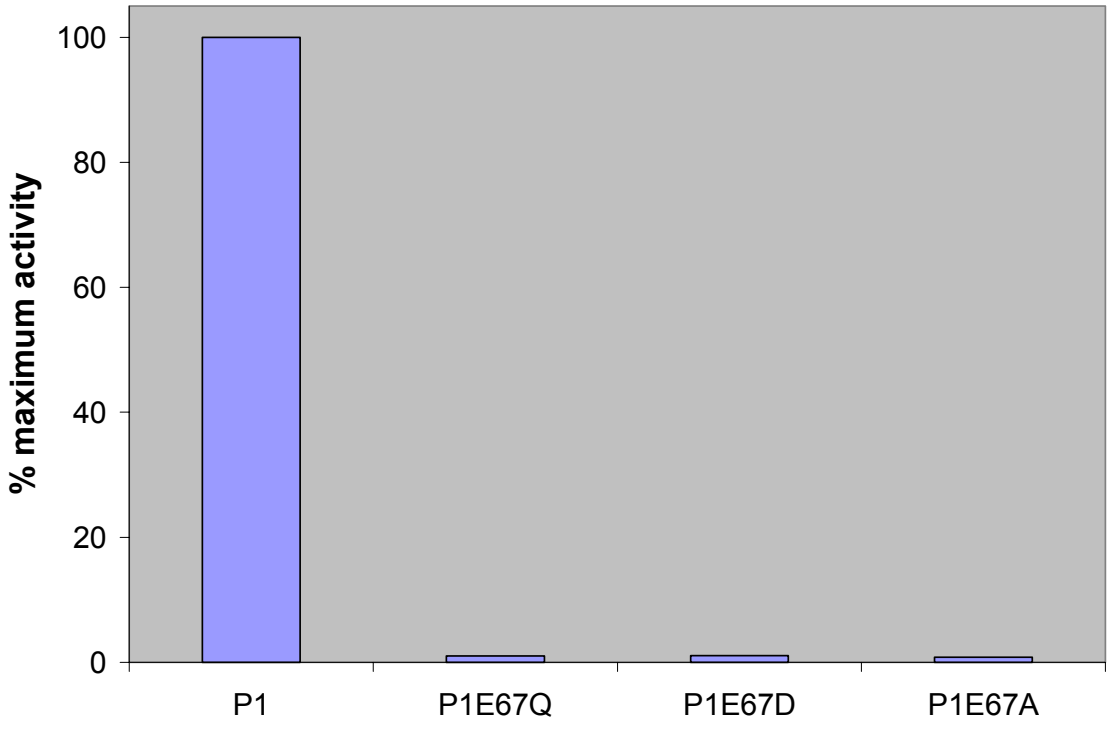
% maximum activity
100
80
60
40
20
0
P1
P1E67Q
P1E67D
P1E67A

Figure 2: (a) Swarm diameter of CheA and CheA E67 mutants. Photographs of swarm assays produced by (b) P1E67A, (c) P1E67D, (d) P1E67Q, and (e) CheA

(a)

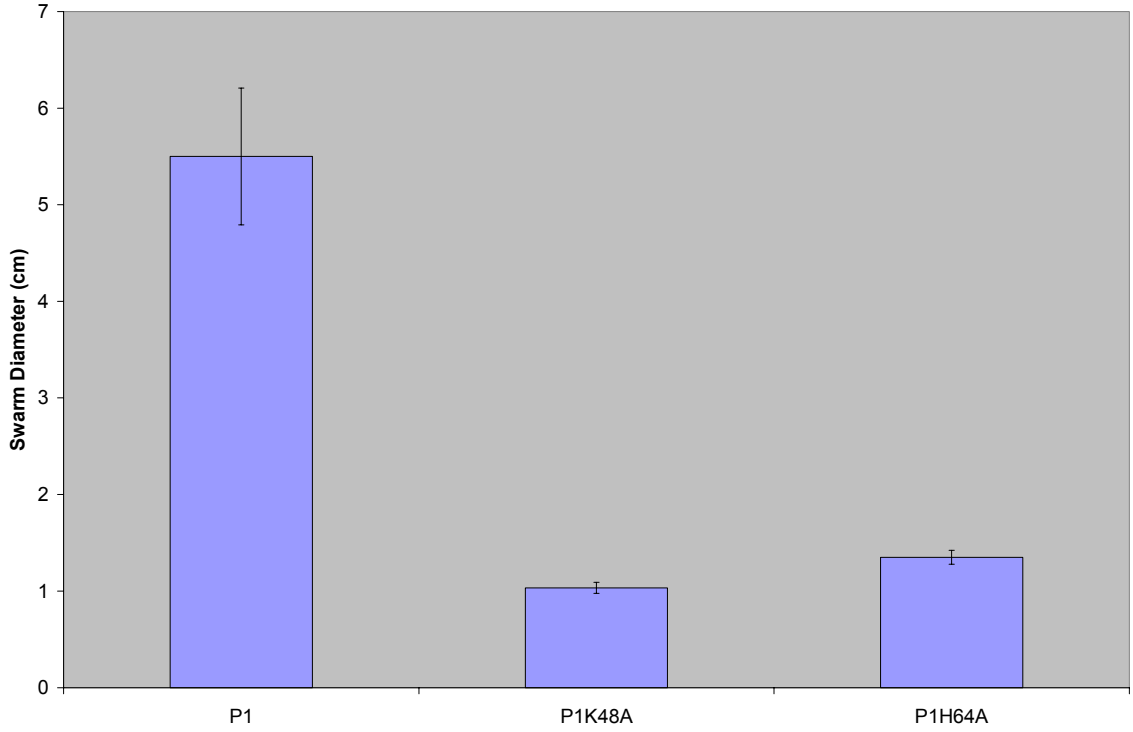

(b) P1E67A (c) P1E67D

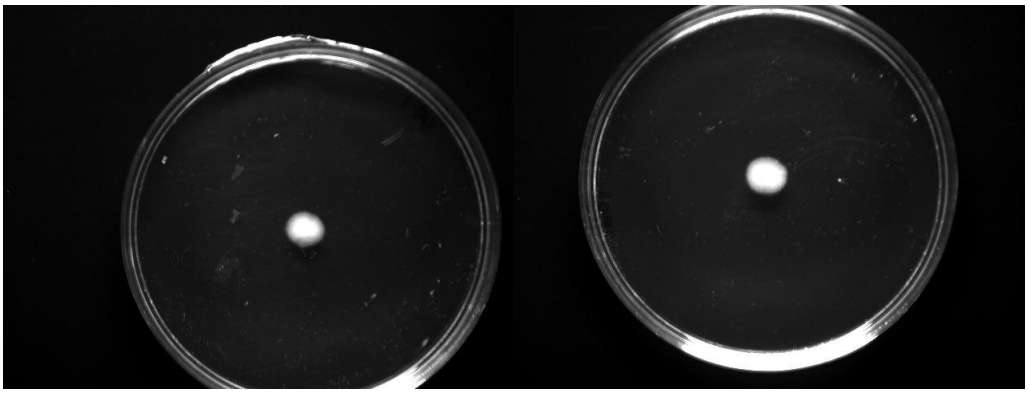

(d) P1E67Q (e) WT

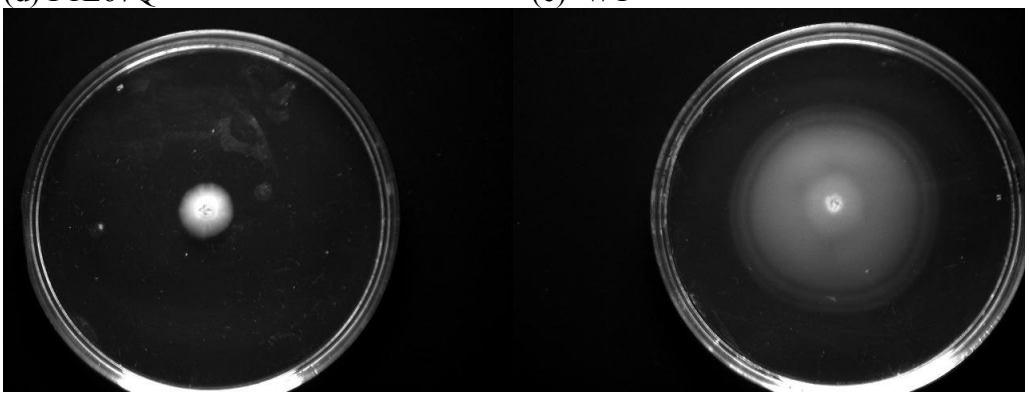

Figure 3: Phosphorylation of mutant proteins CheA E67Q, CheA E67D, and CheA E67A as a function of pH

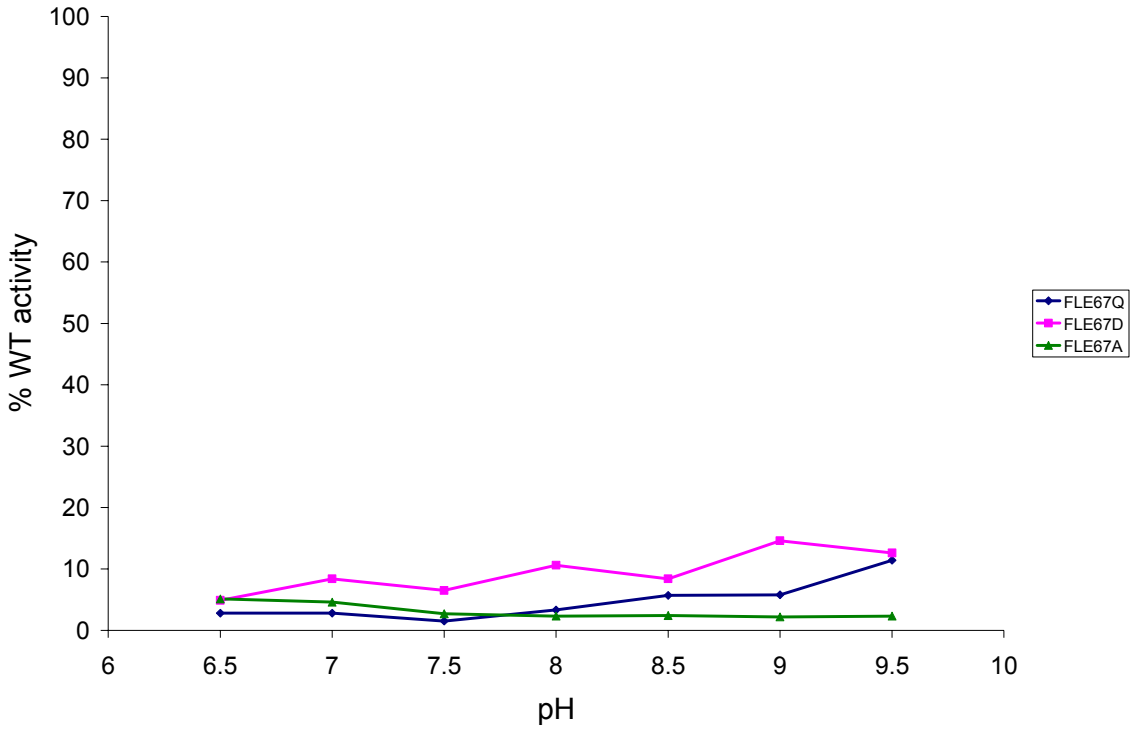
100
90
80
70
60
50
40
30
20
10
0
% WT activity
6
6.5
7
7.5
8
8.5
9
9.5
10
pH
FLE67Q
FLE67D
FLE67A

Figure 4: (a) Far UV-CD spectrum of P1 (diamonds) and P1E67Q (pink square) (b) P1(diamonds) and Δ289 are incubated in a tenfold excess of P1E67Q (squares) and BSA (triangles)

a.)

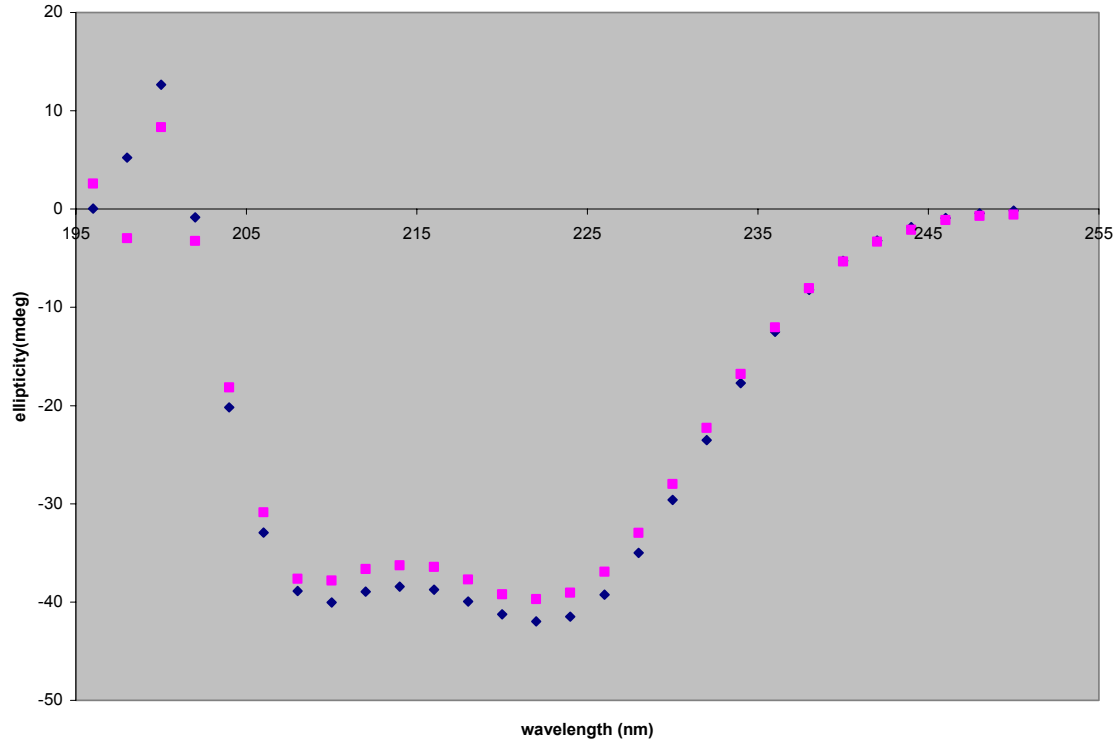
20
10
0
-10
-20
-30
-40
-50
195
205
215
225
235
245
255
ellipticity(mdeg)
wavelength (nm)

b.)

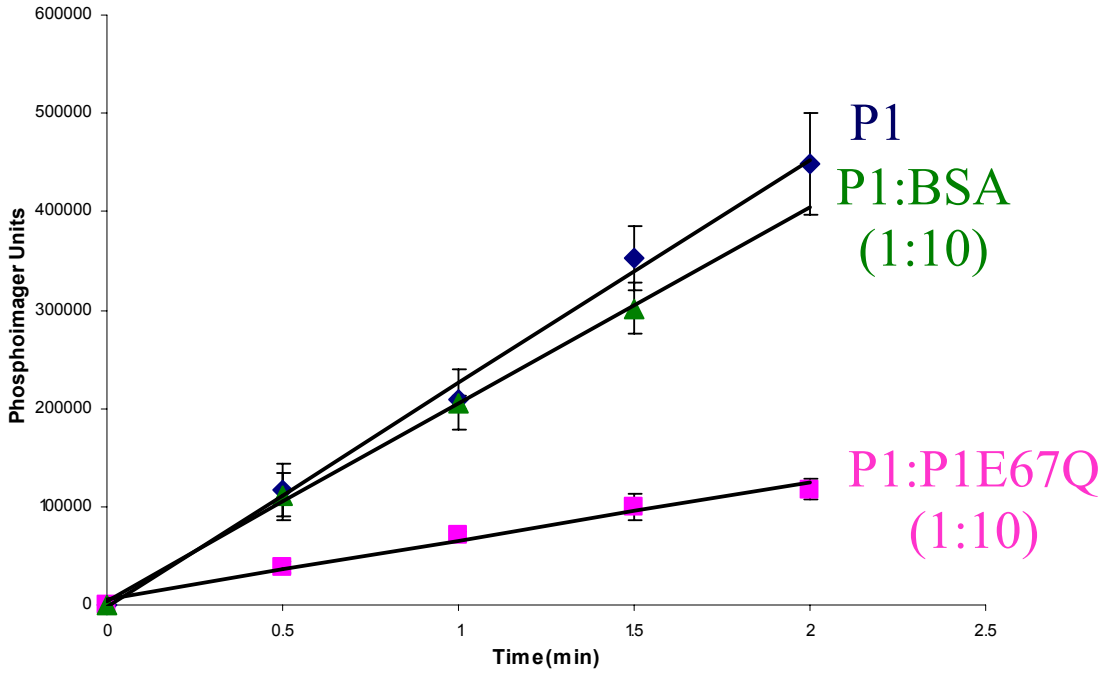
600000
500000
400000
300000
200000
100000
0
0
0.5
1
1.5
2
2.5
Phosphoimager Units
Time(min)
P1
P1:BSA
(1:10)
P1:P1E67Q
(1:10)

Figure 5: 2Fo-Fc electron density map of the 1.1Å structure of P1E67Q. The map is contoured to 2.2σ and 3.2σ.

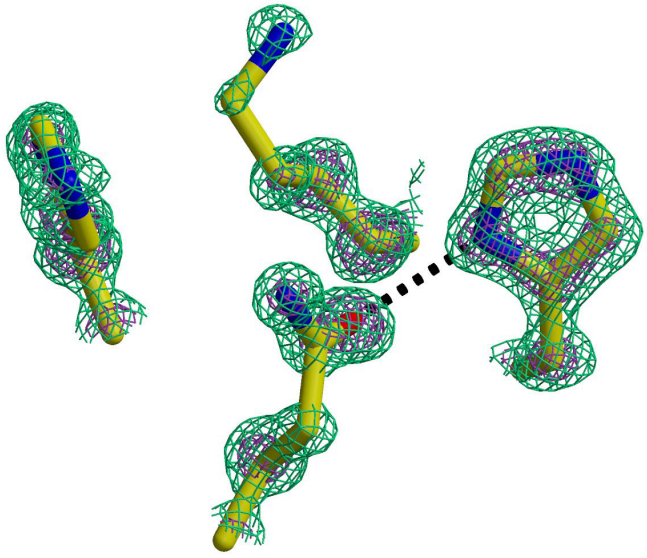

Figure 6: A conservative point mutation disrupts the native hydrogen bonding network of P1

a.)

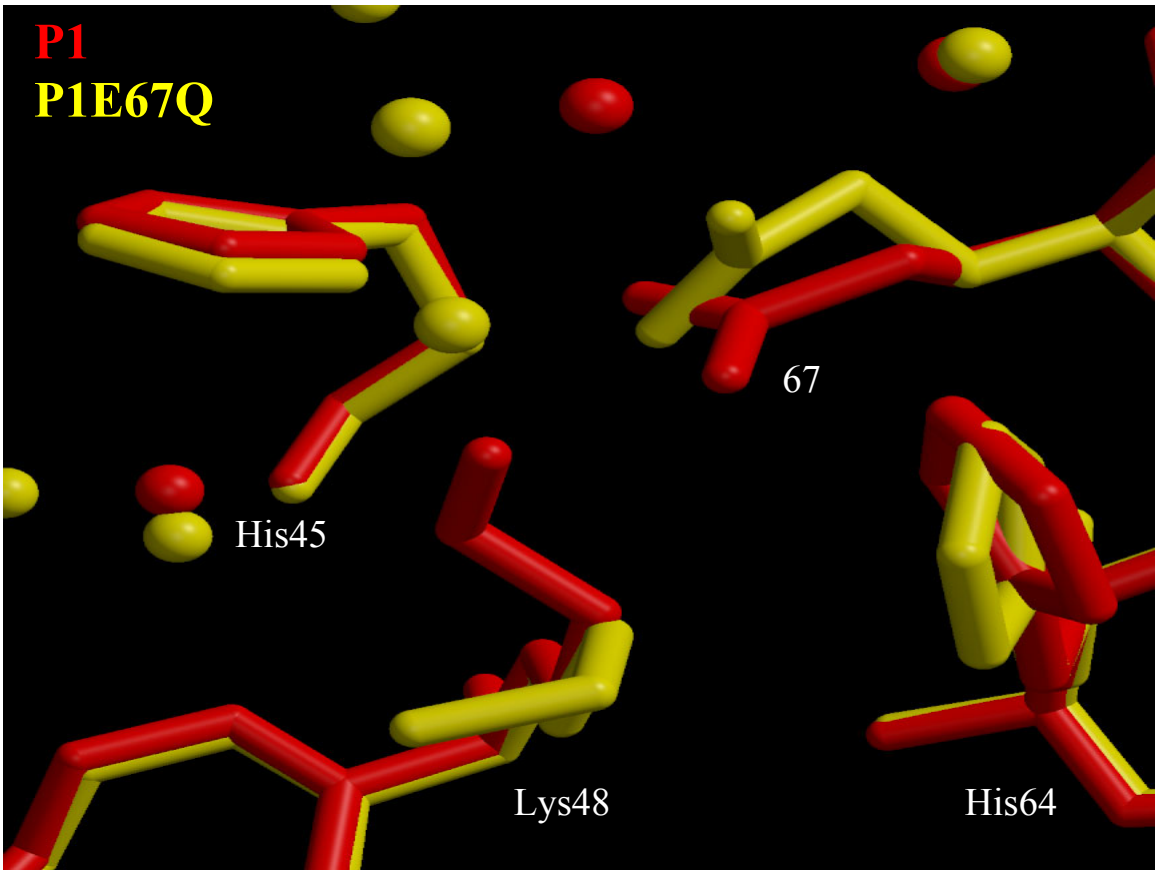
P1
P1E67Q
67
His45
Lys48
His64

b.)

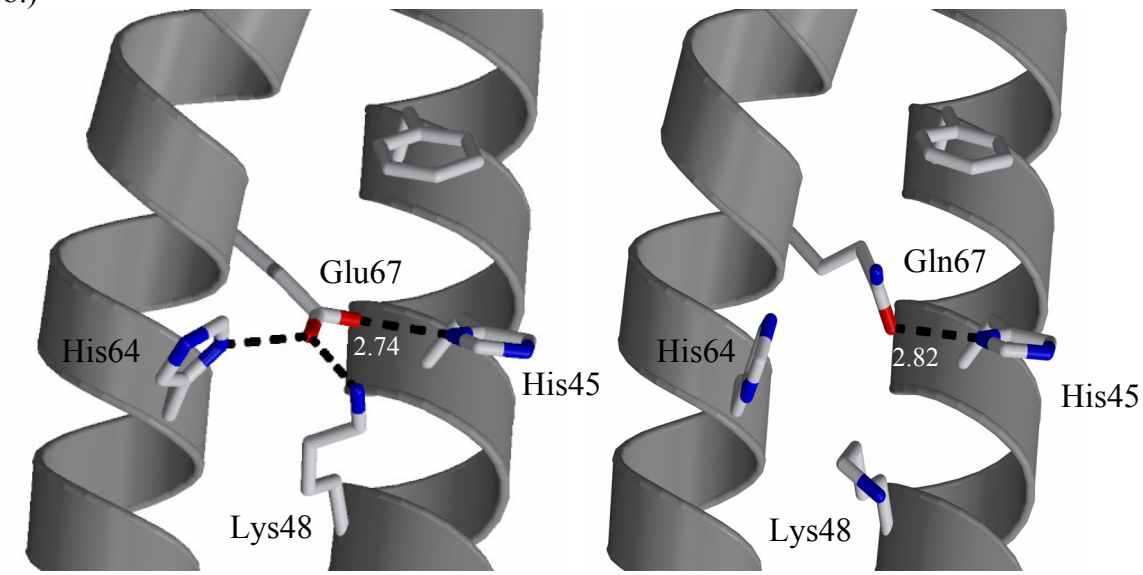
Glu67
His64
2.74
His45
Lys48
Gln67
His64
2.82
His45
Lys48

Figure 7: ^{15}N chemical shifts of P1E67Q (a) His45 (b) His64 and (c) HisTag

(a)

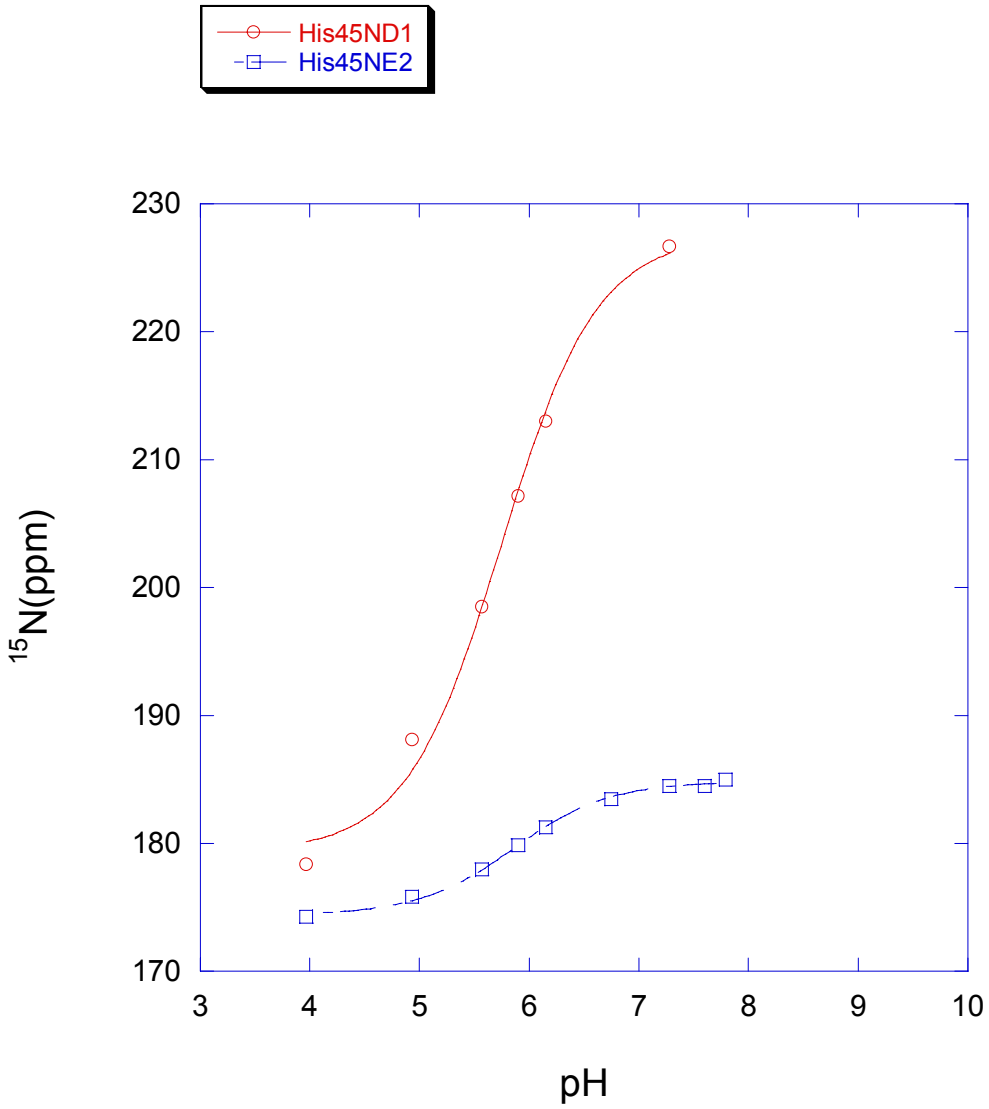
His45ND1
His45NE2
230
220
210
200
190
180
170
3
4
5
6
7
8
9
10
^{15}N(ppm)
pH

(b)

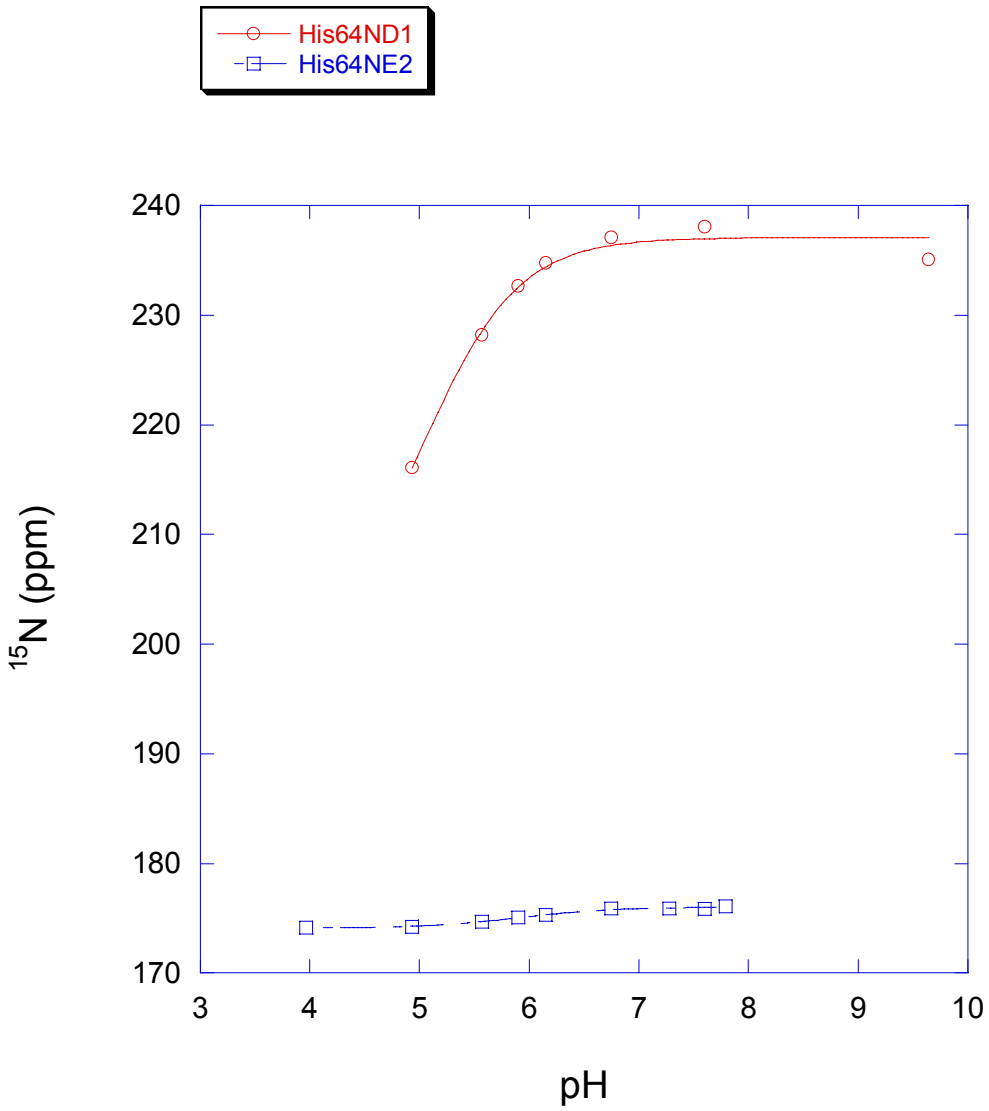
His64ND1
His64NE2
240
230
220
210
200
190
180
170
^{15}N (ppm)
3
4
5
6
7
8
9
10
pH

(c)

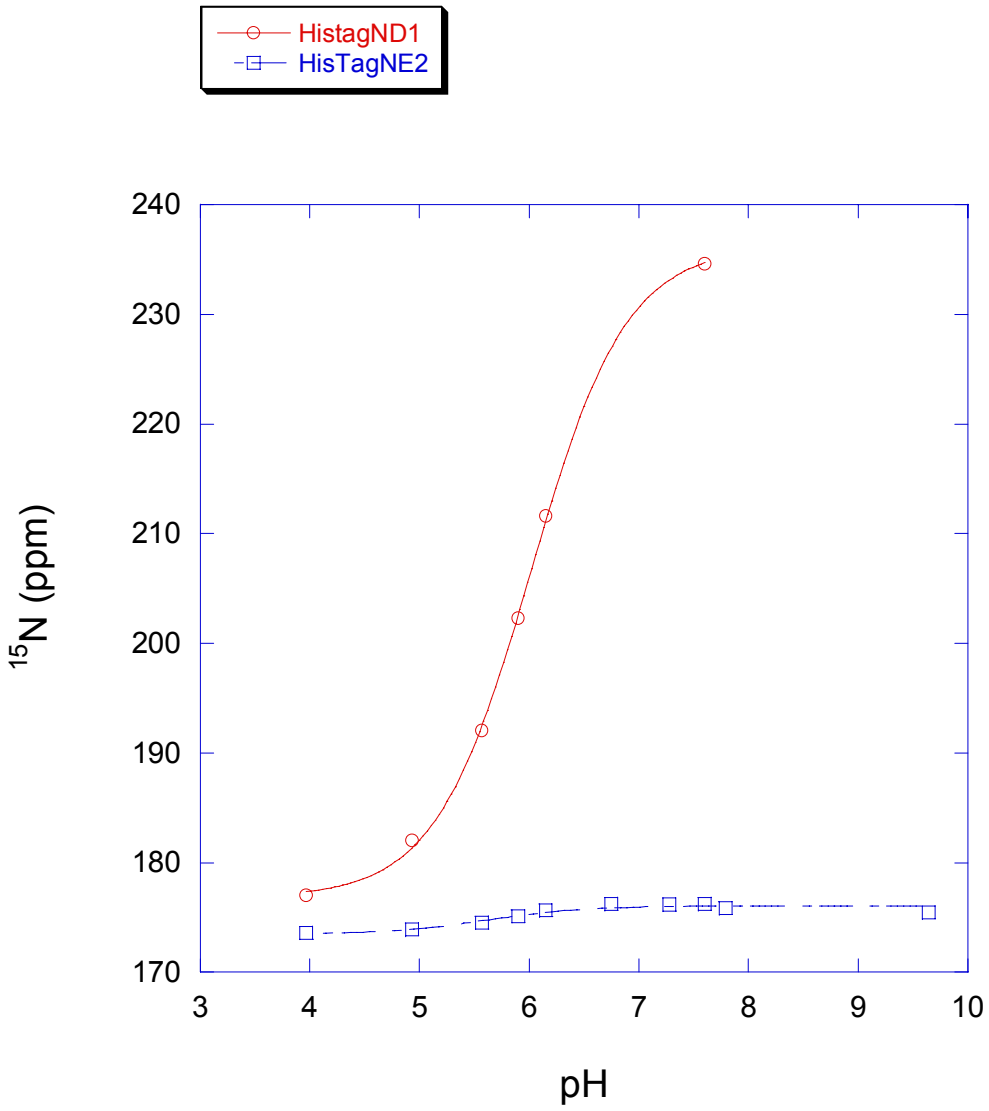
HistagND1
HisTagNE2
240
230
220
210
200
190
180
170
^{15}N (ppm)
3
4
5
6
7
8
9
10
pH

Figure 8: Critical residues to the CheA autophosphorylation reaction are located in the (a) P1 and (b) P4 domains.

(a)

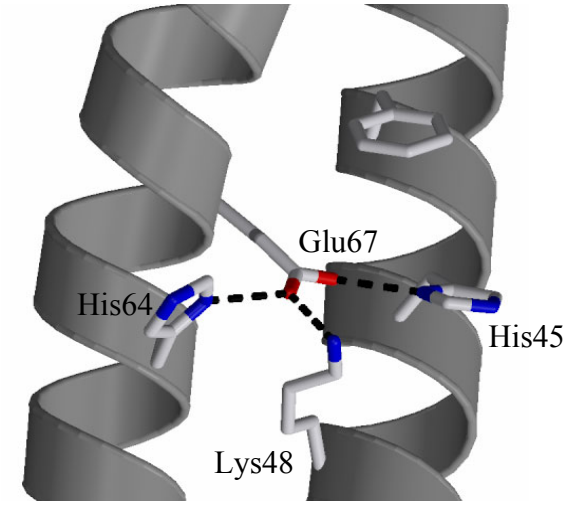
Glu67
His64
His45
Lys48

(b)

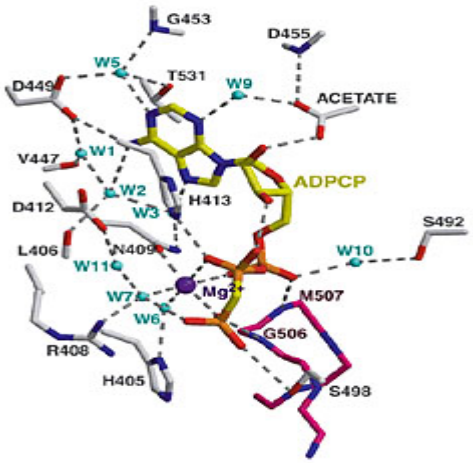
G453
D455
W5
T531
W9
D449
ACETATE
V447
W1
ADPCP
W2
H413
D412
W3
S492
L406
N409
W10
W11
W7
Mg
M507
W6
G506
R408
H405
S498

REFERENCES

1. Parkinson, J.S. and E.C. Kofoid, *Communication modules in bacterial signaling proteins.* Annu. Rev. Genet., 1992. **26**: p. 71-112.

2. Stock, A.M., V.L. Robinson, and P.N. Goudreau, *Two-component signal transduction.* Annu. Rev. Biochem., 2000. **69**: p. 183-215.

3. Inouye, M. and R. Dutta, eds. *Histidine Kinases in Signal Transduction*. 2003, Academic Press. 520.

4. Bilwes, A., et al., *Structure of CheA, a Signal-Transducing Histidine Kinase.* Cell, 1999. **96**: p. 131-141.

5. Bilwes, A.M., et al., *Nucleotide binding by the histidine kinase CheA.* Nature Structural Biology, 2001. **8**(4): p. 353-360.

6. Jackson, A.P. and A. Maxwell, *Identifying the catalytic residue of the ATPase reaction of DNA gyrase.* Proceedings of the National Academy of Sciences, 1993. **90**: p. 11232-11236.

7. Conley, M.P., et al., *pH Dependence of CheA Autophosphorylation in Escherichia coli.* Journal of Bacteriology, 1994. **176**(13): p. 3870-3877.

8. Zhou, H. and F.W.Dahlquist, *Phosphotransfer site of the Chemotaxis-Specific Protein Kinase CheA as Revealed by NMR.* Biochemistry, 1997. **36**: p. 699-710.

9. Zhou, H., et al., *NMR Studies of the Phosphotransfer Domain of the Histidine Kinase CheA from Escherichia coli: Assignments, Secondary Structure, General Fold, and Backbone Dynamics.* Biochemistry, 1995. **34**: p. 13858-13870.

10. Mourey, L., et al., *Crystal Structure of the CheA Histidine Phosphotransfer Domain that Mediates Response Regulator Phosphorylation in Bacterial Chemotaxis.* The Journal of Biological Chemistry, 2001. **276**(33): p. 31074-31082.

11. Otwinowski, A. and W. Minor, *Processing of X-ray diffraction data in oscillation mode.* Methods in Enzymolozy, 1997. **276**: p. 307-325.

12. Perrakis, A., R. Morris, and V.S. Lamzin, *Automated protein model building combined with iterative structure refinement.* Nature Structural Biology, 1999. **6**(5): p. 458-463.

13. Sheldrick, G.M. and T.R. Schneider, *SHELXL:high resolution refinement.* Methods in Enzymology, 1997. **277**: p. 319-343.

14. McRee, D.E., *XtalView: a visual protein crystallographic software system for X11/Xview.* J. Mol. Graph., 1992. **10**: p. 44-47.

15. Zhang, O.W., et al., *Backbone H-1 and N-15 Resonance Assignments of the N-Terminal Sh3 Domain of Drk in Folded and Unfolded States Using Enhanced-Sensitivity Pulsed-Field Gradient Nmr Techniques.* Journal of Biomolecular Nmr, 1994. **4**(6): p. 845-858.

16. Marion, D., et al., *Rapid Recording of 2d Nmr-Spectra without Phase Cycling - Application to the Study of Hydrogen-Exchange in Proteins.* Journal of Magnetic Resonance, 1989. **85**(2): p. 393-399.

17. Roberts, J.D., et al., *A N-15 Nuclear Magnetic-Resonance Study of the Acid-Base and Tautomeric Equilibria of 4-Substituted Imidazoles and Its Relevance to the Catalytic Mechanism of Alpha-Lytic Protease.* Journal of the American Chemical Society, 1982. **104**(14): p. 3945-3949.

18. Munowitz, M., et al., *Acid-Base and Tautomeric Equilibria in the Solid-State - N-15 Nmr-Spectroscopy of Histidine and Imidazole.* Journal of the American Chemical Society, 1982. **104**(5): p. 1192-1196.

19. Harbison, G., J. Herzfeld, and R.G. Griffin, *N-15 Chemical-Shift Tensors in L-Histidine Hydrochloride Monohydrate.* Journal of the American Chemical Society, 1981. **103**(16): p. 4752-4754.

20. Blomberg, F., W. Maurer, and H. Ruterjans, *Nuclear Magnetic-Resonance Investigation of N-15-Labeled Histidine in Aqueous-Solution.* Journal of the American Chemical Society, 1977. **99**(25): p. 8149-8159.

21. Witanowski, M., et al., *Nitrogen-14 Nuclear Magnetic-Resonance of Azoles and Their Benzo Derivatives.* Tetrahedron, 1972. **28**(3): p. 637-653.

22. Pelton, J.G., et al., *Tautomeric States of the Active-Site Histidines of Phosphorylated and Unphosphorylated Iii(Glc), a Signal- Transducing Protein from Escherichia-Coli, Using 2-Dimensional Heteronuclear Nmr Techniques.* Protein Science, 1993. **2**(4): p. 543-558.

23. Bachovchin, W.W., *N-15 Nmr-Spectroscopy of Hydrogen-Bonding Interactions in the Active-Site of Serine Protease - Evidence for a Moving Histidine Mechanism.* Biochemistry, 1986. **25**(23): p. 7751-7759.

24. Schuster, II and J.D. Roberts, *N-15 Nuclear Magnetic-Resonance Spectroscopy - Effects of Hydrogen-Bonding and Protonation on Nitrogen Chemical-Shifts in Imidazoles.* Journal of Organic Chemistry, 1979. **44**(22): p. 3864-3867.

25. Reynolds, W.F. and C.W. Tzeng, *Determination of Preferred Tautomeric Form of Histamine by C-13 Nmr-Spectroscopy.* Canadian Journal of Biochemistry, 1977. **55**(5): p. 576-578.

26. Wolfe, A. and H. Berg, *Migration of bacteria in semisolid agar.* Proceedings of the National Academy of Sciences, 1989. **86**: p. 6973-6977.

27. Ikegami, T., et al., *Solution Structure and Dynamic Character of the Histidine-Containing Phosphotransfer Domain of Anaerobic Sensor Kinase ArcB from Escherichia coli.* Biochemistry, 2001. **40**: p. 375-386.

28. Xu, Q. and A.H. West, *Conservation of Structure and Function Among Histidine-containing Phosphotransfer (HPt) Domains as Revealed by the Crystal Structure of YPD1.* Journal of Molecular Biology, 1999. **292**: p. 1039-1050.

29. McEvoy, M.M., et al., *Nuclear Magnetic Resonance Assignments and Global Fold of a CheY-Binding Domain in CheA, the Chemotaxis-Specific Kinase of Escherichia coli.* Biochemistry, 1995. **34**: p. 13871-13880.

30. Tawa, P. and R.C. Stewart, *Kinetics of Chea Autophosphorylation and Dephosphorylation Reactions.* Biochemistry, 1994. **33**(25): p. 7917-7924.

31. Swanson, R.V., S.C. Schuster, and M.I. Simon, *Expression of Chea Fragments Which Define Domains Encoding Kinase, Phosphotransfer, and Chey Binding Activities.* Biochemistry, 1993. **32**(30): p. 7623-7629.

32. Levit, M., et al., *Active site Interference and Asymmetric Activation in the Chemotaxis Protein Histidine Kinase CheA.* The Journal of Biological Chemistry, 1996. **271**(50): p. 32057-32063.

33. Tawa, P. and R.C. Stewart, *Mutational Activation of Chea, the Protein-Kinase in the Chemotaxis System of Escherichia-Coli.* Journal of Bacteriology, 1994. **176**(14): p. 4210-4218.

34. Hirschman, A., et al., *Active Site Mutations in CheA, the Signal-Transducing Protein Kinase of the Chemotaxis System in Escherichia coli.* Biochemistry, 2001. **40**: p. 13876-13887.

35. Morrison, T.B. and J.S. Parkinson, *A fragment liberated from the Escherichia coli CheA kinase that blocks stimulatory, but not inhibitory, chemoreceptor signaling.* Journal of Bacteriology, 1997. **179**(17): p. 5543-5550.

36. Ellefson, D.D., U. Weber, and A.J. Wolfe, *Genetic analysis of the catalytic domain of the chemotaxis- associated histidine kinase CheA.* Journal of Bacteriology, 1997. **179**(3): p. 825-830.

37. Bourret, R.B., J. Davagnino, and M.I. Simon, *The Carboxy-Terminal Portion of the Chea Kinase Mediates Regulation of Autophosphorylation by Transducer and Chew.* Journal of Bacteriology, 1993. **175**(7): p. 2097-2101.

38. Kato, M., et al., *Refined structure of the histidine-containing phosphotransfer (HPt) domain of the anaerobic sensor kinase ArcB from Escherichia coli at 1.57A resolution.* Acta Crystallographica, 1999. **D55**: p. 1842-1849.

39. Kato, M., et al., *Insights into Multistep Phosphorelay from the Crystal Structure of the C-Terminal HPt Domain of ArcB.* Cell, 1997. **88**: p. 717-723.

40. Jones, B.E., P. Rajagopal, and R.E. Klevit, *Phosphorylation on histidine is accompanied by localized structural changes in the phosphocarrier protein, HPr from Bacillus subtilis.* Protein Science, 1997. **6**(10): p. 2107-2119.

41. vanNuland, N.A.J., et al., *Phosphorylation-induced torsion-angle strain in the active center of HPr, detected by NMR and restrained molecular dynamics refinement.* Protein Science, 1996. **5**(3): p. 442-446.

42. Pullen, K., et al., *Phosphorylation of Serine-46 in Hpr, a Key Regulatory Protein in Bacteria, Results in Stabilization of Its Solution Structure.* Protein Science, 1995. **4**(12): p. 2478-2486.

43. Vannuland, N.A.J., et al., *High-Resolution Structure of the Phosphorylated Form of the Histidine-Containing Phosphocarrier Protein Hpr from Escherichia-Coli Determined by Restrained Molecular-Dynamics from Nmr-Noe Data.* Journal of Molecular Biology, 1995. **246**(1): p. 180-193.

44. Rajagopal, P., E.B. Waygood, and R.E. Klevit, *Structural Consequences of Histidine Phosphorylation - Nmr Characterization of the Phosphohistidine Form of Histidine- Containing Protein from Bacillus-Subtilis and Escherichia-Coli.* Biochemistry, 1994. **33**(51): p. 15271-15282.

45. Pelton, J.G., et al., *Structural Comparison of Phosphorylated and Unphosphorylated Forms of Iii(Glc), a Signal-Transducing Protein from Escherichia-Coli, Using 3-Dimensional Nmr Techniques.* Biochemistry, 1992. **31**(22): p. 5215-5224.

46. Matsushika, A. and T. Mizuno, *Mutational analysis of the histidine-containing phosphotransfer (HPt) signaling domain of the ArcB sensor in Escherichia coli.* Bioscience Biotechnology and Biochemistry, 1998. **62**(11): p. 2236-2238.

47. Janiak-Spens, F. and A.H. West, *Functional roles of conserved amino acid residues surrounding the phosphorylatable histidine of the yeast phosphorelay protein YPD1.* Molecular Microbiology, 2000. **37**(1): p. 136-144.

48. Sculimbrene, B.R., A.J. Morgan, and S.J. Miller, *Enantiodivergence in small-molecule catalysis of asymmetric phosphorylation: Concise total syntheses of the enantiomeric D- myo-inositol-1-phosphate and D-myo-inositol-3-phosphate.* Journal of the American Chemical Society, 2002. **124**(39): p. 11653-11656.

49. Sculimbrene, B.R. and S.J. Miller, *Discovery of a catalytic asymmetric phosphorylation through selection of a minimal kinase mimic: A concise total synthesis of D-myo-inositol-1-phosphate.* Journal of the American Chemical Society, 2001. **123**(41): p. 10125-10126.

50. Laskowski, R.A., et al., *PROCHECK: a program to check the stereochemical quality of protein structures.* J. Appl. Crystallogr., 1993. **26**: p. 283-291.

Chapter 4

Mutations in the conserved hydrogen bonding network of the CheA histidine phosphotransfer domain

In-depth structural and biochemical studies of the kinase domain have identified amino acids involved in CheA autokinase activity and ATP binding [1, 2]. Since the phosphotransfer domain P1 completes the CheA active site, we are interested in further elucidating the functions of key residues in this domain. As an extension to previous NMR [3] and crystallographic studies [4], our laboratory solved an atomic resolution structure of the phosphotransfer domain from the *T. maritima* organism (Chapter 2). A hydrogen bonding network between residues His45, Glu67, Lys48, and His64 was identified. Since these residues are highly conserved in a domain that exhibits low sequence similarity, it is of interest to evaluate their contributions to the CheA autophosphorylation reaction.

Prior NMR studies revealed the phosphoaccepting histidine, His45, exists in the normally unfavored $N^{\delta 1}H$ tautomeric state and exhibits a pKa of 7.8 [5]. This value is unusually high compared to a pKa of approximately 6.9 for a solvent exposed histidine at room temperature [6]. These atypical chemical properties were attributed to the formation of a hydrogen bond between the $N^{\delta 1}H$ atom of His45 and an unknown residue. Based on the structural and sequence similarities between CheA and the ATPase GyrB, a conserved glutamate residue that is postulated to play a key role in the cleavage of the γ-phosphoryl group in GyrB was hypothesized to be located in the P1 domain [2, 7]. Subsequent crystal structure analysis of the phosphotransfer domain confirmed the existence of a hydrogen bond between the $N^{\delta 1}H$ atom of His45 and Glu67 [4] (Chapter2).

Furthermore, a thorough characterization of the conserved Glu67 revealed that it is not only critical to the CheA autophosphorylation reaction but also necessary for the stabilization of the $N^{\delta 1}H$ histidine tautomer and the preservation of an altered pKa

(Chapter 3). The conservative mutation, E67Q, promotes a change in the tautomeric state of the phosphoaccepting histidine to the $N^{\varepsilon 2}H$ species and lowers the pKa by approximately one pH unit (Chapter 3 Figure 7a). These changes in the chemical properties of the histidine residue result in dramatically reduced phosphorylation activity. Hence, the active site histidine must exist in the correct tautomer in order for it to be phosphorylated.

We continue to examine the structural, biochemical, and electronic consequences of disrupting members of the conserved hydrogen bonding network. The native P1 structure shows that Glu67 additionally acts as a hydrogen bond acceptor to two other conserved residues, Lys48 and His64. In this chapter, mutagenic and biophysical studies within the context of mutant crystal structures are used to define the functional roles of Lys48 and His64 in the catalytic mechanism of CheA.

MATERIALS AND METHODS

Cloning, expression, and purification

T. maritima CheA (residues 1-671), Δ289 (residues 290-671), domain P1 (residues 4-133), and a fragment of domain P1 termed $P1_{short}$ (residues 4-105) were subcloned in the vector pET28(a) (Novagen). Alanine mutants of Lys48 and His64 were generated using Quickchange mutagenesis (Stratagene). Proteins were expressed in *E.coli* strain BL21(DE3) (Novagen) in 2L TB cultures and purified by affinity chromatography on Nickel-NTA beads (Qiagen), followed by thrombin digestion and gel filtration as described in the Materials and Methods section of Chapter 2.

Phosphorylation assays

Initial velocities of full length CheA, CheA K48A, CheA H64A, and CheA E67Q, each at a protein concentration of 2 μM, were measured in 50 mM Tris pH 8.5, 50 mM KCl, 5 mM $MgCl_2$, and 2 mM DTT at 50°C. The initial velocities of full length CheA and CheA H64A were also compared to one another at room temperature in the same buffer at pH 7.5. Reactions were initiated upon addition of [γ-^{32}P] ATP. The phosphorylation assays were carried out in the same manner as described in the Materials and Methods section of Chapter 3.

Swarm assays

Bacterial strain RP9535, lacking the CheA gene, was transformed with pAR1:cheA derivatives expressing wild-type CheA, CheA K48A, or CheA H64A. Tryptone swarm plates were stabbed with the transformants and incubated at 37ºC for 12 hours as described in the Materials and Methods section of Chapter 3.

Circular dichroism measurements

Far UV CD spectra were recorded with an AVIV (Lakewood, NJ) 62A DS spectrometer equipped with a Peltier-type temperature control system and using a 0.1cm quartz cuvette (Wilmad). P1K48A, P1H64A, and P1 were at a concentration of 20 μM in 20 mM sodium phosphate buffer at pH 8.0. Protein concentrations were determined by UV spectrophotometry using extinction coefficients calculated from the number of tryptophan and tyrosine residues present in each protein [8]. Data were collected

between 250 to 190nm using an averaging time of 5 seconds and a bandwidth of 1.5nm at 25ºC.

Determination of phosphohistidine stability

The autophosphorylation reaction of CheA and its mutants was initiated with [γ-^{32}P] ATP as described above. After adequate phosphorylation levels were achieved, the reaction was quenched using 2X sodium dodecyl sulfate (SDS) electrophoresis buffer containing 25 mM ethylenediaminetetra acetic acid (EDTA). The reaction tube was kept at 50°C and aliquots were taken and placed at 4°C at designated time points. Samples were then electrophoresed and processed as described in the Materials and Methods section of Chapter 3.

Crystallization, data collection, and structure refinement

Orthorhombic crystals belonging to the $P222_1$ space group of $P1K48A_{short}$ and $P1H64A_{short}$ were obtained via the hanging drop method of crystallization. The protein fragments used for crystallization were composed of residues 4 -104 of the CheA histidine phosphotransfer domain. Crystals were generated by mixing 2 μL of 7-15 mg/ml protein with 2 μL of reservoir solution (32% PEG 4K, 0.1M NaAc pH 4.5, 0.2M AmAc for $P1K48A_{short}$; 30% PEG 4K, 0.1M NaAc pH 4.5, 0.2M AmAc for $P1H64A_{short}$).

Diffraction data were collected on the A1 beamline at the Cornell High Energy Synchrotron Source (CHESS) using a wavelength of 0.9363Å. $P1K48A_{short}$ and $P1H64A_{short}$ crystals diffracted to 1.38Å and 1.4Å, respectively. Data were processed, scaled, and reduced using the DENZO/SCALEPACK suite of programs [9]. The cell

dimensions of P1K48A$_{short}$ are x= 27.680Å, y= 37.627Å, and z=87.517Å. The cell dimensions of P1H64A$_{short}$ are x=27.567Å, y=37.618Å, and z= 87.402Å. The structures of each mutant were refined using SHELXL [10] and the model manually rebuilt in XtalView [11] as described in the Materials and Methods section of Chapter 3. Details of data collection and refinement can be found in Table 1.

General NMR methods and data analysis

Uniformly ^{15}N labeled protein P1K48A and P1H64A was expressed and used to collect NMR data on 500 and 600 MHz Varian UNITY and Inova spectrometers, respectively. These instruments were equipped with ^{1}H [^{13}C/^{15}N] pulsed-field gradient probes. Assignment of specific histidine side chain resonances was done by comparison to wild type values obtained elsewhere (Hamel et al. unpublished results). Procedures and parameters used for 3D ^{15}N-NOESY-HSQC, 2D HSQC-aliphatic and 2D HSQC-aromatic correlation experiments over a pH range of 3.5 to 9.8 are described in the Materials and Methods section of Chapter 3 [12, 13]. The analysis of the NMR data can also be found there.

RESULTS

Mutations of residues involved in the hydrogen bond network inhibit phosphotransfer

Amino acid residues that participate in the conserved hydrogen bond network were mutated. The activities of CheA, CheA K48A, CheA H64A, and CheA E67Q were first compared *in vitro* at 50°C and pH 8.5. The activity of wild type CheA was too rapid to be measured under these conditions. However, it was possible to obtain the relative

levels of mutant phosphorylation (Figure 1a). CheA H64A is approximately 15-fold faster than K48A and roughly 270-fold faster than E67Q. At pH 7.5 and room temperature, the initial velocity of wild type CheA is approximately 60-fold faster than CheA H64A (Figure 1b). The chemotaxis ability of *E. coli* mutants CheA K48A and CheA H64A were also assessed *in vivo*. Swarm assays show that the chemotaxis signaling network cannot tolerate mutations of K48 and H64 (Figure 2).

To assess whether these mutations perturbed the secondary structure of the phosphotransfer domain, we compared the far UV CD spectra of P1H64A and P1K48A to the wild type P1. The results indicate that P1H64A and P1 have similar spectra (Figure 3a). However, P1K48A has lost some secondary structure content (Figure 3b), suggesting that this residue may play a role in stabilizing the helical conformation of the P1 domain.

In order to determine whether despite the observed structural perturbance, P1K48A could still recognize the CheA kinase domain, it was incubated in a 10-fold excess in the presence of P1 and the catalytic fragment Δ289 at room temperature, where its activity is minimal. P1K48A is indeed capable of inhibiting the phosphorylation of wild type P1 by Δ289. The wild type reaction is inhibited by over 50% in the presence of P1K48A (Figure 4).

To further explore putative roles for residues involved in the hydrogen bonding network, their involvement in stabilizing the phosphohistidine complex was investigated. Phospho-labeled CheA and mutants were generated by incubation with [γ-^{32}P] ATP. The reaction was quenched and the phosphorylation level monitored over a period of three hours. The stability of the phosphoramidate bond is not affected by mutations at Lys48,

His64, or Glu67 over this time frame (Figure 5). It is therefore unlikely that these residues directly interact with the phosphate.

Lys48 and His64 contribute to the structural integrity of the active site region.

In order to fully characterize P1K48A and P1H64A, a structural analysis of these mutants was performed. Here we report the crystal structures of P1K48A$_{short}$ and P1H64A$_{short}$. The quality of the data and refinement are summarized in Tables 1 and 2. Neither of these mutations disrupt the general four-helix bundle fold observed in the wild type P1 [3, 4] (Chapter 2 Figure 3). However, as described below, the area surrounding the phosphoaccepting histidine is structurally altered.

The replacement of Lys48 with an alanine disrupts the positions of two other members of the hydrogen bonding network, Glu67 and His64 (Figure 6a). The discontinuous electron density for these side chains reflects prevalent disorder. The conformation of Glu67 that we were able to model revealed that the side chain orientation has swiveled. However, it is still capable of accepting a hydrogen bond from His45. The structural properties of His64 are also affected by the K48A mutation. His64 exists in at least two alternate conformations, and no longer hydrogen bonds to Glu67. Lys48 therefore appears to fix the orientation of Glu67 and His64. An overlay of the P1K48A$_{short}$ and native P1 structure surprisingly revealed that the position of the phosphoaccepting histidine, His45, remains the same (Figure 6b).

The structural changes incurred by the H64A mutation are not as disruptive as those observed for K48A (Figure 7a). The P1H64A$_{short}$ structure revealed that Glu67 is hydrogen bonded to the $N^{\delta 1}$ atom of His45, but exists in a slightly different position.

However, substitution of the His64 side chain for an alanine results in a broken salt bridge between Lys48 and Glu67 due to displacement of the Lys48 side chain. The orientation of His45 oncemore remains unchanged (Figure 7b).

Chemical properties of the phosphoaccepting histidine in the mutants K48A and H64A

Alanine substitutions for Lys48 and His64 both diminish the autophosphorylation of CheA; but do they affect the reactivity of the phosphoaccepting histidine as previously documented for Glu67 (Chapter 3). NMR spectroscopy is ideally suited to study the electronic properties of histidine residues. To further explore the functional roles of Lys48 and His64, the HSQC spectra [14] of ^{15}N labeled proteins at several pH values were evaluated in the mutants P1K48A and P1H64A. Data points obtained from the histidine side chains were plotted as a function of pH and fit to equation 1 (Chapter 3) using least squares fitting. Relevant chemical shifts are listed in Table 2.

The titration curves for the $N^{\varepsilon 2}$ and $N^{\delta 1}$ resonances of the P1K48A His45 side chain are shown in Figure 8. The pKa value for the imidazole ring was determined to be 6.8. The larger shift of the $N^{\varepsilon 2}$ atom at high pH reveals that the $N^{\delta 1}H$ tautomer is dominant. This tautomer is stabilized through the hydrogen bond to Glu67. In fact, the $N^{\delta 1}$:$N^{\varepsilon 2}$ tautomeric ratio is 2.6:1, as observed for the native protein (Table 4) (Hamel, et al. unpublished results)[5].

Identical NMR experiments were performed on the P1H64A mutant. The resonances of the His45 imidazole side chain also demonstrate a dependence on pH (Figure 9). The phosphoaccepting histidine exhibits similar properties to the wild type. It possesses an altered pKa of 6.8 and its chemical shifts at high pH reveal the existence

of a predominantly $N^{\delta 1}H$ tautomeric state. The $N^{\delta 1}H$:$N^{\varepsilon 2}H$ ratio was calculated to be 2.6:1. The tautomeric and protonation states of each histidine is listed in Table 3 and compared to wild type protein and a previously characterized mutant P1E67Q (Chapter 3). The titration curves, chemical shifts, and tautomeric states of the remaining histidines in P1 can be found in Appendix 1.

DISCUSSION

The work presented in this paper has further elucidated the roles of conserved residues in the CheA phosphotransfer domain. By implementing mutagenesis studies, macromolecular protein crystallography, and two-dimensional NMR techniques, we have further investigated the functional roles of conserved residues in the phosphotransfer domain. The effects mutations at Lys48 and His64 exert on the structure of the P1 domain and on the chemical properties of the phosphoaccepting histidine are examined.

An intact hydrogen bond network optimizes the histidine phosphotransfer reaction

Mutagenic analysis of His64 revealed that it is the least disruptive of the mutants studied (Figure 1). Its secondary structure, as revealed by the far UV CD spectrum, remains intact (Figure 3a). The 1.4Å crystal structure demonstrated that the only major difference between the native and mutant structure is the position of the Lys48 side chain. Both the phosphoaccepting histidine, His45, and the activating Glu67 maintain their side chain orientation. 2-D NMR studies confirmed that the reactivity of His45 is unaltered. The phosphorylatable histidine exists in the normally unfavored $N^{\delta 1}H$ tautomeric state

possessing a $N^{\delta 1}H$:$N^{\varepsilon 2}H$ ratio that is very similar to that of the wild type (Table 3). Additionally, this mutation does not affect the stability of the phospho-histidine complex (Figure 5). Hence, the observed decrease in phosphorylation activity of the H64A mutant can be likely attributed to a decrease in binding affinity to the kinase domain.

The active site residues may form part of the binding interface to the kinase domain

Lys48 appears to play a critical role in stabilizing the active site structure. As demonstrated by CD and crystallography, Lys48 disrupts the secondary structure of the phosphotransfer domain (Figures 3b and 6). It is located towards the C-terminus of helix B and may play a role in stabilizing the negative charge of the helix dipole, thereby stabilizing the P1 helical structure. Its removal results in residue disorder, as shown by the alternate conformations of His64 and the discontinuous density for the His64 and Glu67 side chains.

Despite this disorder in the active site region, the phosphoaccepting histidine largely retains its original side chain orientation, and most importantly, its reactivity (Figures 6 and 8). It possesses the same properties as the wild type phosphoaccepting histidine, exhibiting an altered pKa of 6.8, and favoring the $N^{\delta 1}H$ tautomeric state. Furthermore, it is not involved in stabilizing the tautomeric state of the phosphorylated histidine. Together, these results imply that Lys48 does not contribute towards the k_{cat} of the autophosphorylation reaction. Instead, it maintains the structural integrity of the immediate region surrounding His45 and is perhaps also key to forming the binding interface to the kinase domain P4.

Comparative studies of residues participating in the conserved hydrogen bond network

By exploiting the structural and chemical information obtained in these experiments, we are better able to interpret the observed differences in phosphorylation activity between the P1 mutants K48A, H64A, and E67Q. Although the structures of H64A and E67Q revealed disruption to the native hydrogen bond network, both structures only exhibited minor perturbations to the side chain orientations of residues (Figure 7 and Chapter 3 Figure 6). In both structures, the Lys48 side chain swings out of hydrogen bonding distance from Glu67.

Despite minimal structural perturbations, the phosphorylation of the P1H64A mutant is approximately 270-fold faster than that of P1E67Q. The major differences between these two mutants are the tautomeric state of the phosphoaccepting histidine and the pKa value. As in the wild type P1 domain, His45 of the P1H64A mutant exists in the $N^{\delta 1}H$ tautomeric state and has a pKa of 6.9 at 50°C. The correct orientation of the Lys48 side chain hence contributes to optimal phosphotransfer, perhaps by being an important residue involved in binding the kinase domain. This infers that although P1E67Q is largely a k_{cat} mutant, its diminished phosphorylation could also result from some loss of binding affinity to P4 due to the altered position of Lys48. Further support for this hypothesis is obtained by comparing the results of competition studies between wild type P1 and the mutants P1K48A and P1E67Q. P1E67Q acts as a better inhibitor of the P1 phosphorylation reaction than P1K48A (Chapter 3 Figure 4b and Figure 4).

Although the mutation of Lys48 led to the most significant disruption of secondary structure, it was still more amenable to phosphorylation than E67Q (Figure 1a). Neither P1K48A nor P1E67Q stabilize the phosphorylated histidine. Moreover,

they do not affect the phosphotransfer activity to the response regulator CheY [4]. P1K48A shares the same chemical properties of the wild type phosphoaccepting histidine, meaning the chemical reactivity of His45 is not altered by the disorder in the neighboring environment. Removal of the positive charge likely affects the binding interaction; therefore in addition to stabilizing the helical structure, a positive charge at this precise location may be important for molecular recognition of the kinase domain P4.

Together, these results imply that among the studied mutations of the P1 hydrogen bonding network, E67Q imparts the strongest chemical perturbation and K48A the greatest structural perturbation to the CheA autophosphorylation reaction. Although much work remains to be done towards elucidating the CheA mechanism, an emerging picture is one where the phosphotransfer domain contains a catalytic dyad, a resonating Glu67 which activates a nucleophilic His45. The active site may be completed by a third residue, His405, in the kinase domain. A mutation to this residue was found to affect the k_{cat} of the CheA phosphorylation reaction, but not the K_m for ATP [1]. We are slowly beginning to better understand the structural and chemical determinants of the CheA autophosphorylation reaction. Further structure-function studies will elucidate the mechanistic basis for the initiation of the His-Asp phosphorelay in bacterial chemotaxis.

Table 1: Data collection and refinement statistics

	P1K48A$_{short}$	*P1H64A$_{short}$*
Data Collection Statistics		
Resolution (Å)	1.38	1.40
Wavelength (Å)	0.9363	0.9363
Total reflections	227.281	176130
Unique reflections	25909	18854
Completeness (%)	97.6 (98.3)	98.1 (87.3)
I/σ(I)	29.0 (4.1)	20.7 (2.7)
Rsym(%)	0.063 (0.288)	0.09 (0.49)
Mosaicity	0.367	0.584
Wilson B (Å^2)	26.2	28.1
Refinement Statistics		
Resolution limits	30 – 1.38	30 – 1.4
R_{work}[c]	0.1770	0.1678
R_{free}[d]	0.2581	0.2488
Ramachandran plot[e] residues in		
Most favored regions (%)	97.9	96.9
Additional allowed regions(%)	2.1	3.1
Generously allowed regions(%)	0.0	0.0
Disallowed regions (%)	0.0	0.0

[a] Numbers in parentheses correspond to values in the highest resolution shell

[b] $R_{sym} = (\Sigma_{hkl}\Sigma_i | I_i(hkl) - < I(hkl) > |)/(\Sigma_{hkl}\Sigma_i I(hkl))$

[c] $R_{work} = \Sigma(|F_{obs}| - |F_{calc}|)/\Sigma|F_{obs}|$

[d] R_{free} is the R-factor calculated for a 5% test set of reflections excluded from the refinement calculation

[e] As determined by PROCHECK [15]

Table 2: Expected and observed ^{15}N chemical shifts for the His45 residue of P1K48A and P1H64A

	Residue	*Nitrogen*	*Protonation State*	δ_{obs} *(ppm)*	δ_{th} *(ppm)*	δ_{obs}-δ_{th}	*Δδ[Nδ1-Nε2]*
P1K48A							
	His45						
		$N^{\delta1}$	protonated	179.4	176.5	2.9	6.2
		$N^{\varepsilon2}$	protonated	173.2	176.5	-3.3	
		$N^{\delta1}$	protonated	*185.3	249.5	-64.2	36.0
		$N^{\varepsilon2}$	deprotonated	221.3	249.5	-28.2	
P1H64A							
	His45						
		$N^{\delta1}$	protonated	180.7	176.5	4.2	7.5
		$N^{\varepsilon2}$	protonated	173.2	176.5	-3.3	
		$N^{\delta1}$	protonated	*185.4	249.5	-64.1	37.4
		$N^{\varepsilon2}$	deprotonated	222.8	249.5	-26.7	

*theoretical values obtained from the limits as calculated by the Henderson-Hasselbach equation

Table 3: The pKa values and predominant tautomeric states of His45 in CheA and its variants

		pKa	*Predominant tautomeric state*	*Nδ1:Nε2*
P1K48A				
	His45	6.8	$N^{\delta 1}H$	2.6:1
P1H64A				
	His45	6.9	$N^{\delta 1}H$	2.7:1
P1E67Q				
	His45	5.8	$N^{\varepsilon 2}H$	1:3.3
P1				
	His45	6.9	$N^{\delta 1}H$	2.6:1

Figure 1: Mutations at the active site hydrogen bonding network. Histidine phosphorylation was measured at (a) pH 8.5 and 50°C and (b) pH7.5 and 25°C.

(a)

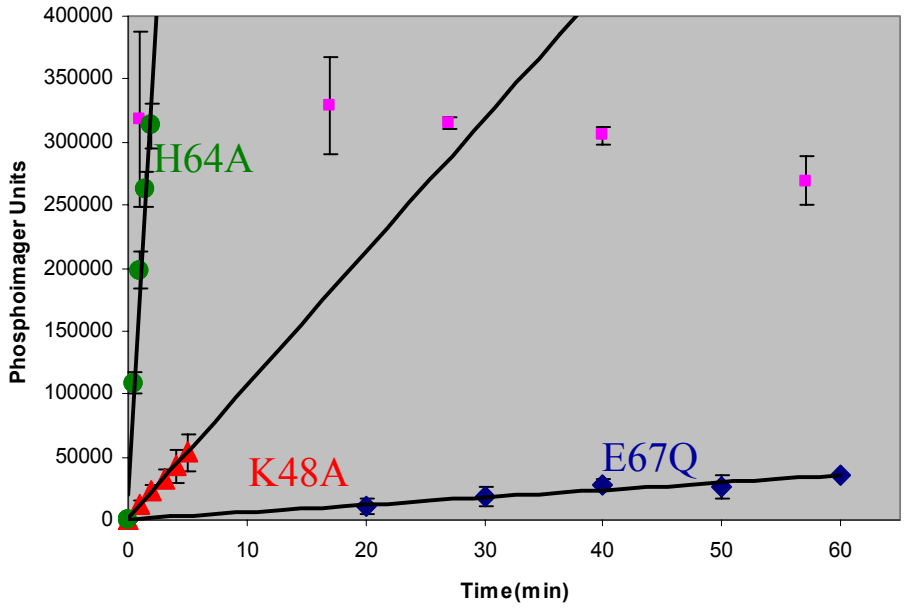
400000
350000
300000
250000
200000
150000
100000
50000
0
Phosphoimager Units
H64A
K48A
E67Q
0
10
20
30
40
50
60
Time(min)

(b)

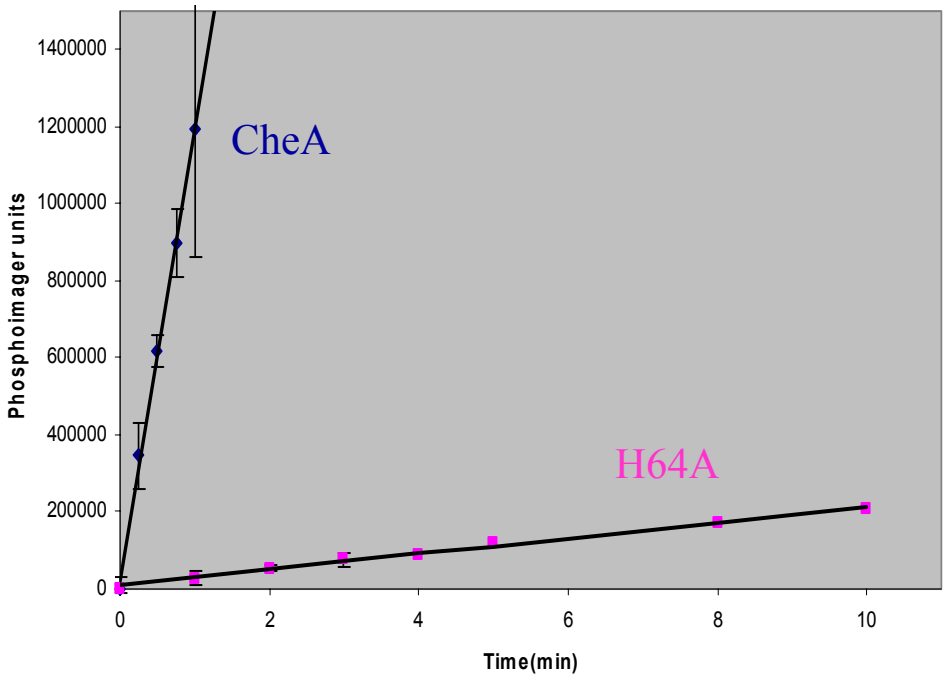
1400000
1200000
1000000
800000
600000
400000
200000
0
Phosphoimager units
CheA
H64A
0
2
4
6
8
10
Time(min)

Figure 2: (a) Swarm Diameter of CheA and its mutants. Photographs of swarm assays produced by (b) CheA, (c) P1K48A, and (d) P1H64A.

(a)

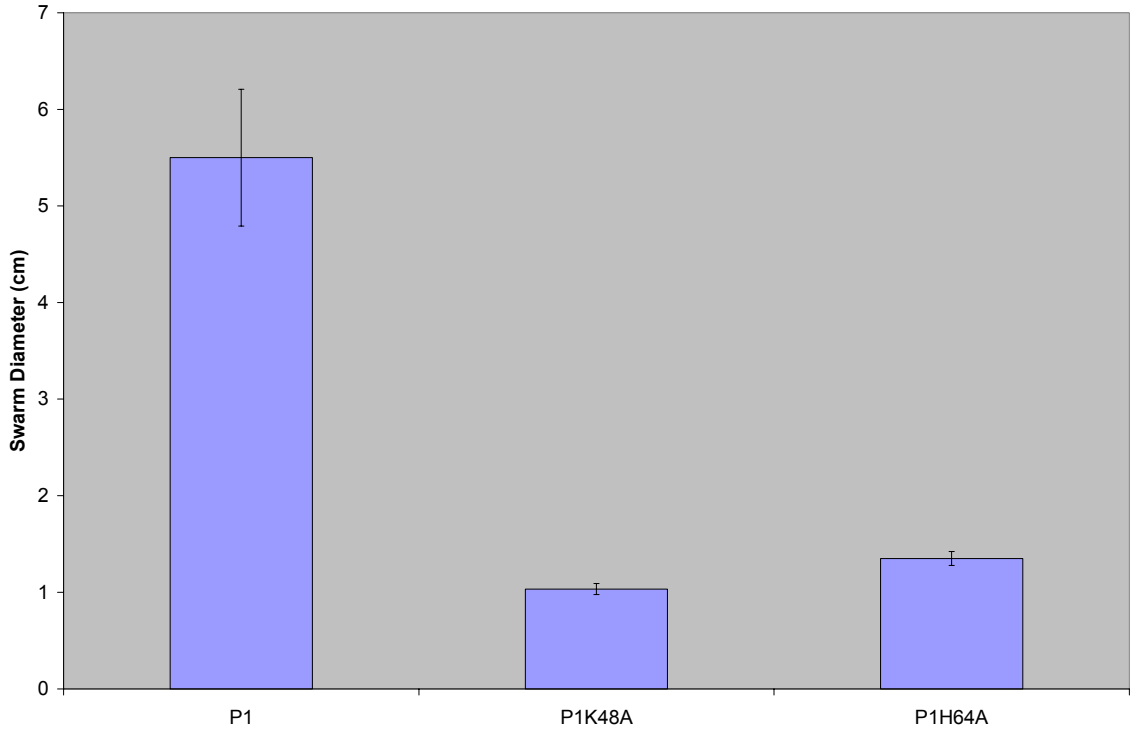

(b) WT, K48A, H64A

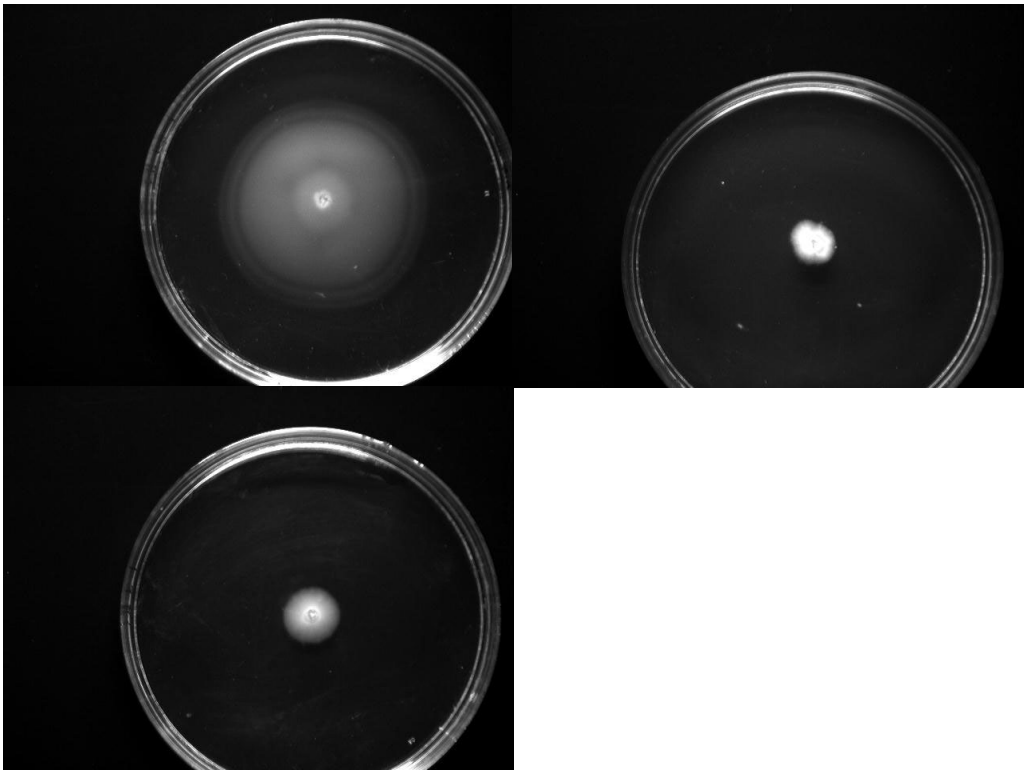

Figure 3: Far-UV CD spectra of (a) P1H64A and P1; (b) P1K48A and P1

(a)

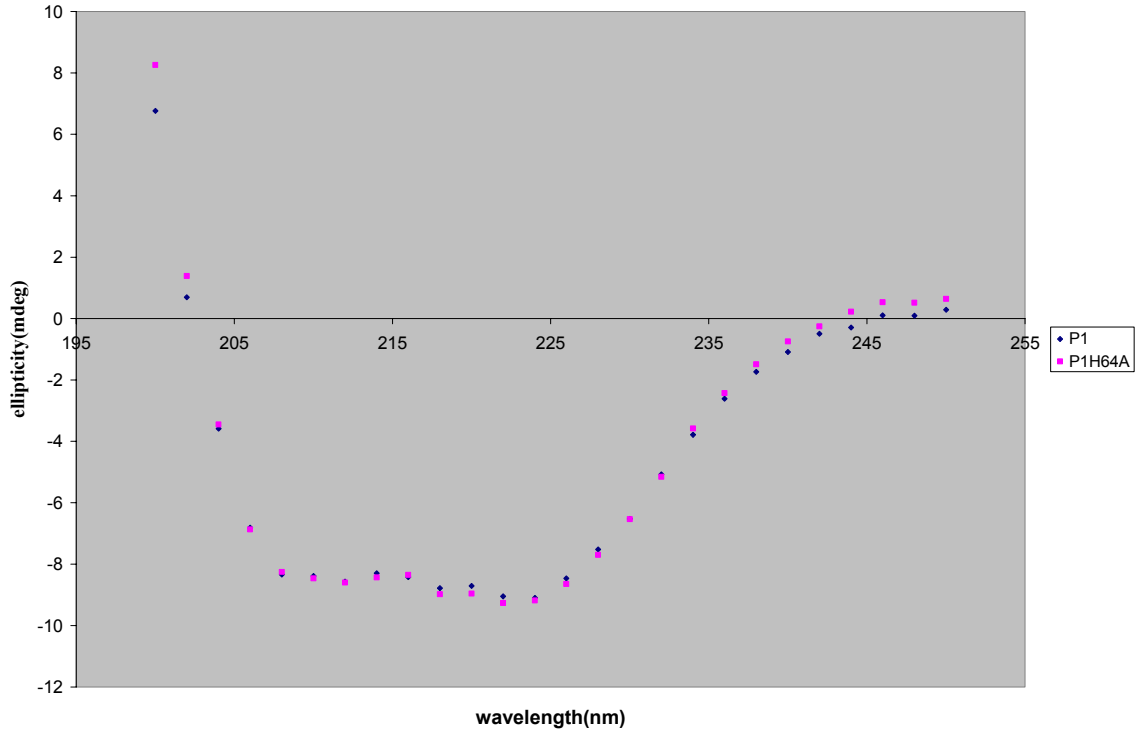
10
8
6
4
2
0
-2
-4
-6
-8
-10
-12
195
205
215
225
235
245
255
ellipticity(mdeg)
wavelength(nm)
P1
P1H64A

(b)

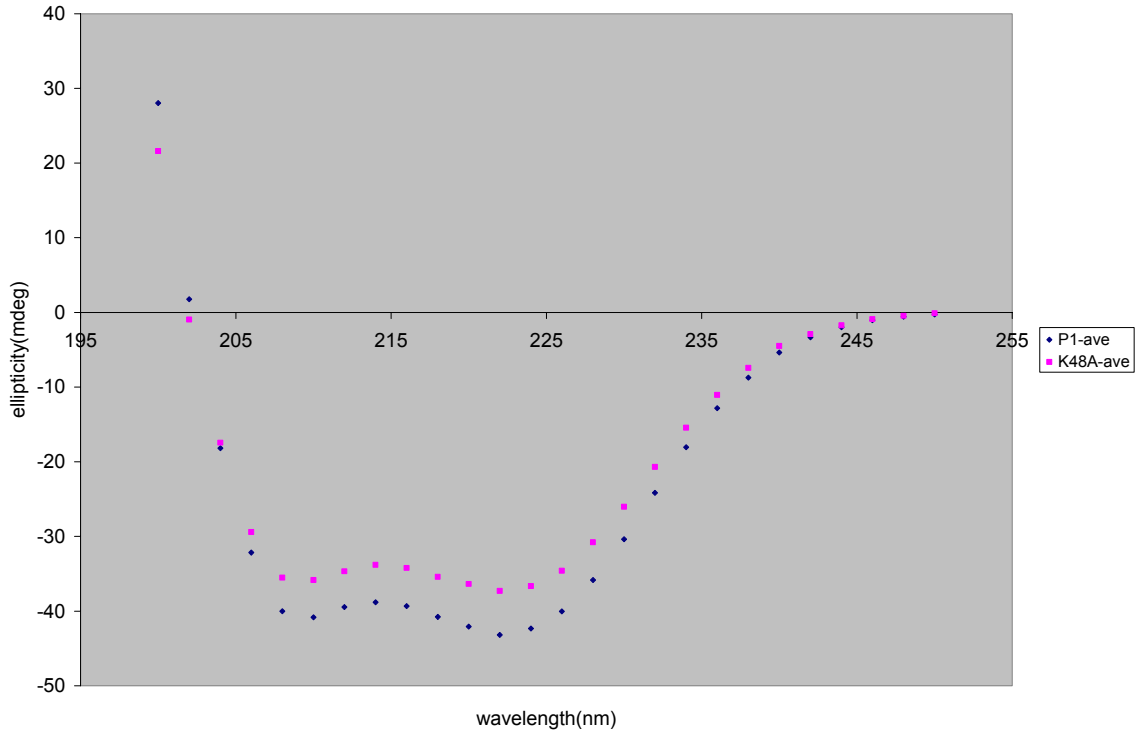
40
30
20
10
0
-10
-20
-30
-40
-50
195
205
215
225
235
245
255
ellipticity(mdeg)
wavelength(nm)
P1-ave
K48A-ave

Figure 4: P1 (diamonds) and the catalytic core Δ289 were incubated together in the presence of a tenfold excess of P1K48A (squares). Approximately 44% of wild type phosphotransfer activity is maintained.

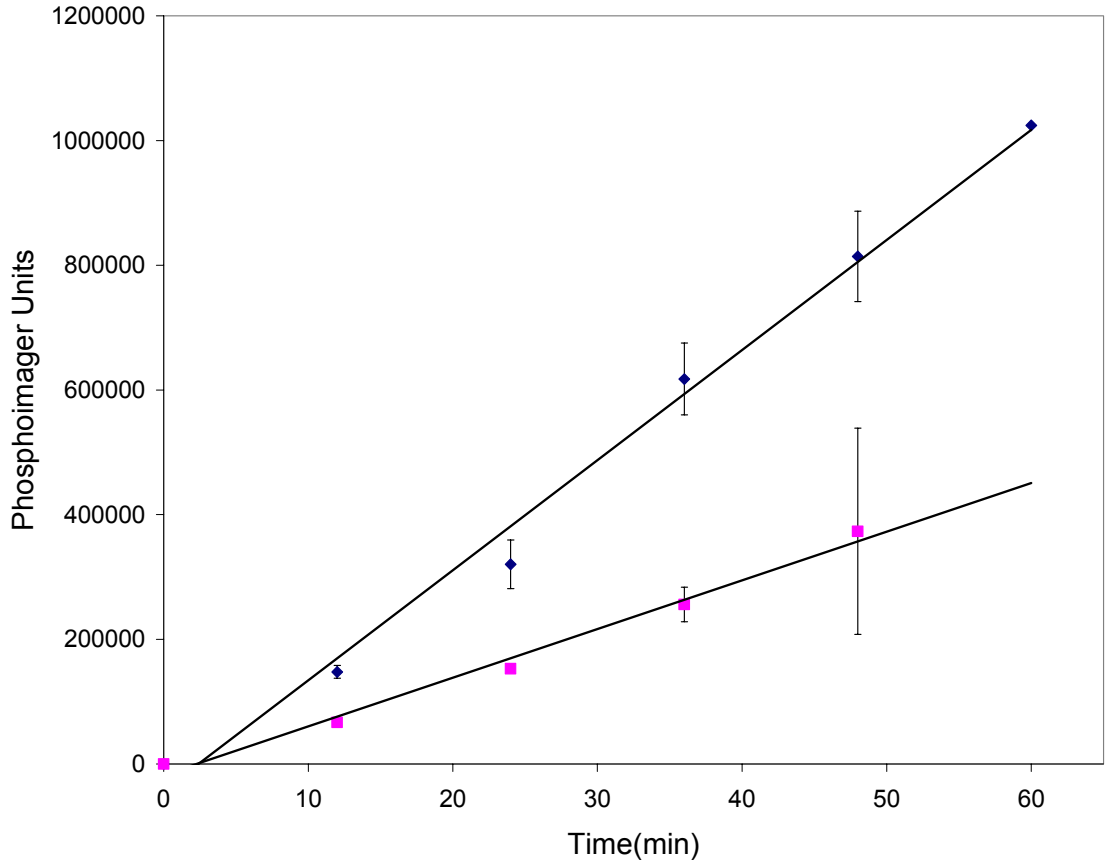
1200000
1000000
800000
600000
400000
200000
0
Phosphoimager Units
0
10
20
30
40
50
60
Time(min)

Figure 5: The stability of the phospho-histidine complex was determined over an extended period of time at 50ºC

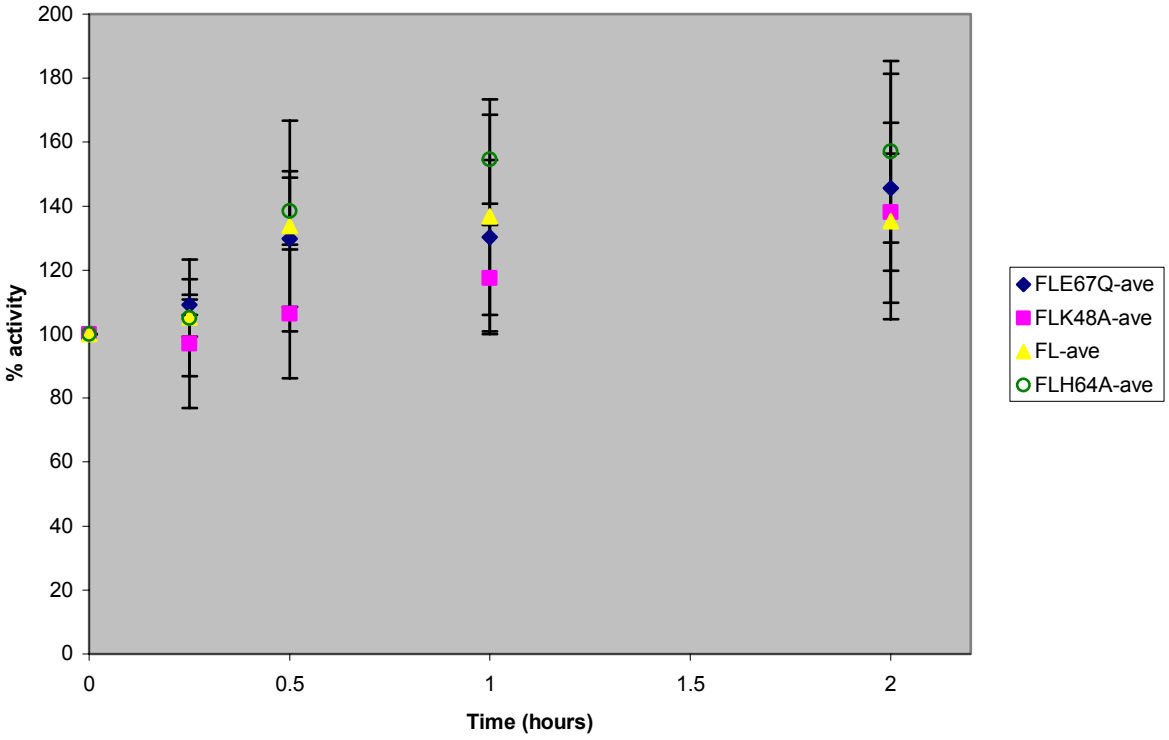
200
180
160
140
120
100
80
60
40
20
0
% activity
0
0.5
1
1.5
2
Time (hours)
FLE67Q-ave
FLK48A-ave
FL-ave
FLH64A-ave

Figure 6: (a) Close-up view of the P1K48A active site (b) overlaid with the native P1 model

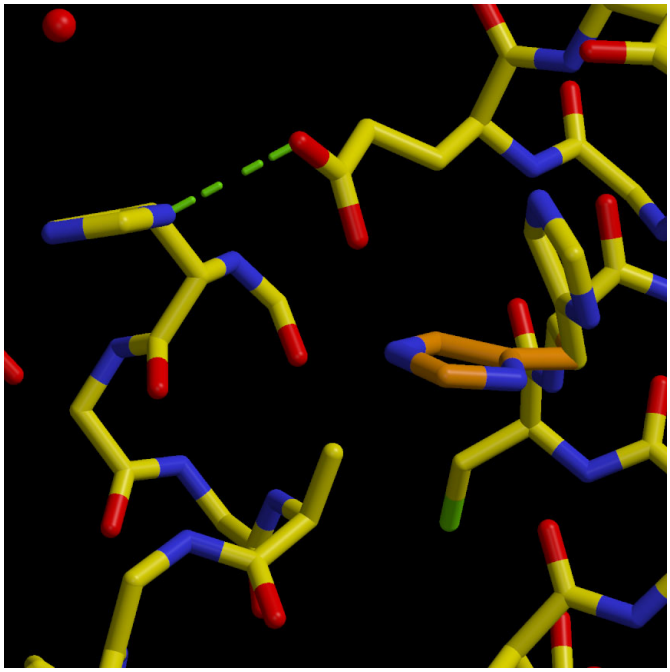

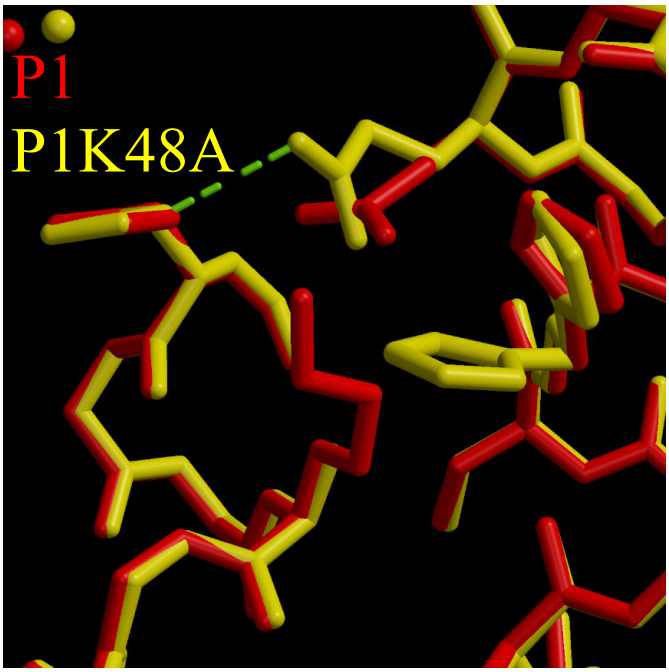
P1
P1K48A

Figure 7: (a.) Close up view of the P1H64A active site (b.) overlaid with the native P1 model

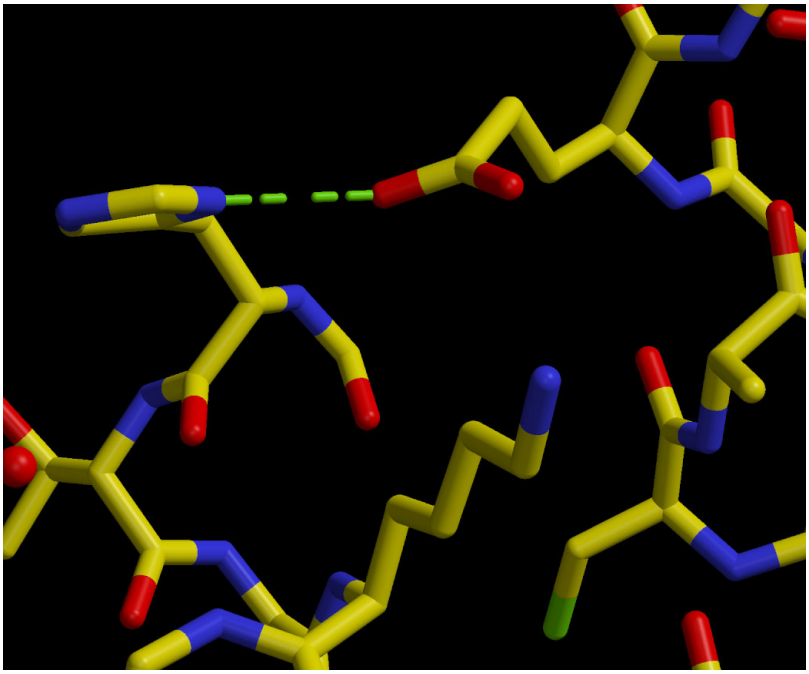

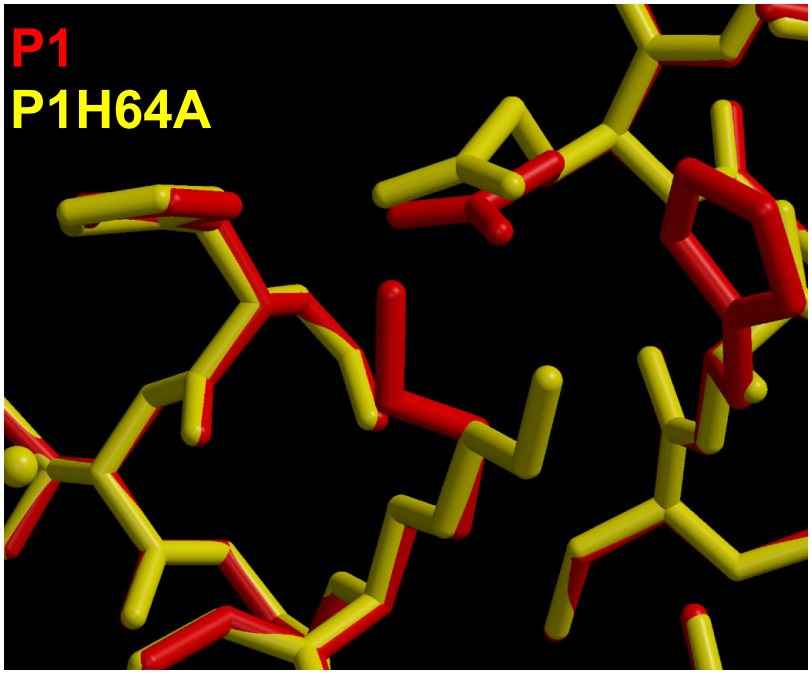
P1
P1H64A

Figure 8: Chemical shifts of the His45 imidazole ^{15}N nuclei of P1K48A as a function of pH. The $N^{\varepsilon 2}$ atom is blue and the $N^{\delta 1}$ is red.

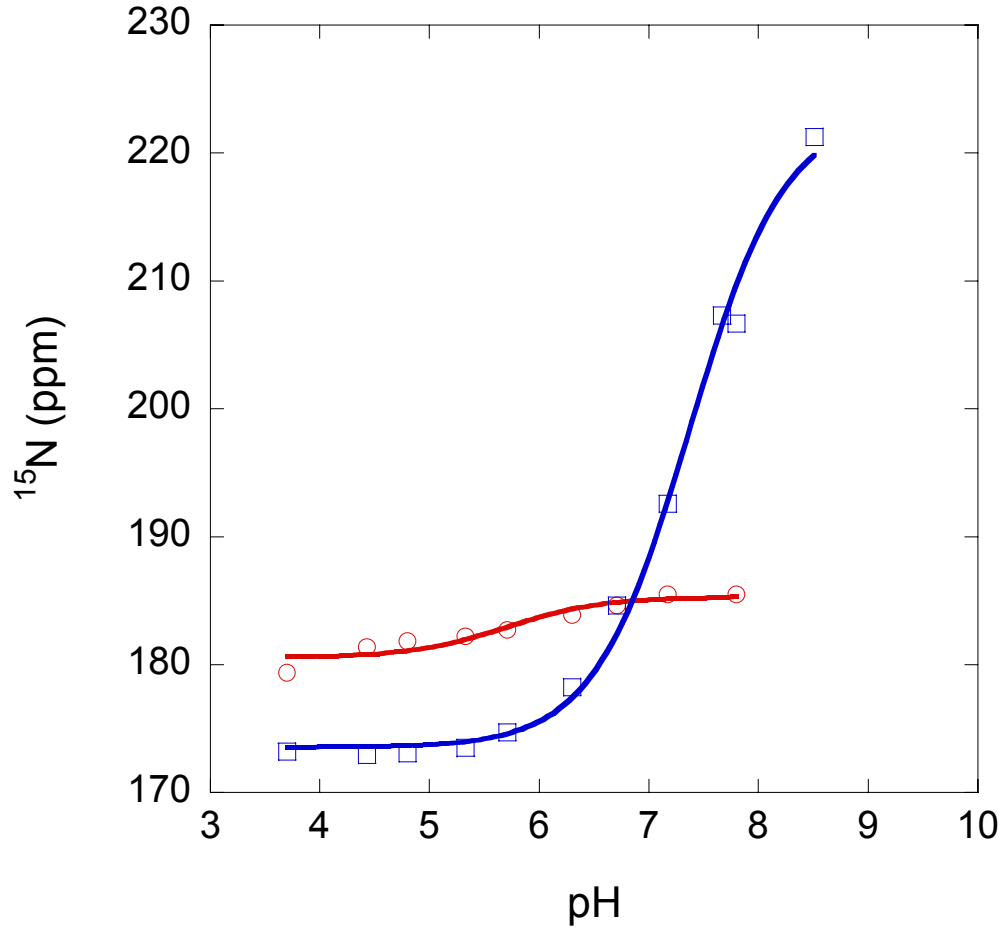
230
220
210
200
190
180
170
3
4
5
6
7
8
9
10
^{15}N (ppm)
pH

Figure 9: Chemical shifts of the imidazole ^{15}N nuclei of P1H64A His45 as a function of pH. The $N^{\varepsilon 2}$ atom is blue and the $N^{\delta 1}$ is red.

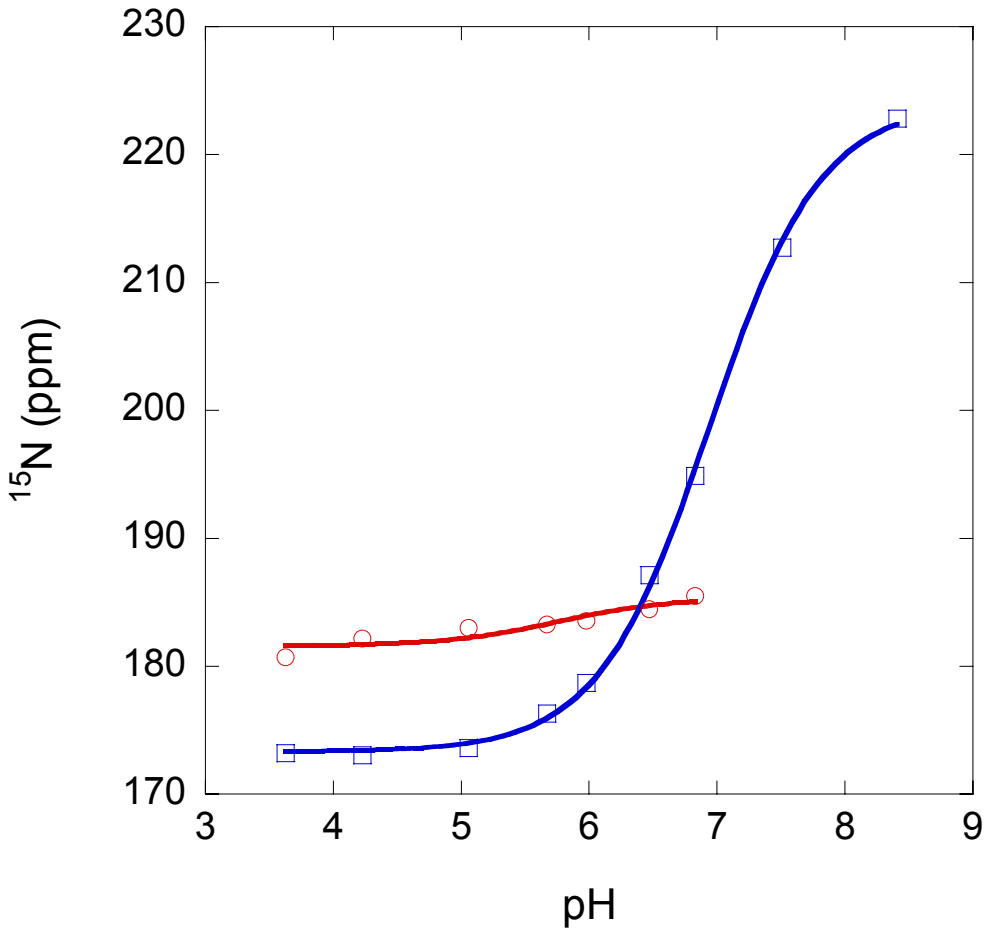
230
220
210
200
190
180
170
^{15}N (ppm)
3
4
5
6
7
8
9
pH

REFERENCES

1. Hirschman, A., et al., *Active Site Mutations in CheA, the Signal-Transducing Protein Kinase of the Chemotaxis System in Escherichia coli.* Biochemistry, 2001. **40**: p. 13876-13887.

2. Bilwes, A.M., et al., *Nucleotide binding by the histidine kinase CheA.* Nature Structural Biology, 2001. **8**(4): p. 353-360.

3. Zhou, H., et al., *NMR Studies of the Phosphotransfer Domain of the Histidine Kinase CheA from Escherichia coli: Assignments, Secondary Structure, General Fold, and Backbone Dynamics.* Biochemistry, 1995. **34**: p. 13858-13870.

4. Mourey, L., et al., *Crystal Structure of the CheA Histidine Phosphotransfer Domain that Mediates Response Regulator Phosphorylation in Bacterial Chemotaxis.* The Journal of Biological Chemistry, 2001. **276**(33): p. 31074-31082.

5. Zhou, H. and F.W.Dahlquist, *Phosphotransfer site of the Chemotaxis-Specific Protein Kinase CheA as Revealed by NMR.* Biochemistry, 1997. **36**: p. 699-710.

6. Markley, J.L., *Observation of Histidine Residues in Proteins by Means of Nuclear Magnetic-Resonance Spectroscopy.* Accounts of Chemical Research, 1975. **8**(2): p. 70-80.

7. Bilwes, A., et al., *Structure of CheA, a Signal-Transducing Histidine Kinase.* Cell, 1999. **96**: p. 131-141.

8. Gill, S.C. and P.H. Vonhippel, *Calculation of Protein Extinction Coefficients from Amino-Acid Sequence Data.* Analytical Biochemistry, 1989. **182**(2): p. 319-326.

9. Otwinowski, A. and W. Minor, *Processing of X-ray diffraction data in oscillation mode.* Methods in Enzymolozy, 1997. **276**: p. 307-325.

10. Sheldrick, G.M. and T.R. Schneider, *SHELXL:high resolution refinement.* Methods in Enzymology, 1997. **277**: p. 319-343.

11. McRee, D.E., *XtalView: a visual protein crystallographic software system for X11/Xview.* J. Mol. Graph., 1992. **10**: p. 44-47.

12. Zhang, O.W., et al., *Backbone H-1 and N-15 Resonance Assignments of the N-Terminal Sh3 Domain of Drk in Folded and Unfolded States Using Enhanced-Sensitivity Pulsed-Field Gradient Nmr Techniques.* Journal of Biomolecular Nmr, 1994. **4**(6): p. 845-858.

13. Marion, D., et al., *Rapid Recording of 2d Nmr-Spectra without Phase Cycling - Application to the Study of Hydrogen-Exchange in Proteins.* Journal of Magnetic Resonance, 1989. **85**(2): p. 393-399.

14. Ikegami, T., et al., *Solution Structure and Dynamic Character of the Histidine-Containing Phosphotransfer Domain of Anaerobic Sensor Kinase ArcB from Escherichia coli.* Biochemistry, 2001. **40**: p. 375-386.

15. Laskowski, R.A., et al., *PROCHECK: a program to check the stereochemical quality of protein structures.* J. Appl. Crystallogr., 1993. **26**: p. 283-291.

Appendix 1

^{1}H and ^{15}N Chemical shifts of P1 histidine residues

Table 1: Expected and observed imidazole ^{15}N chemical shifts for P1K48A and P1H64A

	Residue	Nitrogen	Protonation State	δ_{obs} (ppm)	δ_{th} (ppm)	δ_{obs}-δ_{th}	$\Delta\delta$[Nδ1-Nε2]
P1K48A							
	His64						
	low pH	$N^{\delta1}$	protonated	177.1	176.5	0.6	3.5
		$N^{\varepsilon2}$	protonated	173.6	176.5	-2.9	
	high pH	$N^{\delta1}$		*194.7	249.5	-54.8	23.3
		$N^{\varepsilon2}$	deprotonated	218.0	249.5	-31.5	
	HisTag						
	low pH	$N^{\delta1}$	protonated	176.7	176.5	0.2	3.3
		$N^{\varepsilon2}$	protonated	173.4	176.5	-3.1	
	high pH	$N^{\delta1}$	deprotonated	240.2	249.5	-9.3	65.2
		$N^{\varepsilon2}$	protonated	175.0	249.5	-74.5	
P1H64A							
	HisTag						
	low pH	$N^{\delta1}$	protonated	176.6	176.5	0.1	3.0
		$N^{\varepsilon2}$	protonated	173.6	176.5	-2.9	
	high pH	$N^{\delta1}$	deprotonated	*237.4	249.5	-12.1	62.0
		$N^{\varepsilon2}$	protonated	175.4	249.5	-74.1	

Table 2: The tautomeric states and pKas of histidine residues found in the CheA P1 domain

		pKa	Predominant Tautomeric State	Nδ1:Nε2
P1K48A				
	His45	6.8	$N^{\delta1}H$	2.6:1
	His64	6.5	$N^{\delta1}H$	1.8:1
	His1	6.0	$N^{\varepsilon2}H$	1:9.6
P1H64A				
	His45	6.9	$N^{\delta1}H$	2.7:1
	His1	5.9	$N^{\varepsilon2}H$	1:4.3
P1E67Q				
	His45	5.8	$N^{\varepsilon2}H$	1:3.3
	His64	5.31	$N^{\varepsilon2}H$	1:4.3
	His1	5.9	$N^{\varepsilon2}H$	1:4.8
P1				
	His45	6.9	$N^{\delta1}H$	2.6:1
	His64	5.6	$N^{\varepsilon2}H$	1:3.4

Figure 1: ^{1}H chemical shifts for the histidines of P1E67Q (a) His45 (b) His64 (c) HisTag

(a)

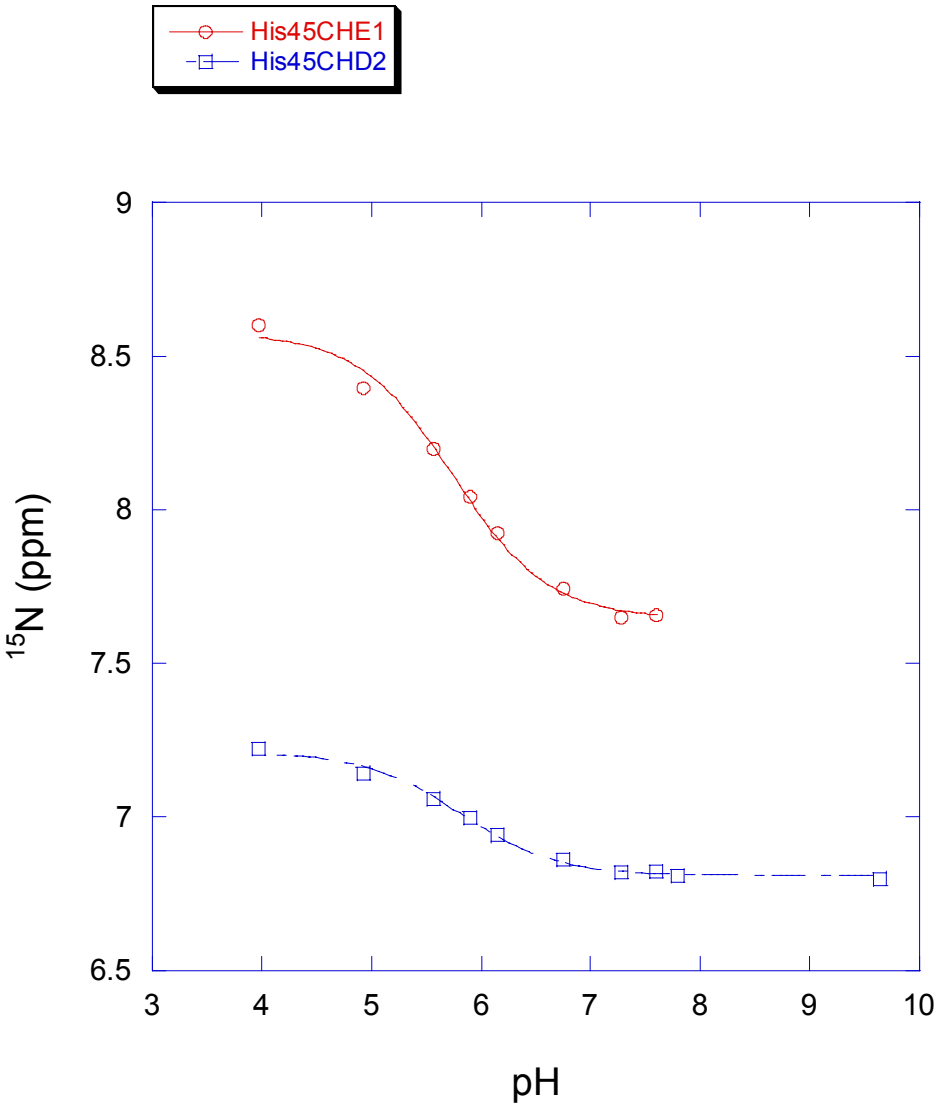

(b.)

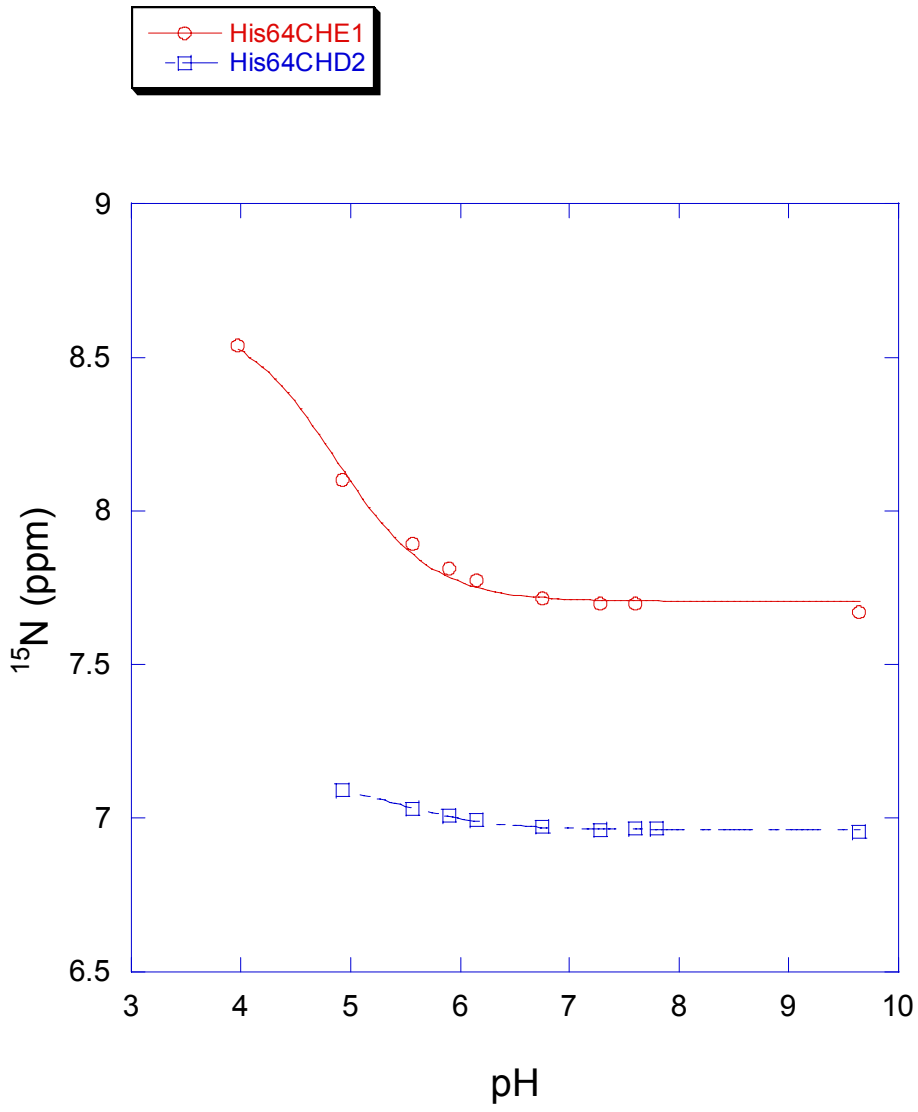

(c)

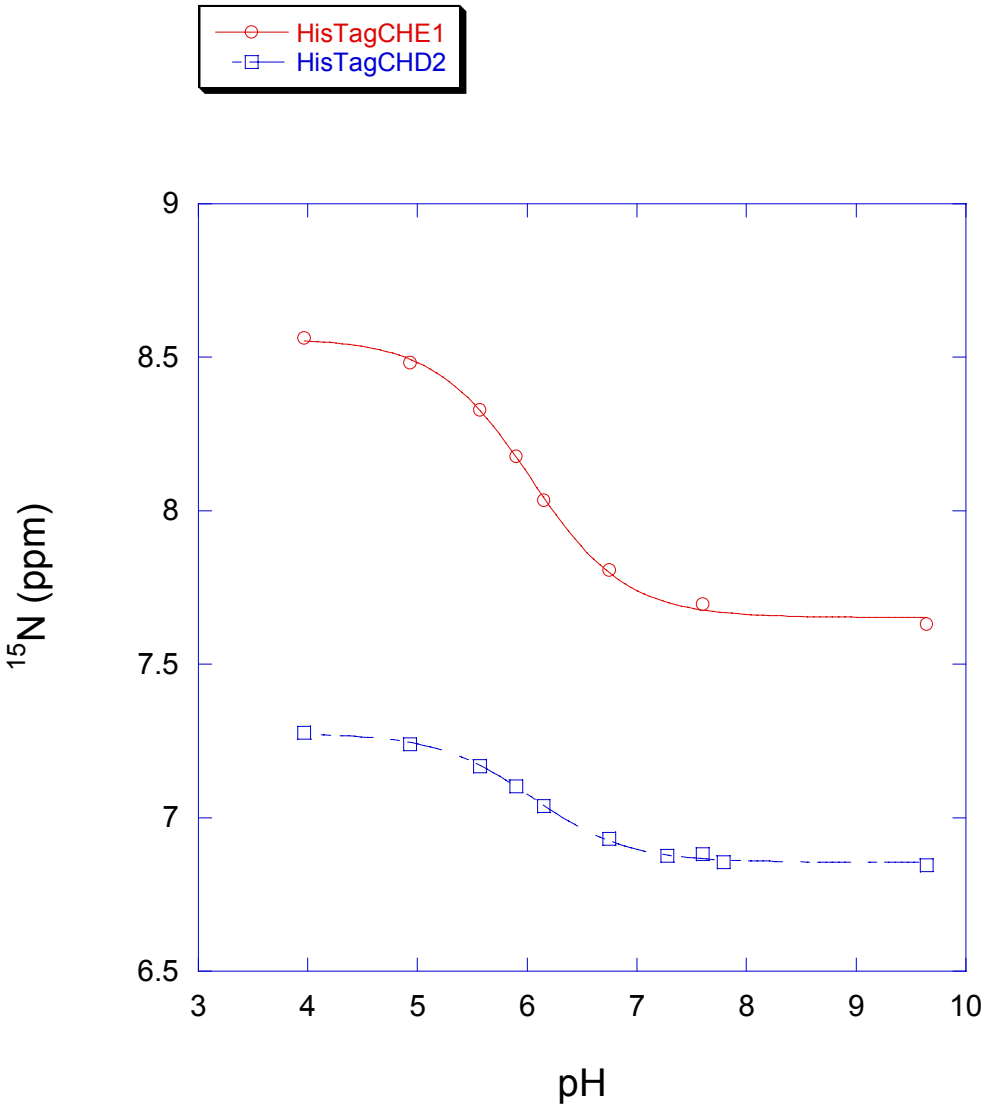

Figure 2: ^{1}H chemical shifts for the histidines of P1K48A (a) His45 (b) His64 (c) HisTag

(a)

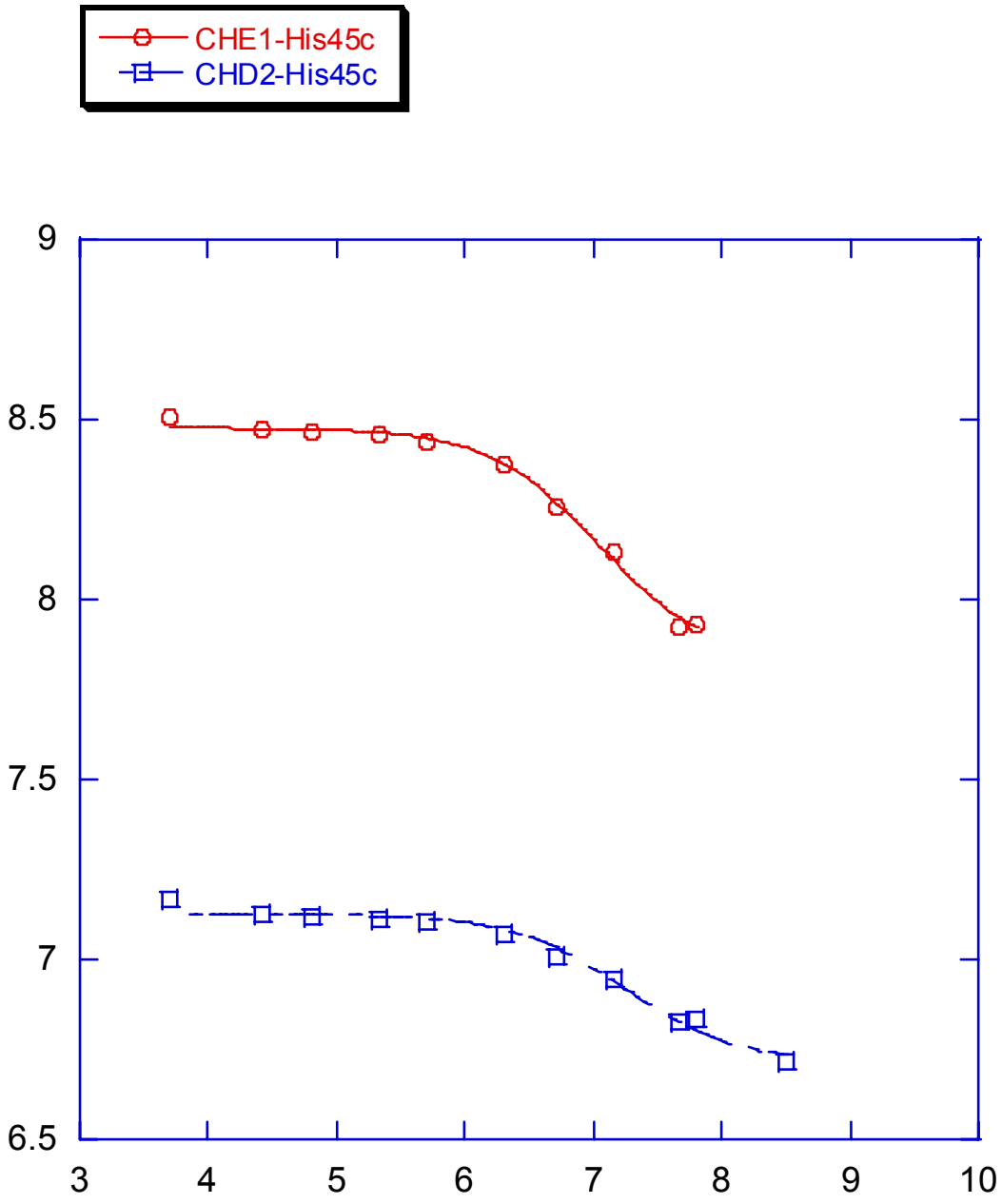

(b)

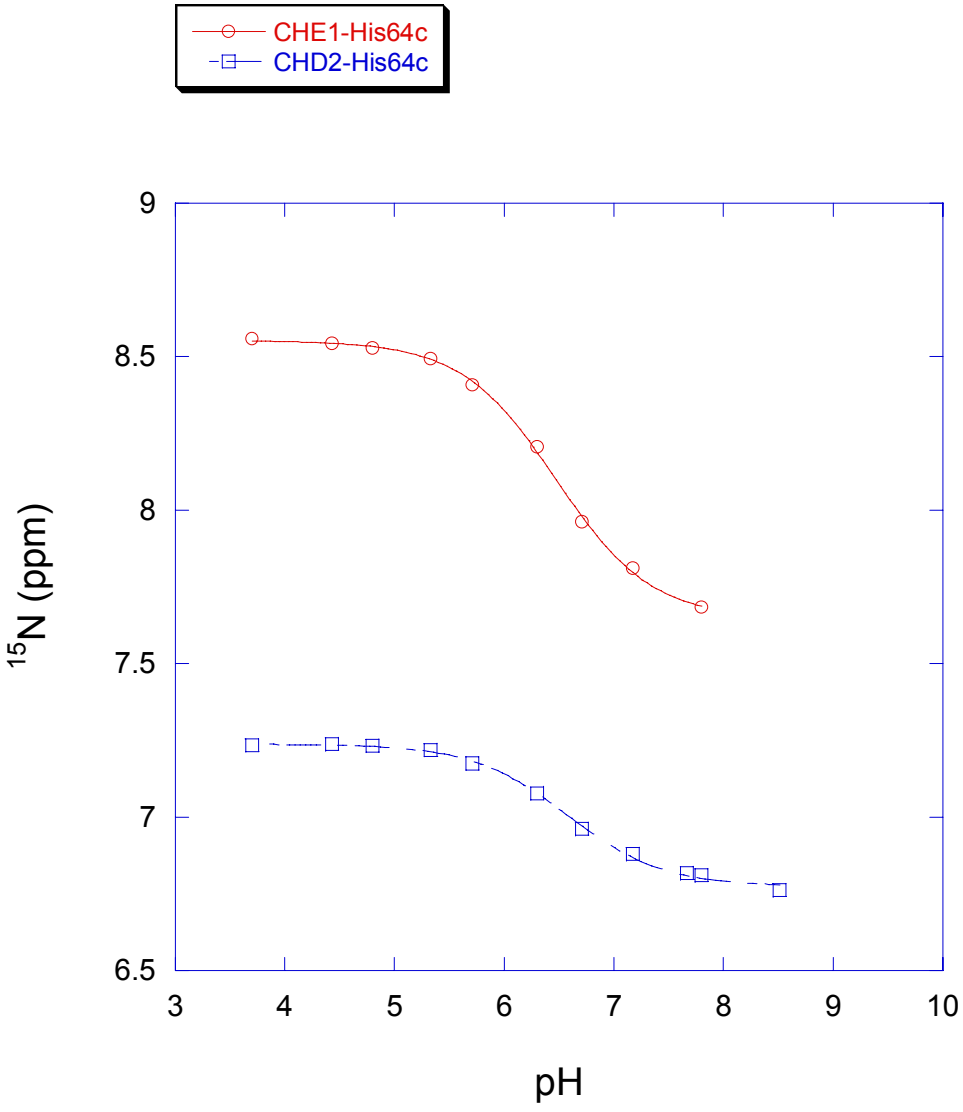

(c)

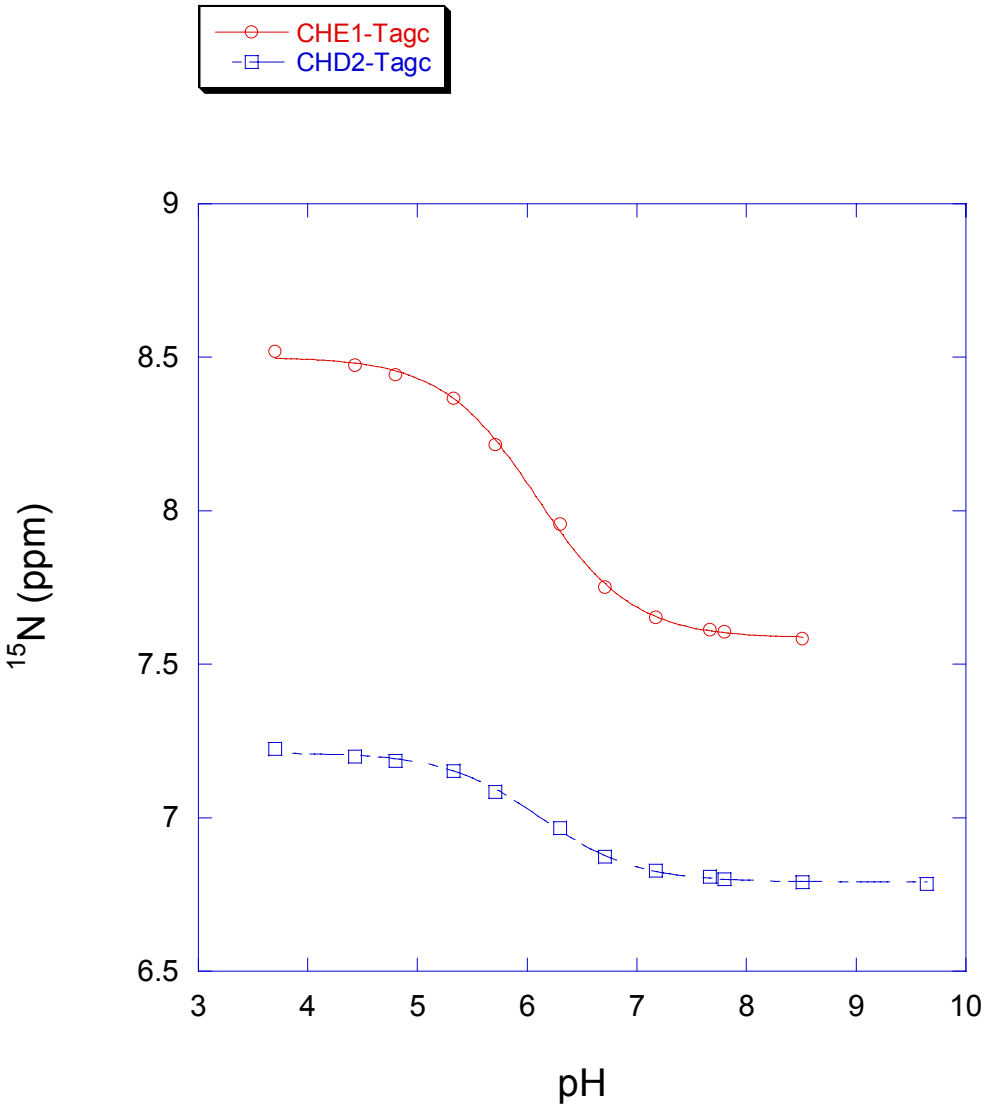

Figure 3: ^{1}H chemical shifts for the histidines of P1H64A (a) His45 (b) HisTag

(a)

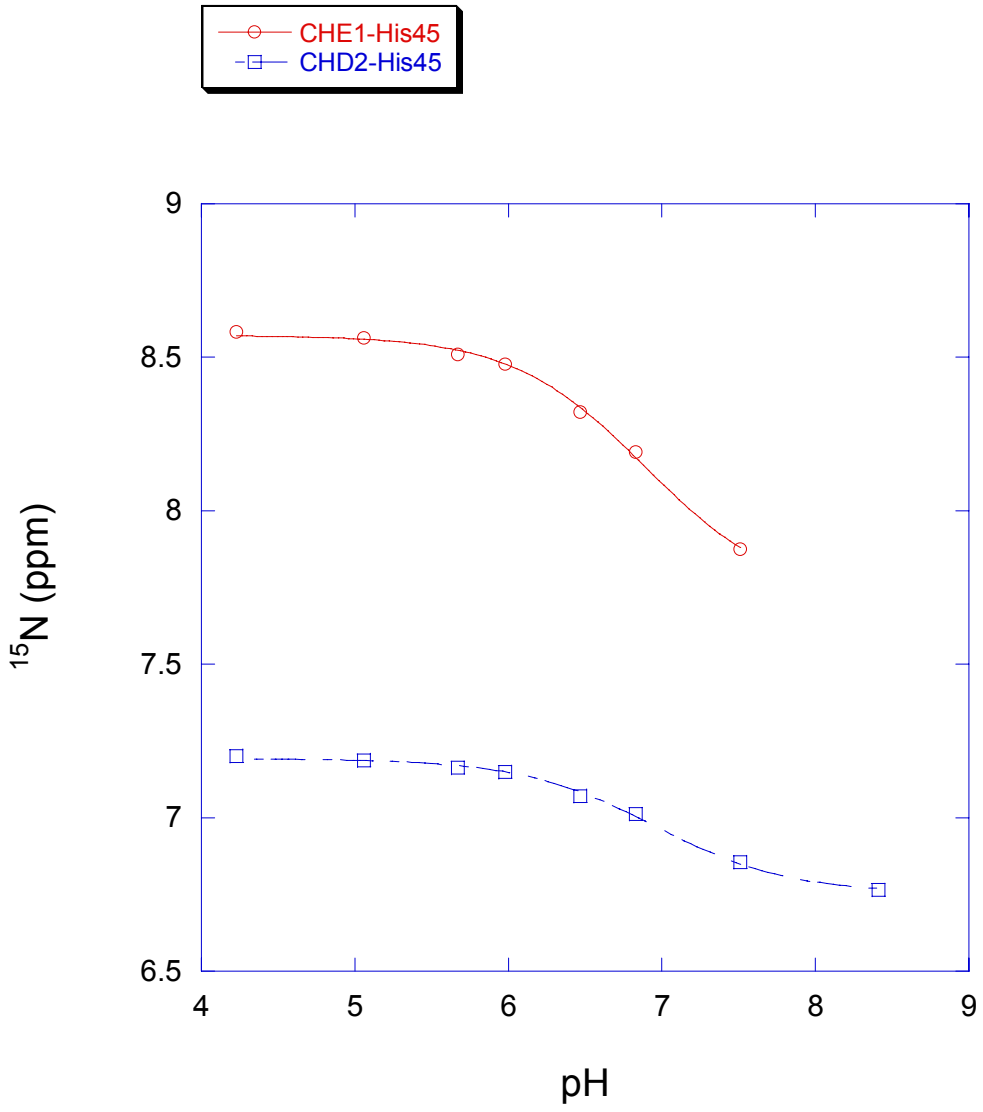

(b)

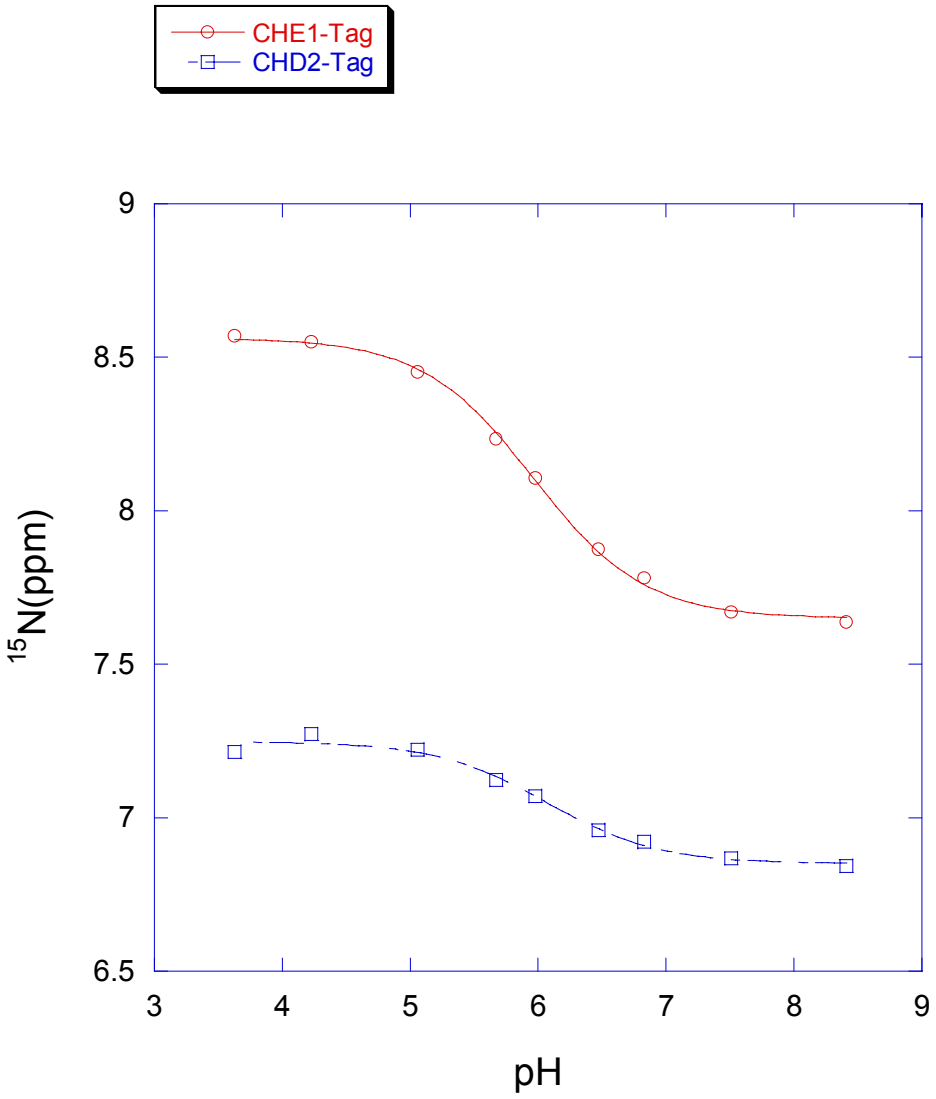

Appendix 2

Biochemical Characterization of CheA domains

The phospho-histidine bond is not stable at high temperatures

The ability of P1 to be phosphorylated by Δ289 was monitored as a function of temperature (Figure 1a). Although this hyperthermophilic organism has an optimal growth temperature of 80°C and a maximal growth temperature of 90°C (Huber, Langworthy et al. 1986), maximal phosphorylation activity was surprisingly observed at 60°C. The stability of the P1 phospho-histidine complex was subsequently tested as a function of time (Figure 1b). The phospho-histidine bond is stable for up to 3 hours at 25°C and 40°C. However, at 50°C, the bond becomes slightly less stable. A drastic reduction in the stability of the phospho-histidine complex is observed at temperatures above 60°C. The bond is rapidly broken as evidenced by the lack of phosphorylation signal observed after two hours.

Figure 1: Temperature dependence of phosphorylation activity (a) and the stability of the P1 phospho-histidine complex (b): The phosphorylation of P1 by Δ289 was allowed to reach saturation levels. The reaction was then terminated and placed at 4°C. Aliquots of the phosphorylation reaction were taken at the indicated time points as described in Materials and Methods.

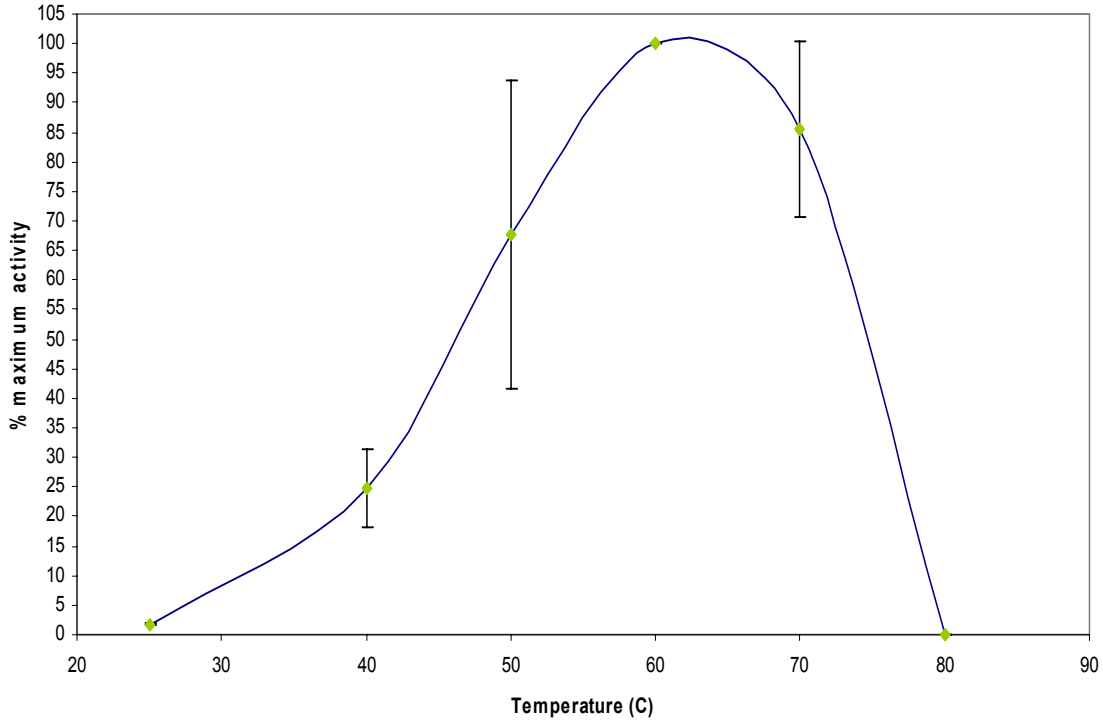
% maximum activity
105
100
95
90
85
80
75
70
65
60
55
50
45
40
35
30
25
20
15
10
5
0
20
30
40
50
60
70
80
90
Temperature (C)

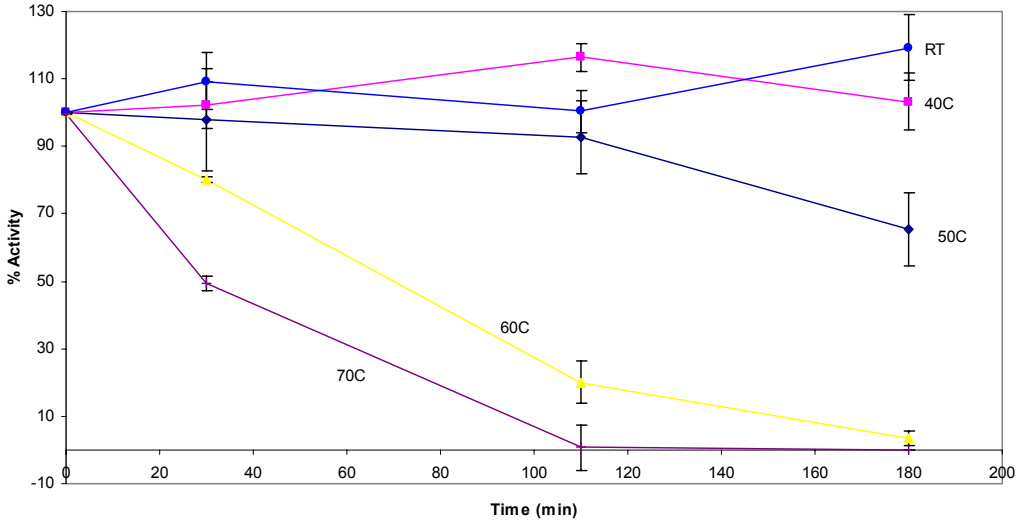
130
110
90
70
50
30
10
-10
% Activity
0
20
40
60
80
100
120
140
160
180
200
Time (min)
RT
40C
50C
60C
70C

MATERIALS AND METHODS

Temperature Dependence and Phosphostability Studies

The initial velocities of P1(30μM) phosphorylation by Δ289(2μM) were measured at 25°C, 40°C, 50°C, 60°C, 70°C and 80°C as described above. To measure the stability of the phospho-histidine complex, the phosphorylation reaction was quenched with 4X sodium dodecyl sulfate (SDS) electrophoresis buffer containing 25mM ethylenediaminetetra acetic acid (EDTA). The reaction tube was kept at the respective temperature and aliquots were placed at 4°C at designated time points. Samples were then electrophoresed and processed as previously described.